Thin Film Formation of a Solution Processed Pentacene

Daniel C Huang

Electrical Engineering and Computer Sciences
University of California at Berkeley

Technical Report No. UCB/EECS-2009-74
http://www.eecs.berkeley.edu/Pubs/TechRpts/2009/EECS-2009-74.html

May 20, 2009

Thin Film Formation of a Solution Processed Pentacene

by

Daniel Huang

B.S. (University of California, Berkeley) 2002
M.S. (University of California, Berkeley) 2006

A dissertation submitted in partial satisfaction of the

Requirements for the degree of

Doctor of Philosophy

in

Electrical Engineering and Computer Sciences

in the

Graduate Division

of the

University of California, Berkeley

Committee in charge:

Professor Vivek Subramanian, Chair
Professor Tsu-Jae King Liu
Professor Oscar Dubon

Spring 2009

The dissertation of Daniel Chien-Hau Huang is approved:

Chair _____ Date _____

_____ Date _____

_____ Date _____

University of California, Berkeley

Abstract

Thin Film Formation of a Solution Processed Pentacene

by

Daniel Huang

Doctor of Philosophy in Electrical Engineering and Computer Sciences

University of California, Berkeley

Professor Vivek Subramanian, Chair

Pentacene has one of the highest carrier mobility among organic semiconductors. Unfortunately, due to its tight packing density, giving it its high mobility, pentacene does not readily dissolve in common solvents, making it difficult to incorporate into printed electronics. Solution processable pentacene through a precursor route is a promising method of incorporating pentacene into printed electronics. Here, the thin film formation of pentacene through a precursor route is detailed. Specifically, the thin film formation of pentacene on oxide is compared with thin film formation of pentacene on oxide through evaporation methods. Then thin film formation of pentacene through the precursor is detailed and compared on different substrates important to printed electronics. Finally, the performance of pentacene thin film transistors is tested by using different heat treatments for processing the pentacene precursor. The heat treatments were based on the thin film studies of pentacene thin film formation and seek to optimize pentacene TFT performance.

Acknowledgements

Funding for this work was from SRC. This dissertation was made possible through the talents and generous contribution of many extraordinary people at UC Berkeley. Jean Frechet's group in the department of Chemistry has been a great for support in organic chemistry. In particular Clayton Mauldin has always been available for discussions and equipment training. In the Organic Electronics Lab, special thanks to Shong Yin and Kanan Puntambekar for trememdous help in X-ray analysis. Thanks also to Steven Volkman and Kinyip Phoa for help with materials characterization. AFM work would not have be possible without the aid of Alejandro de la Fuente Vornbrock. Thanks to Frank Liao who helped me in whatever way was humanly possible for him. In addition, thanks to Paul Chang and Tuyen Le who taught me the ins and outs of research as I was getting started. Of course, many thanks to my advisor Vivek Subramanian who has been mentor these past years and taught me not only research but also football.

Dedicated to my cousin Titus Jahng

Somehow he also decided to study engineering

Table of Contents

List of Figures

List of Tables

List of Equations

1 Introduction

Printed electronics has been an area of increased research in these past years. It promises to reduce the cost of manufacturing electronics, which would allow for low-cost electronics in an application space which currently does not exist. Applications can include flexible displays,[1] electronic noses,[2] RFID tags[3] and e-textiles.[4] All these applications do not necessarily require high switching speeds; instead they require flexible substrates and low cost manufacturing.

Printed electronics is a technology which uses a different paradigm than traditional semiconductors. While silicon technology strives for electronics with high switching speeds and high integration density to fit in a small area, printed electronics is useful for applications where small areas, high speed and high integration are not necessary. The purpose of printed electronics is not to compete with current silicon based semiconductors, instead it fills a different application space which current silicon based semiconductors does not address. Specifically, the promise of printed electronics is to create low-cost electronics.

Many people equate printed electronics with organic electronics. Strictly speaking organic electronics does not have to be printed, however a great driver in organic electronics is use printing technology. Even though printed electronics does not have to use organic materials, however a great portion of materials used for printed

electronics is organic. It can be said that it was the discovery of organic semiconductors that allowed for printed electronics to be possible.

This thesis deals with a pentacene precursor for use as a semiconducting material in printed electronics, specifically for a TFT. This chapter will first talk about printed electronics and the place where printed electronics falls in the world of electronics. Next, the materials used for printed electronics is covered. Specifically, the organic semiconductor pentacene and the pentacene precursor will be introduced. Finally, the general organization of this thesis is outlined.

1.1 Printed Electronics

As stated before, printed electronics fills the application space which tradition silicon-based technology does not fill and even spaces which have not yet been thought of because the technology was not present. Specifically it fills the space of low-cost and disposable electronics. Disposable electronics allows for the thought of "smart everything." If electronics can get cheap enough, it would be possible to incorporate electronics into everything. Electronics in clothing would allow for the monitoring of vital signs in soldiers in battle, this is one application in e-textiles. Electronics onto food products allow for real time inventory of items on the shelf. In both these examples, the electronic element will eventually be thrown away, so the cost of manufacturing and integration of the electronics needs to be cheap. Three reasons printed electronics promises low-cost production is the direct printing of electronics onto arbitrary substrates, removal of expensive lithography and high vacuum equipment and the usage of an additive process.

Suppose a traditional processed was used to an RFID tag. The circuit is processed directly on a silicon wafer through a subtractive process. Films of the desired material are deposited onto the substrates, many times using expensive high vacuum equipments. Then using expensive lithographic techniques the films are patterned and the unwanted material is removed, leaving the desired patterns. This overall is a wasteful process. Finally, the wafers are diced and the circuit needs to be attached to the RFID tag.

Printed electronics promises to reduce the cost of this process by manufacturing circuits directly onto the low-cost substrates. Figure 1.1 illustrates the manufacturing of devices through an all additive printing system. Here the low-cost substrate is passed under several deposition stages, where materials are patterned and deposited straight onto the substrate. This is similar to an inkjet printer where paper passes under a printing head and ink is directly deposited onto the paper in the desired pattern. The cost of attachment is now cut out. The printing process being all additive reduces material was, and finally the printing system cuts out the need of high vacuum and lithographic tools.

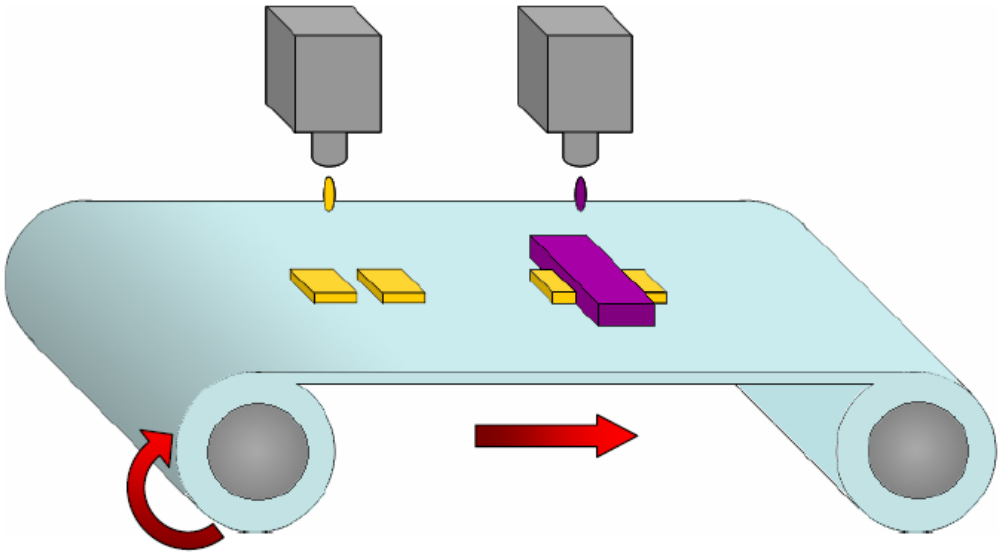

Figure 1-1: An all additive printing process used for the manufacturing of organic electronics.

The equipment for printed electronics is the same conventional printing technology for publishing in order to be used for electronic manufacturing. Such processes include, ink-jet printing, gravure printing, and screen printing. These processes allows for a more flexible range of substrates for electronics production compared to the standard clean room for silicon processing. Furthermore, the traditional clean room equipments require stringent environmental conditions. With printing, atmospheric pressures are sufficient for the deposition of materials, which further reduces costs and allows for flexibility in substrates.

The great innovation in printed electronics is the inks which are used in printed electronics are different from conventional printing. Therefore this field attracts talents form chemistry, material science, and engineering of all disciplines.

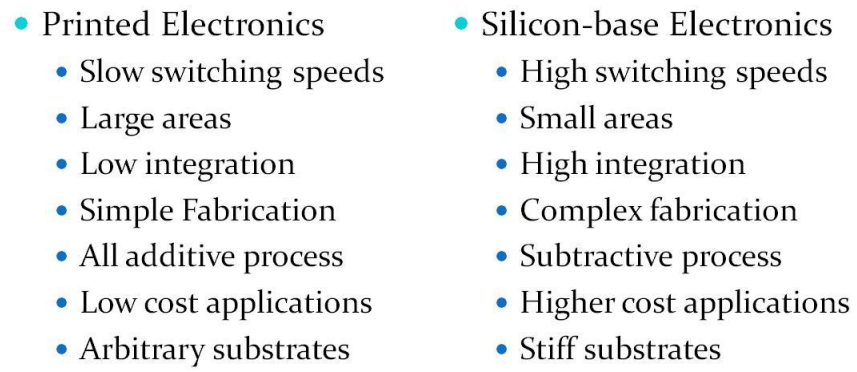

Figure 1-2: Comparison of Printed electronics paradigm with silicon-based electronics

1.2 Organic Semiconductors for Printed Electronics

It was the discovery of conduction in organic materials which allowed to printed electronics. This particular field can be credited to Alan J. Heeger, Alan G. MacDiarmid, and Hideki Shirakawa, who were jointly award the Nobel Prize in 2000 for their pioneering work in the field of organic electronics.

The work by Heeger et al. was published in 1977; however the study of conduction in organic materials dates before 1977. The fundamentals of quantum mechanism were well in place by the 50s. This lead to the understanding in the fundamentals of semiconductors physics was well as physical organic chemistry. There was a large amount of research in the understanding of wavefunctions in solids which lead to our current understanding of solid-state physics. At the same time, molecular orbital theory was developed by physical chemists which lead to our understanding of organic chemical reaction as well as organic crystals.

In the 50s and early 60s the presence of charge carriers were measured in iodine perylene complexes.[5] This lead to much research in conductivity in organic materials. In

the 60s much effort was placed in understanding organic crystals structure, such as benzene crystals.[6] The first conducting polymer, polypyrrole, was demonstrated in 1963.[7-9] This discovery was the forerunner to the 1977 paper showing conductivity in polyacetylene.[10] In 1974, the first organic semiconducting device was demonstrated; switching was demonstrated in a common biological molecule, melanin.[11] The carrier mobility in all these semiconducting materials was extremely low. Therefore, at that time organic semiconductors could not be realistically used for any useful applications. However, the research on polyacetylene caused a move to research conduction in conjugated organic polymers, resulting in materials such as polythiophenes in the 80s.[12]

In the 80s photoluminescence was discovered in organic materials. This led to the development to the organic LED (OLED), using materials such as phthalocyanines.[13,14] In 1997, the OLED was included into consumer applications, showing maturity in organic semiconductor research.

In the 90s work on organic TFTs led to an interest in small molecules, such as oligothiophenes and polyacenes. Small molecules show higher packing density and better ordering than polymeric systems. Higher packing density increases the mobility of the semiconductor. These systems have showed the potential to have mobility which rival the mobility of amorphous silicon.[15]

In recent years polymeric systems have once again gained traction with polythiophene based materials showing mobilities which are comparable that of small molecules.[16] Polymeric systems are highly attractive, because they are usually engineered to be soluble in common solvents. Due its tight packing, small molecules are generally insoluble in solvents. Printed electronics require molecules to be soluble;

therefore different schemes have been implemented in order to confer solubility to organic semiconductors.

1.2.1 Conferring Solubility to Organic Semiconductors

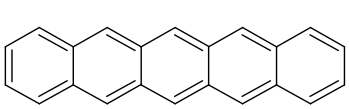

Pentacene

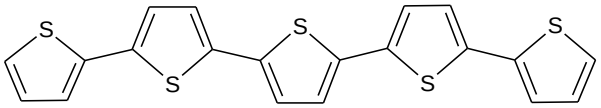

Oligothiophene

Prophyrin

Phthylocyanine

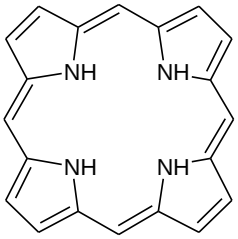

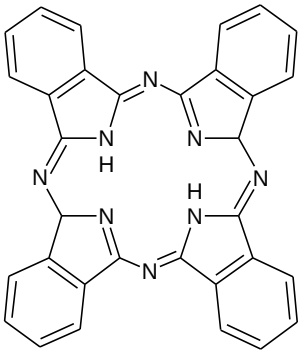

Figure 1-3: Different types of organic semiconductors

There are essentially three types of organic semiconductors: polyacenes, thiophene and porphyrins. All the different types of organic semiconductors are derivatives of these three materials. Polyacenes are chains of fused benzene rings together. Polythiophenes are a chain of thiophene rings. Porphyrins are a highly conjugated cyclic biological molecule. Certain iron containing porphyrins are called heme, which is what transports oxygen in blood. More typically used than prophyrin is its derivative phthylocyanine. Note the high level of conjugation in each semiconductor, which is what enables conduction in each material. Pentacene is one of the most

common and studied organic semiconductor because of its high mobility which is on par with the mobility of amorphous silicon.[15]

The high mobility organic semiconductors that have been commonly cited to have mobilities of over 1 cm^2/Vs[17] are usually small organic semiconducting molecules, which need to be deposited through thermal evaporation and high vacuum. Some of these small molecules are pentacene, oligothiophenes and single crystalline rubrene, which have been shown to have mobilities ranging from 1-15 cm^2/Vs.[17] These materials are insoluble in common solvents. It has been shown that some degree of solubility can be imparted to these materials when placed in heated solvents.[18] However, this is not conducive to spin coating, drop casting, inkjet printing or gravure printing, as the solvent needs to be maintained the high temperatures until after deposition.

The most common soluble organic semiconductors are polymeric systems, where the polymer chains have been functionalized with side-chains in order impart solubility. The trade-off is that the polymeric systems have much lower mobilities compared the thermally evaporated small molecules, usually less than 0.1 cm^2/Vs.[19] The mobility decrease is attributed to crystallinity and unordered packing as compared to small molecules. Small molecules readily form crystalline structures through a very tight herring-bone packing structure (figure 1.4). The tight packing of the small molecules allows for a high degree of p-orbital overlapping between molecules, which increases the mobility of the material. It is unfortunately for this reason, which also causes these organic semiconductors to be insoluble in common solvents. It would be desirable to impart solubility to small organic semiconducting molecules and maintain its tight

packing even after deposition. There have been many schemes to impart solubility to these small molecules.

Figure 1-4: The tradition herring-bone structure of pentacene. Each line represents a top down view of a single small organic semiconducting molecule.

1.2.1.1 Oligothiophenes Precursors

Different schemes have been implemented to improve the performance of the oligothiophenes. There are schemes, which attempt to increase oxygen stability of the semiconductor. Other schemes seek to the increase ordering of the molecules, thereby increasing mobility. Of courses there are also schemes to allow oligothiophenes to become dissolvable in common organic solvents for the possibility of solution processing

Oligothiophenes have been shown to have mobilities of 1.0 cm^2/Vs,[20] which is lower than pentacene and rubrene, however oligothiophenes chemistry allows for highly flexible addition of side chains, which may be favorable for tuning of solubility of oligothiophenes. Figure 1.5 shows a molecule made by the Fréchet group,[20-22] which functionalizes polythiophenes by the addition of active ester groups on to the ends of the oligothiophene. The ester groups with long chain alkanes impart solubility to the oligothiophene groups, but through a thermolysis reaction, is removed and only the

oligothiophene is left.

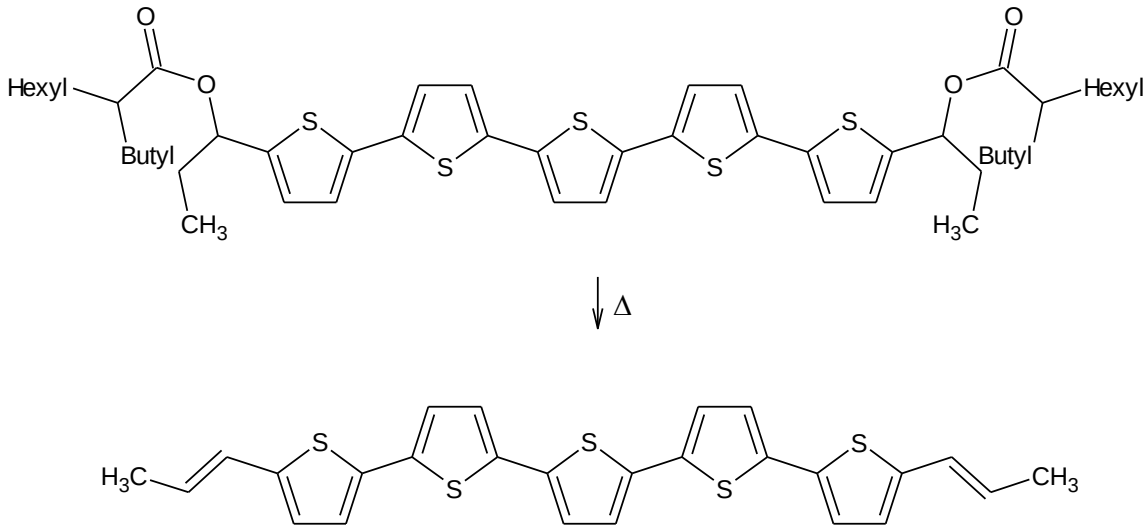

Figure 1-5: Oligothiophenes have been modified with specific side chains to make them soluble in organic solvents. The side chain can be removed with heat after deposition.

1.2.1.2 Soluble Pentacene

Since pentacene has shown high air stability, creation of a soluble pentacene has always been highly desirable. Significant work has been focused on pentacene chemistry in order to impart solubility to pentacene. Anthony's group has have success in adding a bulky side chain on to the middle ring of pentacene, which first serves to impart solubility to pentacene (figure 1.6),[23] it also changes the packing of molecule to go from the traditional herring-bone structure to move to a face-to-face packing (figure 1.7). Using this scheme, Anthony's group has been able to achieve up to 1.0 cm^2/Vs mobilites. These are some of the highest reported mobilities for small organic semiconducting molecules. This type of molecule unfortunately does not allow for multilayer solution processing on top of the semiconductor, since the semiconductor can be dissolved if another layer is printed on top of the existing semiconductor.

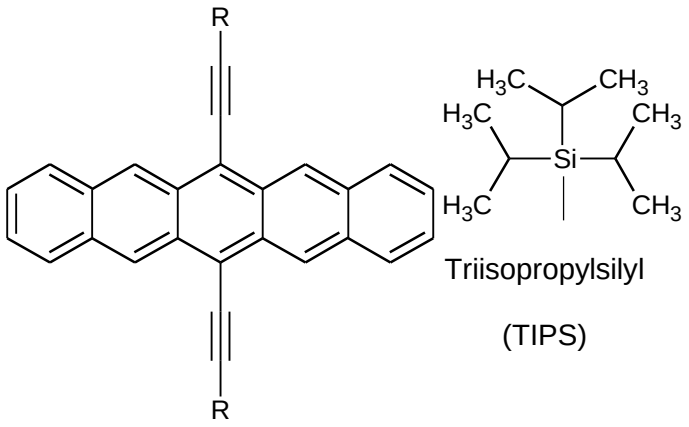

Figure 1-6: Pentacene with TIPS side groups to allow for solubility and increased ordering upon deposition

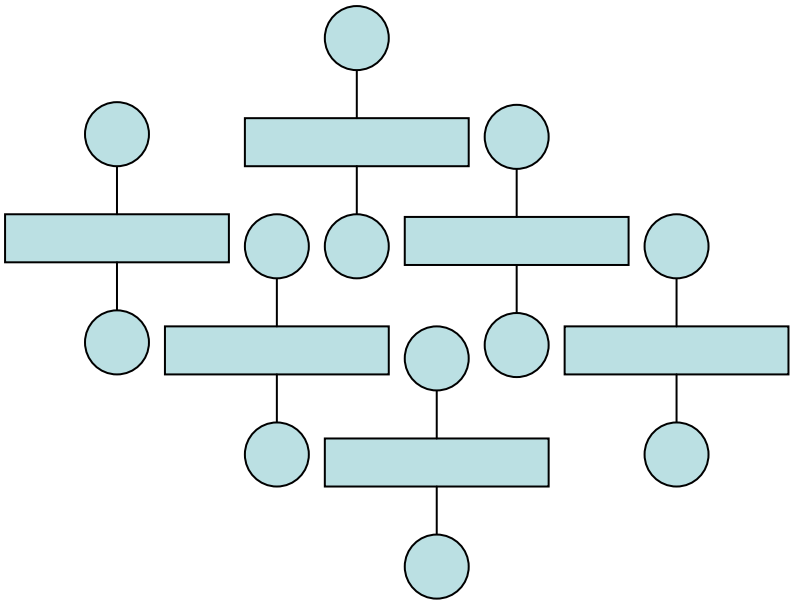

Figure 1-7: The packing of TIPS pentacene is no longer a traditional herring-bone packing, but instead face to face packing.

1.2.1.3 Soluble Pentacene Precursors

Another way to impart to impart solubility to pentacene is to create a pentacene precursor, similar in concept to the oligothiophene precursor. The basic concept of the

precursor is to disrupt the conjugation within the pentacene by adding bulky groups to the center ring of the pentacene. The bulky group breaks up conjugation within the pentacene molecules, as well as disturbs p-orbital overlapping between molecules and confers solubility through the bulky side chains. The first attempt at a pentacene precursor, chemists added a chlorinated ring structure into the center ring of pentacene ring (figure 1.8).[24]

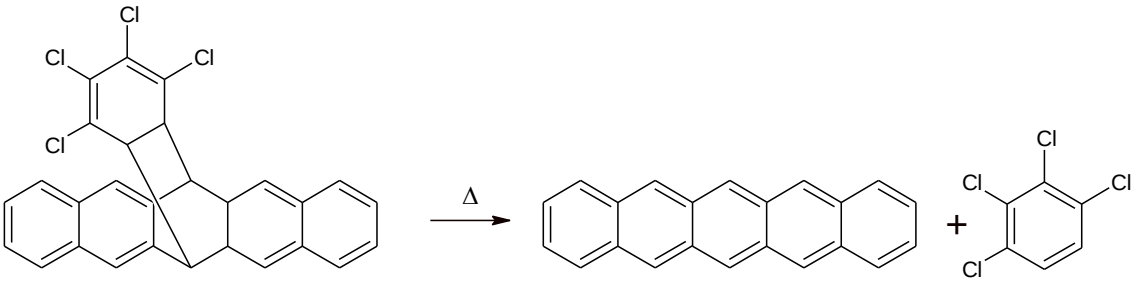

Figure 1-8: The first soluble pentacene precursors

A more successful attempt was down by Afzali et al. from IBM, which added an N-Sulfinylacetamide to the center ring through a Diels-Alder reaction (figure 1.9, 1.10).[25] Mobilities were reported up to 0.8 cm^2/Vs. The success of the pentacene precursor is that after deposition pentacene is converted back to its original form and then is unaffected by its bulky side chains, the original properties of pentacene is preserved. There have been many other precursors which have followed this scheme.[26-29]

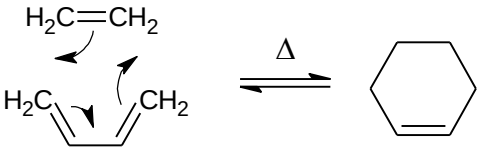

Figure 1-9: The concerted Diels-Alder reaction

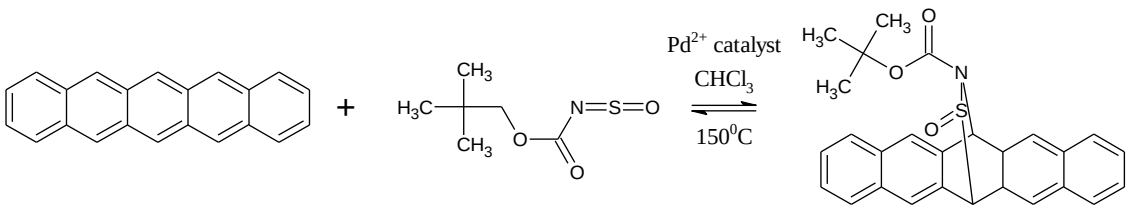

Figure 1-10: The Diels-Alder reaction making pentacene soluble in organic solvents

The pentacene precursor from IBM (13,6-N-Sulfinylacetamidopentacene or SAP) has been successfully used for fully printed organic TFT,[30] showing mobilities in the 0.1cm^2/Vs range. Beyond using this material for use into a printed TFT, little else has been studied regarding this material. This thesis will deal with the thin film formation of pentacene from the degradation of SAP.

1.3 Inorganic Nanoparticles

Up until this point only organic materials have been mentioned. However, it would be incomplete to not at least briefly mention that there is also research being done with inorganic materials to be used in printed electronics, mainly with synthesis of inorganic nanoparticles.

The usage of inorganic materials is promising and should not be neglected because the mobilities reported from inorganic materials TFTs are much higher than what is has been seen with organic materials. Contrary to organic materials which have been reported to be predominately p-type, n-type inorganic materials have been demonstrated.

. The reason for using nanoparticulate materials is for solubility. Inorganic semiconducting crystals do not dissolve in common solvents. However, nanoparticles can be encapsulated with functional groups which would allow for them to be dissolved

in common solvents. Or additives can be added into solution in order stabilize nanoparticles in order to form colloidal suspensions of the nanoparticles.

A second property of nanoparticles is the low melting or sintering temperature of particles. Elemental nanoparticles have been found to have depressed melting temperatures which are far below the bulk melting temperature, making incorporation of these semiconductors on to plastics possible. By using a soluble semiconductor nanoparticles, these nanoparticles can first be deposited through printing. The deposited film probably would have low carrier mobility because of the small crystal size of deposited film. However the film can then be heated in order to sinter nanoparticles. After sintering of nanoparticles, the final crystal sizes of the semiconductors would grow large enough to allow for decent conduction.

Early usage of nanoparticle semiconductors for printed electronics was done by MIT media labs, where CdSe and CdTe were printed onto a substrate gated structure.[31] Mobilities were reported to be approximately 1 cm^2/Vs. A more recent used thiol encapsulated ZnO and gave mobilites of 0.2 cm^2/Vs.[32] The use of ZnO was promising, because first ZnO is a n-type material, which potentially can be coupled with p-type organic materials to form CMOS. Also ZnO is transparent, which allows for ZnO to be potentially incorporated into a display.

1.4 Organic Thin film Transistors

The TFT structure is the typical choice to creating organic transistors. Organic semiconductors cannot easily be made into a mechanically stable substrate which transistors can be built upon, as in silicon. Instead, transistors are built on top a mechanically stable substrate such as glass or plastic and the organic semiconductor is

deposited and processed along with the other materials in the fabrication process. There are different types of configurations which the OTFT can take, namely the bottom-gate top contact OTFT, the bottom-gate bottom contact OTFT, the top-gate OTFT, substrate gated bottom contact OTFT or substrate gated top contact OTFT.

As can be seen in figure 1.11, the top-gate OTFT is the most difficult to make. The top gate OTFT requires a dielectric and metal gate to be processed on top of the semiconductor. The organic semiconducting material is usually the most sensitive material in an OTFT process, so it is always easier to deposit the organic semiconductor last instead of first. For semiconductor material testing, the substrate-gated bottom contact OTFT is the easiest to make and the most useful for testing. The whole OTFT structure minus the semiconductor can be mass produced and stored before testing. Then these substrates can then be used at a later time with a variety of different semiconductors, which only needs to be deposited on top of the substrate to complete the OTFT. One substrate can contain many devices with different W/L for testing, making testing quick and the process highly repeatable. For the sake manufacturing simplicity and testing, all OTFTs used in these studies were substrate gated bottom contact OTFTs.

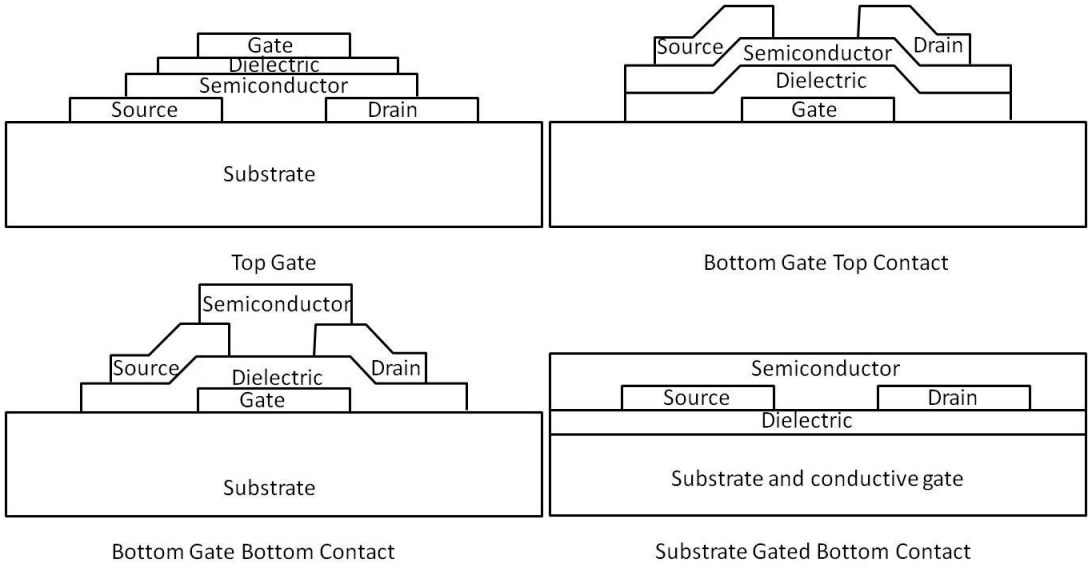

Figure 1-11: Different OTFT configurations

1.4.1 Operation of OTFTs

Due to the presence of traps caused by disorder in organic semiconductors it is difficult for organic semiconductors to become depleted. Therefore, OTFTs are run in accumulation mode. A negative bias is placed on the gate electrode. The negative bias attracts positive carriers of the, generally p-type, semiconductor to form on the semiconductor to dielectric interface creating a channel between the source and drain electrode, allowing conduction to occur between the source and the drain (figure 1.11).

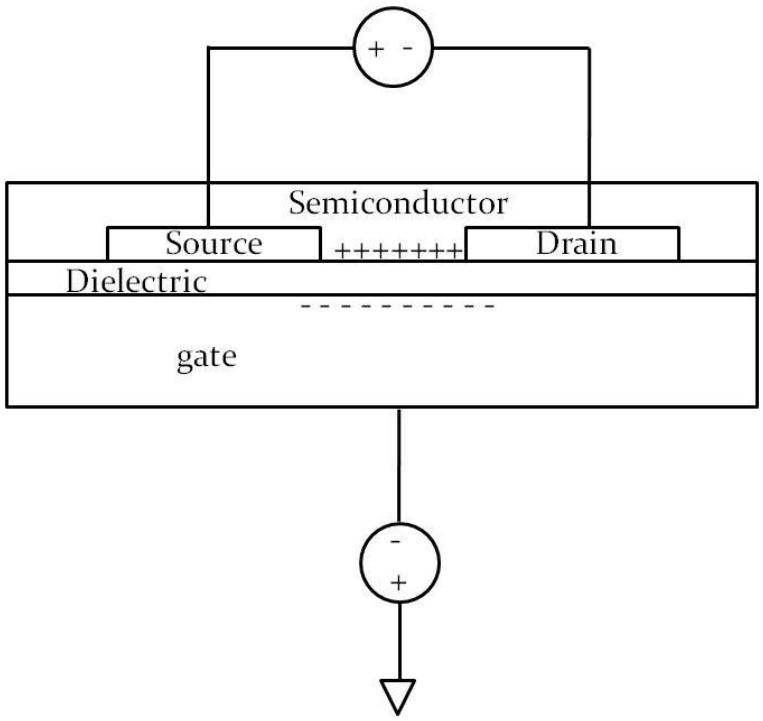

Figure 1-12: Operation of a p-OTFT

If stronger negative bias is placed on the gate electrode more holes are gathered to the dielectric/semiconductor interface allowing for more conduction. Figure 1.12 shows the I-V characteristics of a typical OTFT. The shape generally looks similar to what is seen in a typical single crystalline silicon MOSFET. Hence, the square-law (equation 1.1) which describes typical silicon MOSFETs is also used to describe an OTFT.

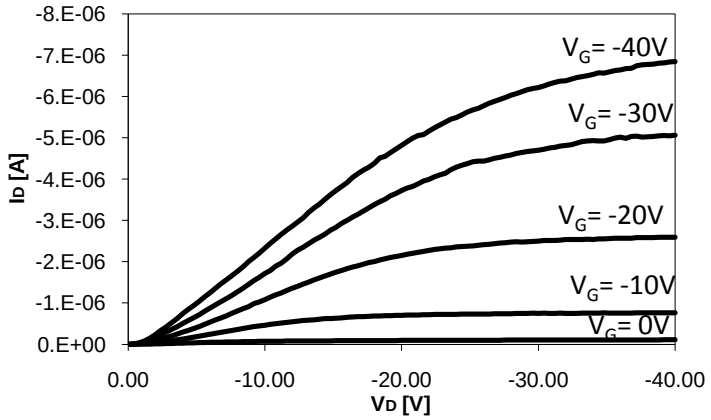

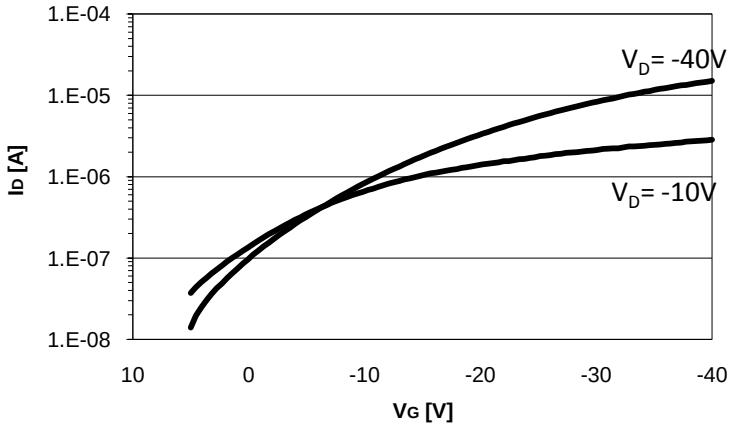

Figure 1-13: IV Characteristics of a typical OTFT. (top) Output characteristics and (bottom) transfer characteristics of a pentacene OTFT with1000Å of oxide (W/L = 125µm/15 µm).

$$I_{DS} = \frac{W}{L}\mu C_{OX}(V_{GS} - V_T - \frac{V_{DS}}{2})V_{DS}$$

$$I_{DS} = \frac{W}{2L}\mu C_{OX}(V_{GS} - V_T)^2$$

Equation 1-1: Square-law equations for triode (top) and saturation (bottom).

1.4.2 Transport in OTFTs

Even though OTFTs apparently functions in the same manner as a bulk silicon MOSFET, however, this is only a model. Carrier transport in an organic semiconductor is quite different than in single crystalline silicon. Organic semiconductors are generally polycrystalline or amorphous, these highly disordered systems have many implications which are not found in single crystalline silicon. In the next sections, the origin of conduction inorganic semiconductors is describe and the effects of disorder on conduction is discussed.

1.4.2.1 Conduction in organic materials

Conduction occurs in metals because of metallic bonding because there is a "sea" of delocalized electrons. These delocalized electrons are not strongly bound to any particular atom, hence can moved around allowing for conduction. Metallic bonding is usually contrasted with covalent bonding where electrons forming the bonds are spatially fixed and are not capable of long range movements.

In inorganic semiconductors, taking silicon as an example, silicon atoms interact with each other through covalent bonding. Specifically the bonding is σ bonding of sp^3 hybridized orbital. Conduction in silicon is also difficult, however by the usage of dopants, conduction can be increased. Dopants, are merely impurities which when added into the semiconductor is able to introduce weakly bound electrons and hence are delocalized in the silicon crystal lattice. With dopants, conduction is made easier, because just like in the case of the metallic bond, there is now a sea of delocalized electron in which conduction can take place.

In order for conduction to occur in organic materials, there needs to be delocalized electrons in the organic material. This can be done within a single molecule through π bonds and conjugations. When a carbon atom is sp^2 hybridized, the three sp^2 orbitals form directional σ bonds with neighboring atoms. The remaining p-orbital, usually form a π-bond with a neighboring p-orbital. When two carbons interact through a σ-bond and a π-bond bond, this called a double bond. Whereas the electrons involved in the σ-bond are fixed in location, the π-bond electrons are able to interact with neighboring π-bonds. Therefore, if a molecule has a chain of interacting π-bonds, then, within that molecule, the electrons in the π-bonds are delocalized; this is called conjugations. Conjugation allows for electrons to move beyond its π-bond and move a longer distance, conjugation also gives added stability to the molecules through resonance.

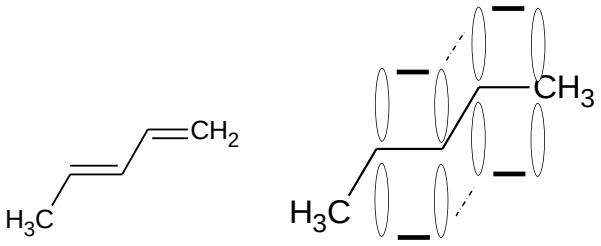

Figure 1-14: The left shows a simple alkadiene in its usually line representation. On the right the same molecule is shown with the π-bond specifically drawn showing the interaction of the p-orbitals

Now for transport of electrons between organic molecules occurs by π-bond overlapping between molecules. In an organic crystal, molecules are held together by van der Waals forces, or more specifically, London dispersion forces.[33] These interactions are relatively weak and therefore distances between molecules are relatively

large. Lattice spacing is much large for organic crystals and bandgaps in organic semiconductors are also relatively large. Conduction in organic molecules is thereby much lower than in inorganic semiconductors. If, the intermolecular distances can be forced together more closely, bandgaps can be reduced, carriers can travel from molecule to molecule easier and conduction can also be increased.

The origin of bandgaps in organic materials comes from the interactions of HOMO/LUMO levels of each individual molecule.[34] The HOMO (highest occupied molecular orbital) is usually analogous to the valence band in inorganic semiconductors. The LUMO (lowest unoccupied molecular orbital) is analogous to the conduction band of inorganic semiconductors. The energy difference between the HOMO/LUMO levels is the definition of the band gap for an organic semiconductor. When multiple HOMO/LUMO levels interact, a continuum is formed becoming the energy bands for organic semiconductors.

1.4.2.2 Multiple Trap and Release (MTR)

A defining feature of organic crystals is the lack of covalent bonds between organic molecules. In inorganic systems the crystal is held together tightly with covalent bonds, keeping lattice points close together and keeping crystals relatively well order, all resulting in high mobility. Organic crystals are held together with van der Waals forces, keeping molecules far apart and crystals are highly susceptible to crystal defects. Organic crystals are generally polycrystalline; crystal boundaries also imperfections and are considered defects.

These crystal defects lead to localized energy perturbation and form traps states. These traps greatly effect the ability for carriers to travel through the semiconductor film.

Two effects of these trapped states is, thermally activated transport and field dependent mobility.

There are many models which try to describe the effect of traps on the TFT mobility in semiconductors. One prevalent model is the multiple trap and release model (MTR). MTR was first used to describe transport in hydrogenated amorphous silicon TFTs[35] and now it has been adapted to describe OTFTs.

The following discussion of MTR is taken from Merlo et al.[36] In MTR the traps originating from both grain boundaries as well as internal crystalline defects are assumed to be distribution of trap states is to assume that the states both from grain boundaries and internal crystal defects are uniformly distributed throughout the semiconductor film. The trap states are assumed to be in an exponential distribution of states in the band gap.

Most carriers are trapped in the exponential trap states. When carriers are trapped they have no mobility and thereby are unable to move. When carriers are freed from the traps, these free carriers are then able to move around. In short, carriers generally are trapped in shallow traps and through thermal perturbation carriers may be release, but then trapped again by another trap, hence the name multiple trap and release.

MTR states that the effective mobility (μ_{eff}) is related to the free carrier mobility (μ_0) and the ratio of free holes (N_V) and total induced holes ($N_V + N_T$) by by the following relationships shown in equation 1.2.

$$\mu_{eff} = \mu_0 \frac{N_V}{N_V + N_T} = \frac{\mu_0}{1 + \frac{N_V}{N_T}}$$

$$N_V = N_{V0} \exp\left(\frac{E_F - E_V}{k_B T} \right)$$

$$N_T = N_{T0} \exp\left(\frac{E_T - E_F}{k_B T} \right)$$

$$\mu_{eff} = \mu_0 \frac{1}{1 + \frac{N_{T0}}{N_{V0}} \exp\left(\frac{E_F - E_V}{k_B T} \right)} \approx \mu_0 \exp\left(\frac{-E_A}{k_B T} \right)$$

Equation 1-2: MTR equations

Here N_V is the aerial density of free holes and N_T is the aerial density of trapped holes. N_{V0} and N_{T0} are the effective density of free and trapped states respectively, k_B is the Boltzmann constant, E_f is the Fermi level and E_v is the valence band edge. The results show that the effective mobility can be approximated with an Arrhenius relationship with an activation energy E_A. The activation energy is the energy necessary to release trapped carriers. Of course the trap depth is not a discrete value, but instead an exponential distribution.

From the Arrhenius equation it is very clear that the mobility is thermally activated. As temperature is increased more carriers are "activated" increasing the effective mobility, which increases the current of a TFT. A physical explanation states that as temperature is increased, the trapped carrier gain enough energy to leave traps to become free. This causes the ratio of free to trapped carrier increases, so the effective mobility also increases.

The less apparent effect which can be seen in the MTR equation is electric field induced mobility. As gate electric field is increased, the activation energy is also

decreased. The activation energy is the difference between the Fermi level and the valence band edge. Increasing the gate electric field moves the Fermi level closer to the valence band edge, effectively decreasing activation energy. Physically, moving the Fermi level is equivalent to filling traps making the exponential trap distribution more shallow, which allows carriers to be freed more easily.

Both these effects have been observed experimentally. As a result the extraction of mobility from OTFTs is extremely difficult. The extraction of mobility will be covered in more detail in the next chapter.

1.5 Organization

This thesis deals with the processing of the IBM pentacene precursor in order for use in printed electronics. Even though it has already been used an tested as printable materials with relatively high performance, however the mechanism of thin film formation is unknown. The rest of this thesis describes experiments which deduce the film formation mechanism of the IBM precursor.

Chapter 2 goes through the details of manufacturing and testing a pentacene transistor. All the fabrication steps are specifically for a substrate gated TFT. Testing details are given for electrically probing the TFT and extracting the mobility and on/off ratio. Then details are given for using AFM, SEM and GIXD in order to test the semiconducting material. The descriptions of AFM, SEM and GIXD are given specifically for the measurements to be used throughout this thesis.

Chapter 3 begins looking at the chemistry of the pentacene precursor with UV-vis. The reaction rate and activation energy is extracted, and simple conclusions are

drawn about the solid-state degradation reaction. This knowledge allows for further study of pentacene thin film growth.

While chapter 3 only looks at the reaction rate of the pentacene precursor forming a thin film, chapter 4 looks into the details of the solid-state reaction of the precursor transforming into pentacene with amorphous SiO_2 as the substrate. Oxide will not be used as a material in printed electronics, however it still the most common material used for TFT testing. The growth of pentacene through evaporation on oxide is well studied, therefore serves as a model for the growth of pentacene through a precursor. The purpose of this chapter is to understand how this material converts from the precursor form into a thin film of pentacene. This knowledge aids in the understanding of tuning the pentacene precursor for usage in transistors. The reaction is traced using SEM, AFM and GIXD. Specifically, temperature dependence of nucleation density, mechanism of crystal growth, surface topology and crystal size are described.

Chapter 5 goes on to look at pentacene films formation on five different substrates. These substrates are all materials which are useful in organic semiconductor. This chapter is similar to chapter 4, however moves away from oxide as the substrate to grow pentacene. Understanding how pentacene grows on these other substrates is imperative for printed electronics. The growth of pentacene thin films on each substrate is compared and contrasted with each other. This also gives further insight on the growth of thin-films through a precursor system.

Chapter 6, the pentacene precursor is subject to different heat-treatments in order to improve TFT performance. To date, the processing of precursor systems has been limited to only one temperature. This chapter explores the processing of the pentacene

precursor using two temperature heating steps. Two temperature processing promises to create higher performance TFTs than single TFTs processed at a single temperature. The microstructure of the pentacene thin films made using two temperature processing is compared with thin films made with the traditional one step processing. TFTs fabricated with this method are also compare with TFTs fabricated using the tradition processing. This chapter shows that using different heat-treatments can tune the performance of a semiconductor formed from a precursor system.

Finally, chapter 7 summarizes the results in this thesis and give suggestions for future work.

1.6 References

1. Lovinger, A. & Rothberg, L. Electrically active organic and polymeric materials for thin-film-transistor technologies. *JOURNAL OF MATERIALS RESEARCH* **11**, 1581-1592(1996).
2. Liao, F., Chen, C. & Subramanian, V. Organic TFTs as gas sensors for electronic nose applications. *SENSORS AND ACTUATORS B-CHEMICAL* **107**, 849-855(2005).
3. Steudel, S. et al. Comparison of organic diode structures regarding high-frequency rectification behavior in radio-frequency identification tags. *JOURNAL OF APPLIED PHYSICS* **99**, (2006).
4. Lee, J. & Subramanian, V. Weave patterned organic transistors on fiber for e-textiles. *IEEE TRANSACTIONS ON ELECTRON DEVICES* **52**, 269-275(2005).
5. Read, S.F.J. Dynamic Nuclear Polarization in a Perylene---Iodine Complex. *J. Chem. Phys.* **36**, 3098-3099(1962).
6. Shoda, T. et al. Molecular packing analysis of benzene crystals. Part 2. Prediction of experimental crystal structure polymorphs at low and high pressure. *Journal of Molecular Structure: THEOCHEM* **333**, 267-274(1995).
7. McNeill, R. et al. Electronic Conduction in Polymers. I. The Chemical Structure of Polypyrrole. *Australian Journal of Chemistry* **16**, 1056-1075(1963).
8. Bolto, B. & Weiss, D. Electronic Conduction in Polymers. II. The Electrochemical Reduction of Polypyrrole at Controlled Potential. *Australian Journal of Chemistry* **16**, 1076-1089(1963).

9. Bolto, B., McNeill, R. & Weiss, D. Electronic Conduction in Polymers. III. Electronic Properties of Polypyrrole. *Australian Journal of Chemistry* **16**, 1090-1103(1963).
10. Shirakawa, H. et al. Synthesis of electrically conducting organic polymers: halogen derivatives of polyacetylene, (CH)x. *J. Chem. Soc., Chem. Commun.* 578-580(1977).
11. McGinness, J., Corry, P. & Proctor, P. Amorphous semiconductor switching in melanins. *Science* **183**, 853-5(1974).
12. Tsumura, A., Koezuka, H. & Ando, T. Macromolecular electronic device: Field-effect transistor with a polythiophene thin film. *Appl. Phys. Lett.* **49**, 1210-1212(1986).
13. Blochwitz, J. et al. Low voltage organic light emitting diodes featuring doped phthalocyanine as hole transport material. *Appl. Phys. Lett.* **73**, 729-731(1998).
14. Tang, C.W. & VanSlyke, S.A. Organic electroluminescent diodes. *Appl. Phys. Lett.* **51**, 913-915(1987).
15. Lin, Y. et al. Stacked pentacene layer organic thin-film transistors with improved characteristics. *Electron Device Letters, IEEE* **18**, 606-608(1997).
16. Kline, R.J. et al. Significant dependence of morphology and charge carrier mobility on substrate surface chemistry in high performance polythiophene semiconductor films. *Appl. Phys. Lett.* **90**, 062117-3(2007).
17. Kelley, T.W. et al. Recent Progress in Organic Electronics: Materials, Devices, and Processes. *Chemistry of Materials* **16**, 4413-4422(2004).
18. Tao, C. et al. Solution processed pentacene thin films and their structural properties. *Materials Science and Engineering: B* **140**, 1-4(2007).

19. Chang, J. et al. Enhanced Mobility of Poly(3-hexylthiophene) Transistors by Spin-Coating from High-Boiling-Point Solvents. *Chemistry of Materials* **16**, 4772-4776(2004).
20. Murphy, A.R. et al. Organic Thin Film Transistors from a Soluble Oligothiophene Derivative Containing Thermally Removable Solubilizing Groups. *Journal of the American Chemical Society* **126**, 1596-1597(2004).
21. Murphy, A.R. et al. Self-Assembly, Molecular Ordering, and Charge Mobility in Solution-Processed Ultrathin Oligothiophene Films. *Chemistry of Materials* **17**, 6033-6041(2005).
22. Chang, P.C. et al. Film Morphology and Thin Film Transistor Performance of Solution-Processed Oligothiophenes. *Chemistry of Materials* **16**, 4783-4789(2004).
23. Sheraw, C. et al. Functionalized Pentacene Active Layer Organic Thin-Film Transistors. *Advanced Materials* **15**, 2009-2011(2003).
24. Brown, A.R. et al. Precursor route pentacene metal-insulator-semiconductor field-effect transistors. *J. Appl. Phys.* **79**, 2136-2138(1996).
25. Afzali, A., Dimitrakopoulos, C. & Breen, T. High-performance, solution-processed organic thin film transistors from a novel pentacene precursor. *JOURNAL OF THE AMERICAN CHEMICAL SOCIETY* **124**, 8812-8813(2002).
26. Weidkamp, K.P. et al. A Photopatternable Pentacene Precursor for Use in Organic Thin-Film Transistors. *Journal of the American Chemical Society* **126**, 12740-12741(2004).

27. Afzali, A., Dimitrakopoulos, C. & Graham, T. Photosensitive pentacene precursor: Synthesis, photothermal patterning, and application in thin-film transistors. *ADVANCED MATERIALS* **15**, 2066-+(2003).
28. Afzali, A., Kagan, C. & Traub, G. N-sulfinylcarbamate-pentacene adduct: A novel pentacene precursor soluble in alcohols. *Synthetic Metals* **155**, 490-494(2005).
29. Okamoto, K. et al. Synthesis and thermolysis of Diels-Alder adducts of 2,9-dialkylpentacenes with diethyl azodicarboxylate. *Journal of Physical Organic Chemistry* **21**, 257-262(2008).
30. Molesa, S. et al. A high-performance all-inkjetted organic transistor technology. *Electron Devices Meeting, 2004. IEDM Technical Digest. IEEE International* 1072-1074(2004).doi:10.1109/IEDM.2004.1419384
31. Ridley, B.A., Nivi, B. & Jacobson, J.M. All-Inorganic Field Effect Transistors Fabricated by Printing. *Science* **286**, 746-749(1999).
32. Volkman, S. et al. A novel transparent air-stable printable n-type semiconductor technology using ZnO nanoparticles. *Electron Devices Meeting, 2004. IEDM Technical Digest. IEEE International* 769-772(2004).
33. Li, L., Meller, G. & Kosina, H. Carrier concentration dependence of the mobility in organic semiconductors. *Synthetic Metals* **157**, 243-246(2007).
34. Elandaloussi, E.H. et al. Effect of Chain Extension on the Electrochemical and Electronic Properties of π-Conjugated Soluble Thienylenevinylene Oligomers. *Journal of the American Chemical Society* **119**, 10774-10784(1997).
35. Schiff, E.A. Trap-controlled dispersive transport and exponential band tails in amorphous silicon. *Phys. Rev. B* **24**, 6189(1981).

36. Merlo, J.A. & Frisbie, C.D. Field Effect Transport and Trapping in Regioregular Polythiophene Nanofibers. *The Journal of Physical Chemistry B* **108**, 19169-19179(2004).

2 Experimental Methods and Characterization Techniques

Since this thesis is primarily concerned with solution processed pentacene for organic TFTs, this chapter shows all the steps used in fabricating and characterizing an OTFT. The first part of the chapter deals with the fabrication and the choice of fabrication steps to make the standard OTFT that will be used in this thesis. Then, all of the different characterization techniques which will be used in this thesis will also be described and explained. The characterization techniques used are, extraction of mobility from OTFT IV curves, SEM for monitoring semiconductor thin-film formation, AFM for looking at semiconductor thin-film topology and GIXD for deducing crystal structure of thin-films. Finally, a section will be given to UV-vis and analyzing UV-vis data.

2.1 OTFT Fabrication and Testing

2.1.1 OTFT Fabrication

OTFT substrates were 4" heavily doped n-type wafers. The gate oxide was grown by wet oxidation at 900^0C and grown to a thickness of 1000Å. The substrate gated OTFT structure is merely a test structure to test semiconducting materials. The thickness of the gate oxide was chosen to mimic the vertical electrical fields which may be used in a fully printed device.

The oxidized wafers are then heated to 120^0C to drive off any water vapor on the oxide, and then placed in HMDS vapor. The HMDS vapor forms a monolayer of HMDS onto the oxide surface which would promote adhesion of photoresist to the oxide surface.

After the deposition of HMDS, positive photoresist is spun on using the standard UC Berkeley microlab process, along with a soft bake of the photoresist. The wafer is patterned through a stepper, which patterns 64 identical dies onto the wafer. Each die contains patterns for OTFT source drain pads defining various W/L ratios. The patterned wafers are developed using the standard process and then hard baked.

Finally, the source/drain pads made by thermally evaporated gold with a chrome adhesion layer. Evaporation was done at a base pressure of approximately 5×10^{-7} torr. The thicknesses of the two metal layers are 500Å of gold and 15Å of chrome, with a rate of 5Å/s and 1Å/s respectively. Lastly the source/drain pads are finally formed by lift off. This is done by placing the wafer into acetone, where all the photoresist and excess gold is removed. The only gold left are the gold which was deposited onto the oxide from the patterned photoresist. Figure 2.1 and figure 2.2 describe the full process.

- Grow 1000Å of wet oxide at 900^0C
- Bake dry wafer for 20 minutes at 120^0C
- Deposited a monolayer of HMDS by placing wafer in HMDS vapor for 20 minutes.
- Spin on photoresist + soft bake
- Pattern photoresist with stepper
- Develop photoresist + Hard bake photoresist
- Evaporate 15Å Cr + 500Å of Au
- Lift off photoresist with acetone

Figure 2-1: Substrate-gated TFT process

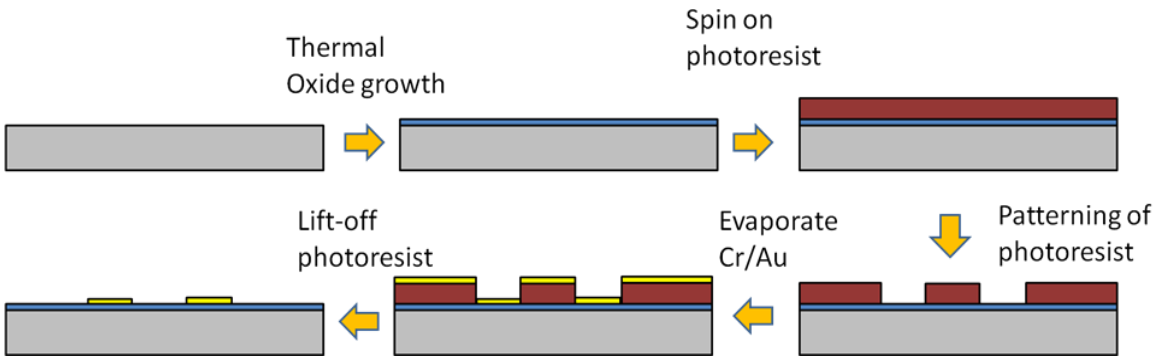

Figure 2-2: Cross-section view of the substrate-gated OTFT process

Because these wafers are many times made in advanced much before semiconducting material will be deposited, there is fear that the wafers may have collected contaminants. Therefore before depositing semiconducting materials, the wafer is cleaned using step 1 of an RCA clean. Step 1 of the RCA clean is a wafer soaks in H_20:NH_4OH:H_2O_2, 5:1:1. This removes all organic contaminants that may have accumulated from the liftoff process and storage. Once again, the wafer is baked dry and

HMDS is redeposited. This time HMDS is applied to help the ordering of organic semiconductors which will be grown on the oxide surface. The reapplication of HMDS is to ensure that HMDS has not been removed by the processing steps between the first HMDS application and the deposition of organic semiconductors. Generally, if it is desired to remove HMDS from oxide surfaces, oxide wafers are placed in oxygen plasma. Even though wafers have not been subjected to plasma treatments, the application of HMDS is simple enough that this extra step was added to ensure that HMDS is still on the oxide surface. At this point semiconducting material can now be deposited through spin, inkjet printing or evaporation, on top of the processed wafer to form a completed TFT.

2.1.2 Electrical testing of OTFT

Electrical testing was done using by probing with a Rucker & Koll probe station under an inert nitrogen ambient in conjunction with an Agilent 4156C parametric analyzer. The gate contact was made by using the probe station chuck contacting the heavily doped substrate. Contacting the source and drain was done by scratching through the semiconducting material as shown in figure 2.3.

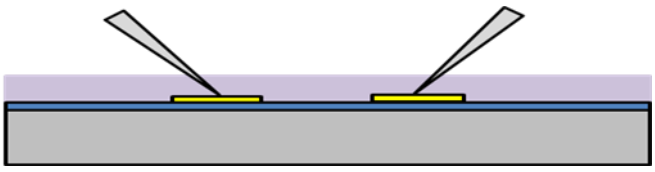

Figure 2-3: Contacting source/drain pads on TFTs

In order to reduce gate leakage, each devices was isolated from the others by scratching the semiconducting material around each device. The standard testing

conditions swept V_{ds} from 10V to -40V and step V_{gs} to -40V. All testing was done under nitrogen ambient.

2.1.3 Mobility extraction

One of the most important benchmarks of an OTFT performance is mobility. This however is also one of the most problematic parameters to extract. The IV characteristic of an OTFT visually looks similar to that of a traditional MOS, therefore the square-law is used to model electrical behavior of the OTFT.

The square law however, fails to model the nonidealities which are significant in OTFT. Issues of at the contacts such as, contact resistance, Schottky barriers, carrier injection are not modeled into the square law. Other issues which are unique to OTFT, such as gate-bias dependent mobility,[1-3] thermally activated transport[1] and ill-defined turn on characteristics[4,5] cannot be addressed using standard MOS equations.

$$I_{DS} = \frac{W}{L}\mu C_{OX}(V_{GS} - V_T - \frac{V_{DS}}{2})V_{DS}$$
$$I_{DS} = \frac{W}{2L}\mu C_{OX}(V_{GS} - V_T)^2$$

Equation 2-1: Square-law equations for triode (top) and saturation (bottom).

Judging from all the aforementioned problems finding the mobility of an OTFT is problematic. Using the standard square-law approach, all the contact effects would be convoluted in the mobility extraction. Even if the contact effects can be removed, knowledge of the threshold voltage is necessary before mobility can be properly extracted.

In OTFTs the threshold voltage is ill-defined, because turn on is gradual. The semiconductor changes from nonconducting to conducting as carriers accumulate and

traps are filled by increasing the electric field over the gate. As more traps are filled, more carriers are available for conduction. Due to this gradual turning of OTFTs, it is difficult to define a specific threshold voltage on OTFTs.

Equation 2.2 and 2.3 shows a way to extract mobility using the slope of the transfer curve and eliminates V_T dependency and assumes no gate voltage dependency.

$$g_m = \frac{\partial I_{DS}}{\partial V_{GS}} = \frac{W}{L}\mu C_{OX}(V_{GS} - V_T)$$

$$g_m = \sqrt{2\frac{W}{L}\mu C_{OX} I_{DS}}$$

$$\mu = \frac{g_m^{\,2}}{2\frac{W}{L}C_{ox} I_{DS}}$$

Equation 2-2: Mobility in saturation

$$g_m = \frac{\partial I_{DS}}{\partial V_{GS}} = \frac{W}{L}\mu C_{OX} V_{DS}$$

$$\mu = \frac{g_m}{\frac{W}{L}C_{ox} V_{DS}}$$

Equation 2-3: Mobility in triode

In this equation, the mobility is extracted from the g_m of the transistor. Due to the slow turning of the transistor, the number carriers for conduction as well as the mobility is clearly gate voltage dependent.[6-11] As a stronger field is place on the gate (more negative voltage), the mobility of holes increase. At extremely high voltages, the mobility has been shown to start decreasing.[3] In practice most of these effects are neglected and, only the highest saturation mobility is reported.[12]

2.2 Scanning Electron Microscopy (SEM)

Scanning electron microscopy was invented in the 1930s.[13] Scanning electron microscopy is one type of electron microscopy where an electron beam scanned across the surface of the sample in a raster scan pattern. The incident bean interacts with the sample and knocks off electrons from the sample and collected by the detector to form the image. Due to the electron interaction with the atoms, information can be extracted about composition, topology and electrical conduction. SEM allow for many high magnification images to be visualized quickly.

In this thesis, visualization of semiconducting films was predominantly done using SEM due to the simplicity and speed of this technique. The LEO 1550 was the SEM used. The base pressure of the main SEM chamber is kept below 2×10^{-5} torr, and the gun is kept below 1×10^{-8} torr. Because organic semiconducting materials are easily destroyed by high energy, the beam energy was always kept below 5kV. Even so, after long use on a single region of a sample, clear "burn" marks are seen. SEM samples were always deposited on oxidized test wafer. Before deposition of samples step 1 of the RCA clean was to clean the substrates.

In this thesis SEM was used predominately for three purposes. First, SEM was utilized to "look" at growing film of pentacene inorder to gain a qualitative understanding for pentacene film formation from a precursor. Second, SEM enabled the nucleation density of growing pentacene crystals to be counted and quantified. The sizes of pentacene crystalline structures are also measured. Lastly, since the electron beam interacts with the pentacene and substrate differently, the wetting and dewetting of pentacene films on substrates can be measured.

SEM pictures are saved in the uncompressed TIFF format. Therefore images can be opened and analyzed with any image processing program. The open-source software The Gimp was used to analyze all the images from SEM. Nucleation site were counted up by hand from the SEM images. The dewetting of films was found by using the threshold feature in The GIMP which creates binary images showing the substrate as a white color and pentacene films as black. The percent coverage of pentacene film is then measured by THE GIMP.

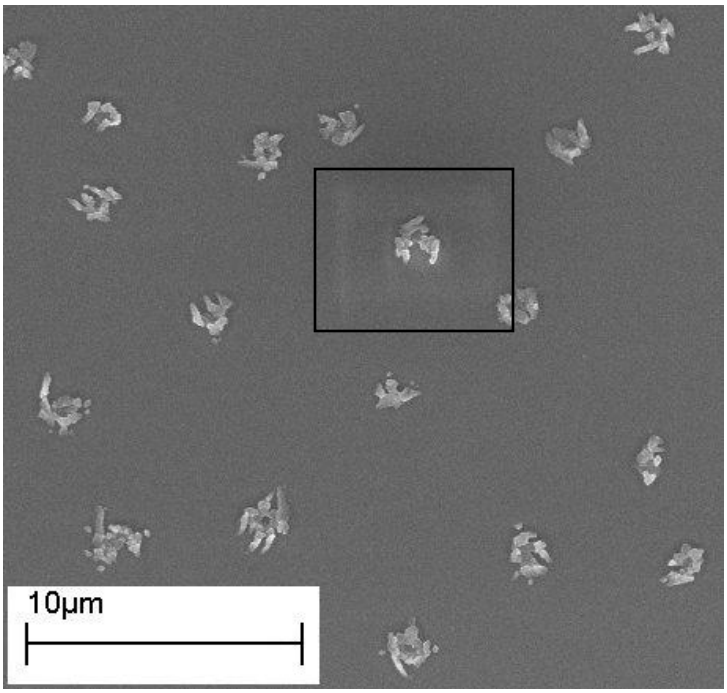

Figure 2-4: Example of SEM image to for counting pentacene nucleation sites. The black square shows an example of sample damage caused by the electron beam from zooming into particular regions.

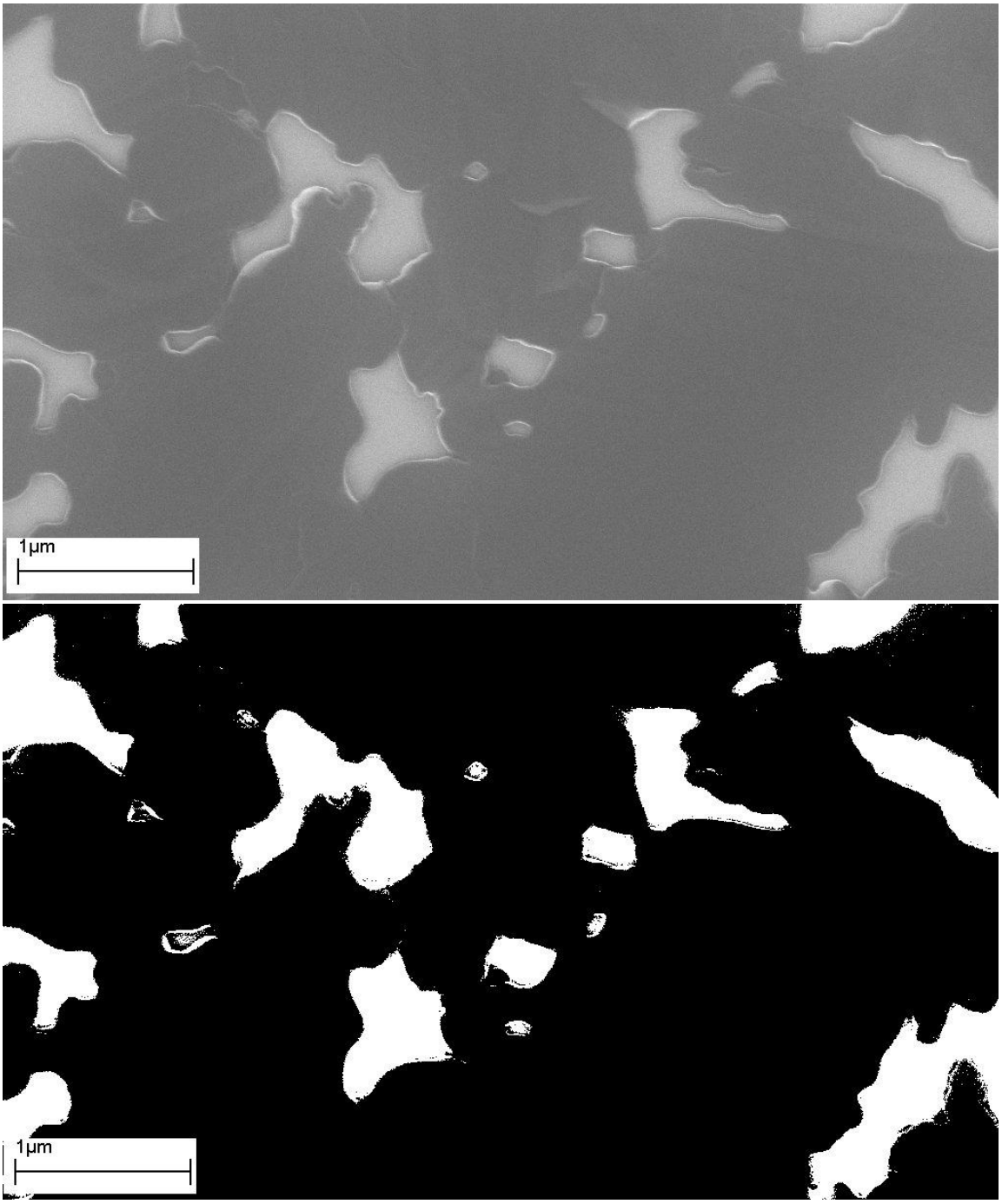

Figure 2-5: (above) A regular SEM image before thresholding. (below) A processed SEM image after thresholding, with black areas indicating pentacene and white areas indicating exposed substrate.

2.3 Atomic Force Microscopy (AFM)

The precursor to the AFM was the scanning tunneling microscope (STM). The STM allowed for high resolution images of conductive material. AFM was invented 1986,[14] which combined the STM with surface profiler. The profiler is a tip with a small mass, which deflects as it moves across the surface. Due to the small mass of the tip, the sample will not be destroyed by the scanning action. By monitoring the deflection of the tip, the surface profile of the sample can be taken. AFM has the benefit of being able to scan a 2-D area much like SEM, but true 3-D information is given.

An AFM probe is a cantilever with a sharp micromachined tip attached to the end of the cantilever. The vertical height of the tip is measured by a laser and photodiode. As the tip is rastered across the surface of a sample the vertical deflection of the tip translates into topological image of the sample. There are two main modes of AFM operation, contact and tapping mode. In contact mode, the tip is scanned across the surface of the sample in constant contact with the sample surface. This has the disadvantage of the probe potentially sticking to samples, especially from water adhesion. Also for extremely soft samples contact mode AFM can potentially damage samples.

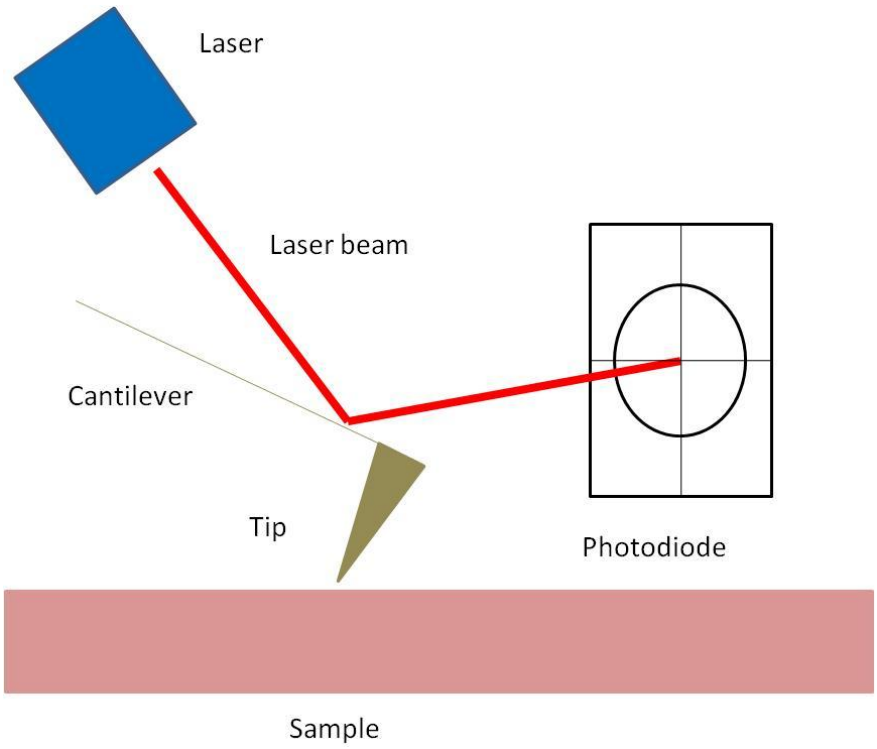

Figure 2-6: A typical AFM tip setup

Tapping mode AFM was invented counter these problems. In tapping mode, the tip vibrates and taps the surface of the sample as the tip scans across the surface. The tip made to resonate/vibrate a fixed frequency and amplitude, creating the "tapping." As the tip rasters across samples the amplitude of the tip changes due to the different features on the sample, which translates to height changes.

The AFM used in these studies was a DI Dimension 3100 AFM. AFM was used to visualize the surface topology on a select few SEM samples where more data was needed. Due to the large number of SEM samples made and the tedium and slow scanning speeds of AFM not all SEM samples were scanned by AFM. Since organic materials are relatively soft, it was found that contact mode AFM was destructive to these samples. All samples, therefore, were scanned in tapping mode. Tap300 tapping mode

tips were purchased from Ted Pella, Inc. The tapping frequency of the tip is approximately 300kHz. The same samples used for SEM were also used for AFM.

For each scan, scanning parameters were adjusted in order to obtain the best images. Parameters adjusted were, scan speed, scan size, lines per sample and amplitudes. Due to the softness of pentacene films it was found that a slow scan rate produced the best images. For images with large roughness, slow scans were imperative inorder for even a reasonable image to be produced. It is due to this reason that SEM was the predominate method of characterizing films. Even though AFM is able to give a true 3-D image, however images are limited to a size of 30×30μm at most, and each image require up to a 20 minute scan.

Data extracted from AFM were analyzed with the open-source software Gwiddyon. For each image, line and plane fitting were performed to normalize the background. AFM was specifically used measure the profiles of cross-sections of images and to find the rms roughness of films.

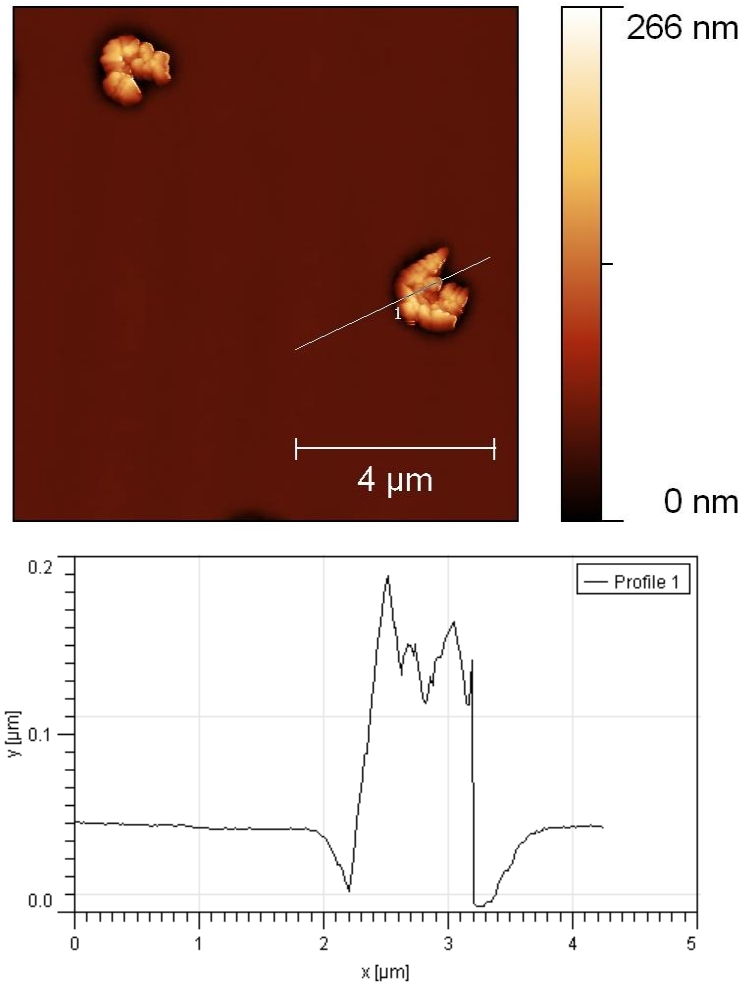

Figure 2-7: AFM image analyzing the profile of a cross-section

2.4 Glancing Angle X-ray Diffraction (GIXD)

X-ray diffraction is used in the thesis in order to deduce the crystal structure of organic semiconducting films. It was developed by William L. Bragg and William H. Bragg, which they were awarded the Nobel Prize.[15] Their discovery can be readily summarized by the famous Bragg's Law:

$$2d\sin(2\theta) = n\lambda$$

Equation 2-4: Bragg's Law

In the equation (equation 2.4), n is an integer, λ is the wavelength of the X-ray, d is the interplanar spacing of the crystal, and θ is the angle between the incident X-ray and the scattering plane. This equation describes the conditions for constructive interference of X-rays, given the angle of the incident X-ray. The generated X-ray diffraction pattern gives the reciprocal lattice of a sample, which is useful to deducing the crystal structure.

Tradition X-ray diffraction on organic materials becomes more problematic because of the weak signals which arise from organic materials and relatively close peaks due to the large inter-plane spacing. Glancing angle X-ray diffraction with a synchrotron source serves to solve these problems.

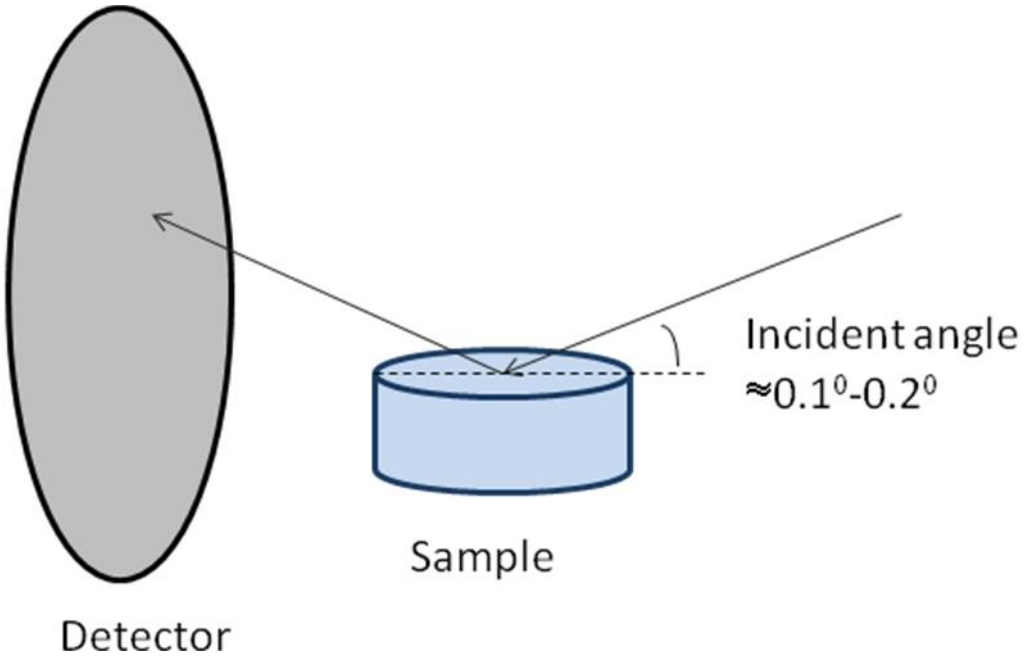

Figure 2-8: Schematic of GIXD setup

GIXD uses an extremely low incident angle (approximately 0.1^0-0.2^0). This limits the amount of X-rays which penetrate the sample, so that the substrate would not interfere with the data of the organic material, therefore the background noise is reduced. Another benefit of the GIXD setup is that crystalline monolayers can be visualized,

where in the traditional setup it cannot. Finally, a synchrotron X-ray source, because the source is brighter and the bandwidth is more narrow, allowing for higher resolutions and stronger diffraction signals.

All GIXD experiments were done at the Stanford Synchrotron Radiation Lightsource on the 11-2 and the 7-2 beamline. The 11-2 beamline gives low resolution 2-D diffraction pattern of the analyzed samples. The 7-2 beamline gives high resolution 1-D xray diffractions. This beamline was specifically used to look at the 100 peak of pentacene in order to estimate crystal size. Diffraction patterns were used to deduce three attributes of the samples; film texturing, pentacene morphotypes and relative crystal size. Texturing can be found by looking at arcing in the in-plane peaks as well as the mixed reflections.

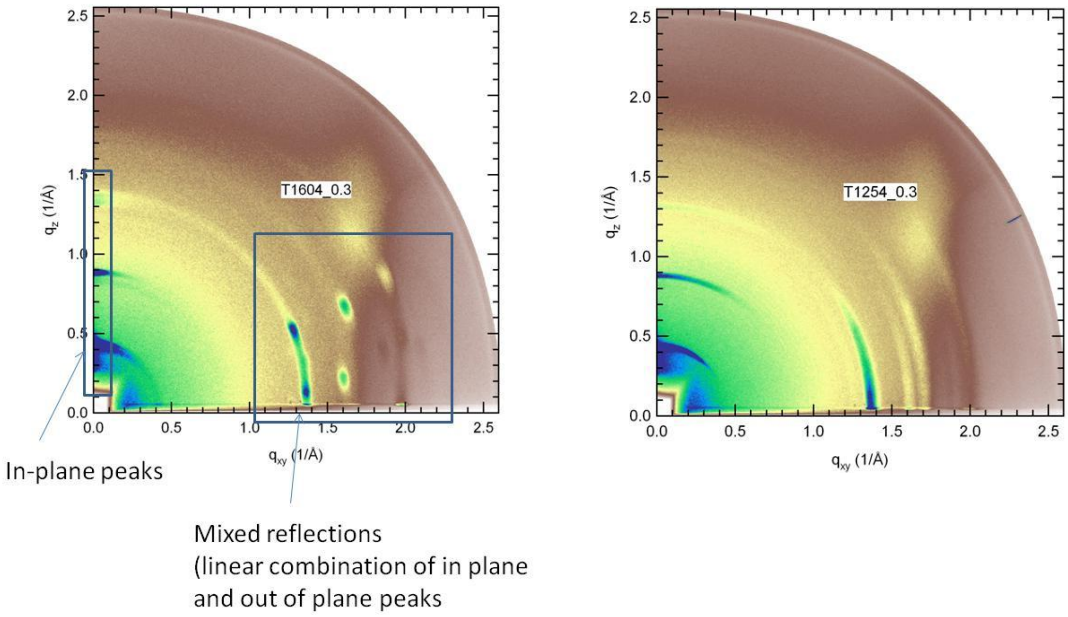

Figure 2-9: (left) GIXD of pentacene film processed at 160^{0}C. (right) GIXD of pentacene film processed at 125^{0}C. In the boxed in-plate peak, from bottom up the identity of the peaks are 100, 200, and 300 respectively.

In the GIXD pattern showing the pentacene film processed at 160^0C in figure 2.9, the in-plane reflections and the mixed reflections are boxed. The in-plane reflections are the same are the reflections seen in regular X-ray diffraction. The out-of-plane reflections are on the x-axis, but are blocked off, because of the beam stop. The mixed reflections are the linear combination of both the in-plane and out-of-plane reflections. There are two ways to look at texturing using the 2-D diffraction patterns.

The first way to look for texturing is to look at the "arcing" in the 100 plane. In a completely disordered polycrystalline film, such as a powder film, distinct peaks will not be seen. Instead "rings" are seen. These rings come from the superposition of identical diffraction patterns rotated at many different angles. As texturing increases and the randomness of crystals decreases, the "rings" shorten into arcs. When crystals are well ordered, then the arcs turn into distinct spots. Therefore by looking at the length of arcs, the texturing of films can be determined, with longer arcs showing high disorder, a full ring indicates no ordering at all, and a isolated point shows perfect ordering. From figure 2.10, the 100 "arc" from a film processed at 125^0C is much larger than the 100 "arc" on a film processed at 160^0C, indicating no low order for film processed at 125^0C and higher order for films processed at 160^0C.

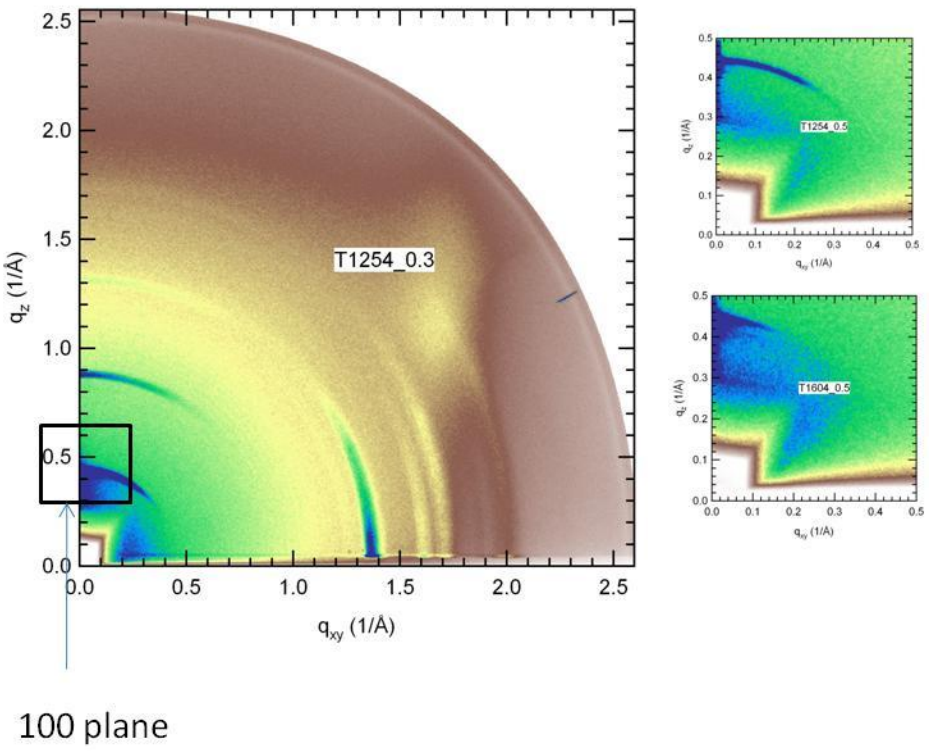

Figure 2-10: (Left) The location of the 100 plane is shown. (Top right) The 100 plane from a film processed at 125^{0}C. (Bottom right) The 100 plane from a film processed at 160^{0}C.

The second way to look at texturing is to look for mixed reflections. When mixed reflections become distinct, that is a good indication of texturing. In disordered polycrystalline samples where diffraction rings are seen, the rings are a blur of all diffraction peaks, both in-plane out-of-plane as well as mixed reflections. When the rings resolve into distinct peaks, blur on the mixed reflection also resolves and is no longer mixed in with the in-plane andn out-of-plane reflections. The film processed at 125^{0}C does not have any distinct mixed reflections showing poor texturing.

There are three morphotypes of pentacene. This is discussed in further detail in chapter 4. The three morphotypes are an orthorhombic monlayer phase,[16] a triclinic thin-film phase[17] and triclinic bluk-like phase.[17]

The existence of different morphotypes of pentacene can be found by looking for doubling of peaks. Both the thin-film phase and the bulk-phase in pentacene have a triclinic crystal structure, however they have different lattice constants. Therefore, if there are two peaks that show up close to each other, this is highly indicative that there are two morphotypes of pentacene present. In figure 2.11, it can be seen that the film processed at 160^0C has two morphtypes of pentacene present while the film at 125^0C does not. The monolayer phase needs more complex methods in order to be identified, so it cannot be determined whether or not it exists. It is assumed that it does not exist, because the monolayer phase needs persists only under specific conditions which the pentacene precursor does not have.

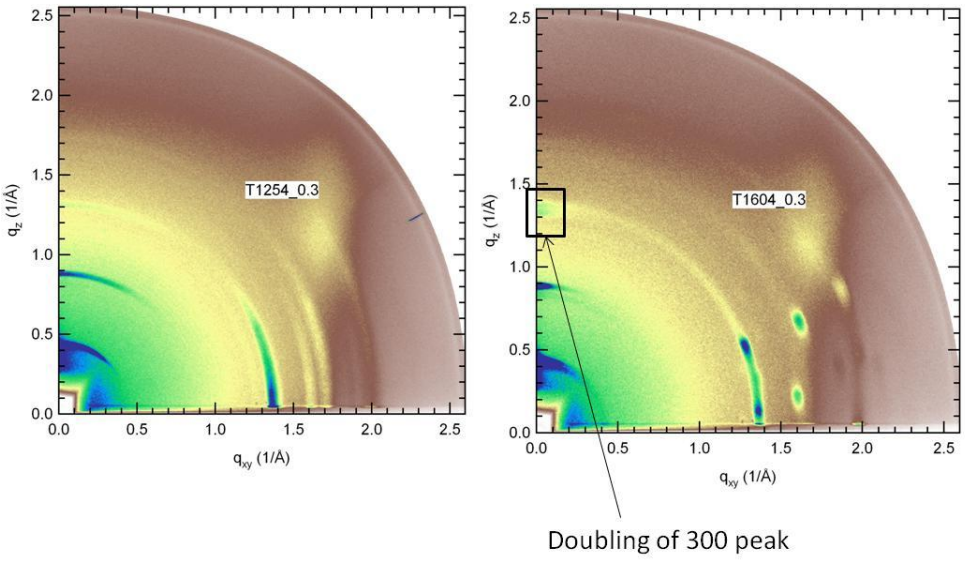

Figure 2-11: (Left) A film processed at 125^0C does not show a double peak. (Right) The A film processed at 160^0C shows a double 300 peak.

Finally, crystallite size is extracted by measuring the full width half maximum of the 100 peak and applying the Debye-Scherer formula. The wider the peak, the smaller the crystallite size. All of the crystallite sizes were extracted using a high resolution X-ray rocking curve, rocked around the 100 plane. Qualitatively, by looking at peak width, a quick comparison of crystal size can be made. Looking back at figure 2.10, the 100 peak at 125^0C is extremely narrow, showing a large crystal compared to the 160^0C film. Only the relative crystal size of the pentacene can be compared, because when extracting the crystal sizes, for simplicity the crystals were assumed to have a cubic crystal structure.

2.5 UV-vis Spectroscopy

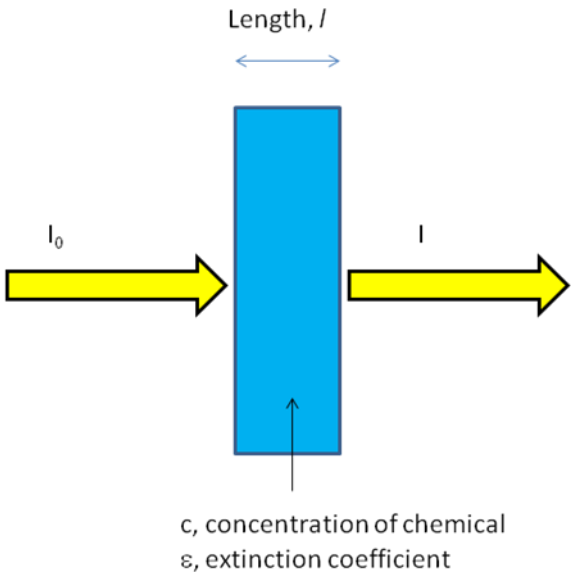

Figure 2-12: Diagram of Beer-Lambert absorption of an incident beam.

From the name UV-vis spectroscopy, it can be inferred that this method measures the interaction of light ranging from UV wavelengths to visible wavelength with a sample. With UV-vis spectroscopy, the measurement can either be absorbance or

transmission of the light at different wavelength. In the study of UV-vis spectroscopy in chapter 3, only absorbance data is used. The use of absorbance is the most typical method for used in UV-vis spectroscopy. UV-vis has with most light spectroscopic techniques operates by Beer-Lambert law.

Beer-Lambert law is the empirical relationship which describes how light is absorbed through a material. This is the principle which data from UV-vis spectroscopy is interpreted. The equation is:

$$\frac{I}{I_0} = 10^{-\varepsilon lc} = 10^{-A}$$

Equation 2-5: Beer-Lambert equation

So the absorbance, A, is related to l, the length of the sample, c the concentration of the chemical, and ε the extinction coefficient. In an UV-vis absorption spectrum, A is plot for different wavelengths of light. For every chemical which absorbs light from the UV to visible light range, a unique pattern of absorption is seen, and can be used to identify the chemical.

Usually samples are soluble in a solvent, and the chemicals are place in a cuvette with a fixed size. Assume now that there are two chemicals in the cuvette. The absorbance, A, is affected by both chemicals and the absorbance is now:

$$A = \varepsilon_1 l c_1 + \varepsilon_2 l c_2$$

Equation 2-6: Absorbance when there are two chemicals

The length are identical for both chemicals, because the size of the cuvette is fixed and both chemicals are dispersed in the cuvette.

Supposed there is a chemical reaction where A→B. Each chemical has an unique UV-vis absorbance spectrum, and A has a sharp peak at 600nm and B does not. Suppose multiple samples are such that each sample is at a different stage of the conversion from A to B. Therefore samples made during the early stage of the reaction will have more A and samples at the end of the reaction will have more B. It can also be assumed that before the reaction starts the samples is 100% A and the end of the reaction 100% of the samples is B (figure 2.13).

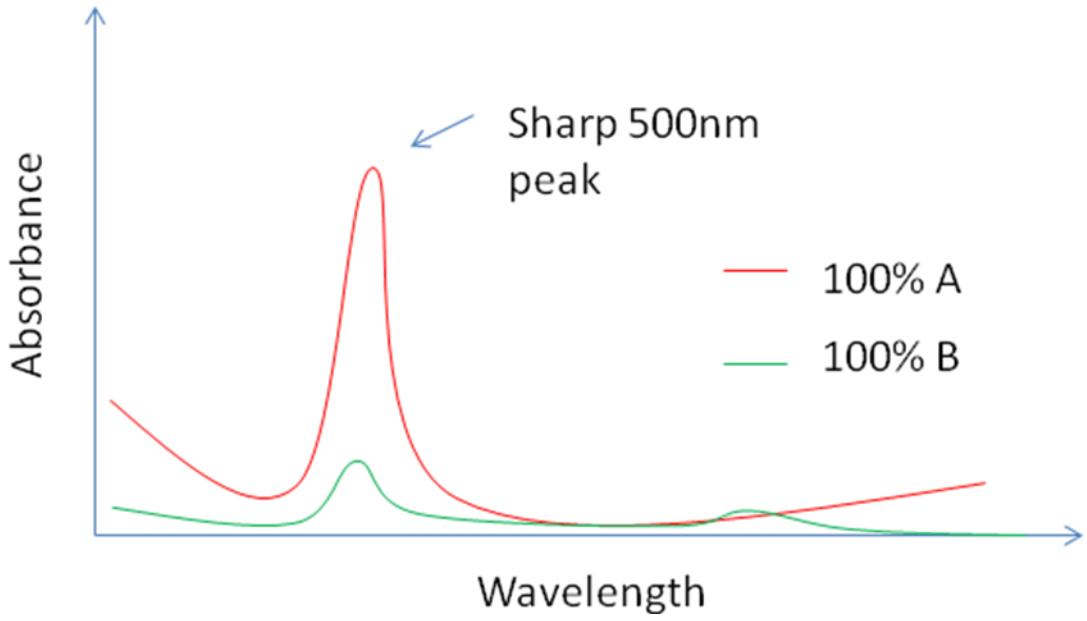

Figure 2-13: UV-vis absorption spectrum of chemical A and B

Once a spectrum is taken for 100% A and 100% B it is very easy to figure out the concentration of A and B for all the intermediate samples where there is a mix of A and B. As the reaction proceeds, A will disappear and B will start appearing. The concentration can be monitored from the absorbance at 600nm. Suppose the sample gives a spectrum as seen by the orange curve in figure 2.14. The % of A left in the vial is found by:

$$A = 1 - \frac{x1}{x2}$$

The % of B which as appeared is found by:

$$B = 1 - \frac{x2}{x1}$$

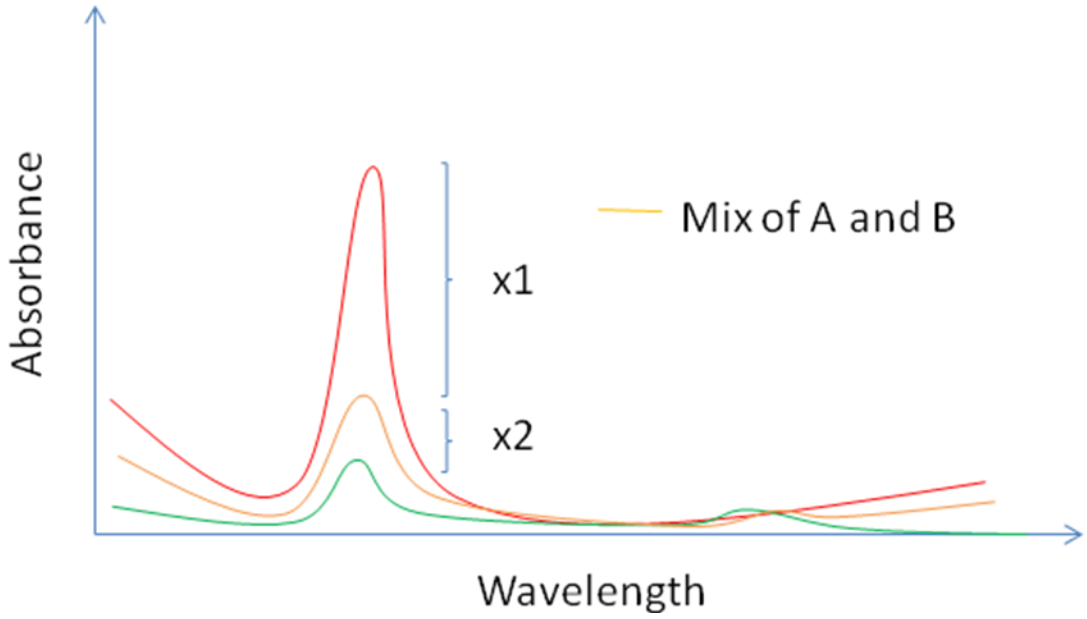

Figure 2-14: UV-vis absorption spectrum of with both A and B present.

In order for this experiment to work, the initial concentration of A used to create each sample must be the same. The length of each cuvette must also must be the same. In the case of a solid-state reaction, samples are not dissolved in a liquid and placed in a cuvette. Instead samples are deposited on glass or quartz slides and then placed in the machine. In sample preparation, each glass slide must be identical, and the thickness of the deposited film must have identical thicknesses. Having identical sample thickness is analogous to using cuvettes of identical size and identical starting chemical concentrations. If this condition is not met, then experimental results would be invalid.

2.6 References

1. Bassler, H. Charge Transport in Disordered Organic Photoconductors a Monte Carlo Simulation Study. *physica status solidi (b)* **175**, 15-56(1993).
2. Merlo, J.A. & Frisbie, C.D. Field Effect Transport and Trapping in Regioregular Polythiophene Nanofibers. *The Journal of Physical Chemistry B* **108**, 19169-19179(2004).
3. Mottaghi, M. & Horowitz, G. Field-induced mobility degradation in pentacene thin-film transistors. *Organic Electronics* **7**, 528-536(2006).
4. Roichman, Y., Preezant, Y. & Tessler, N. Analysis and modeling of organic devices. *physica status solidi (a)* **201**, 1246-1262(2004).
5. Horowitz, G. Organic thin film transistors: From theory to real devices. *JOURNAL OF MATERIALS RESEARCH* **19**, 1946-1962(2004).
6. Podzorov, V. et al. Intrinsic charge transport on the surface of organic semiconductors. *cond-mat/0403575* (2004).at <http://arxiv.org/abs/cond-mat/0403575>
7. Paasch, G., Lindner, T. & Scheinert, S. Variable range hopping as possible origin of a universal relation between conductivity and mobility in disordered organic semiconductors. *SYNTHETIC METALS* **132**, 97-104(2002).
8. Li, L., Meller, G. & Kosina, H. Influence of traps on charge transport in organic semiconductors. *Solid-State Electronics* **51**, 445-448(2007).
9. Li, L., Meller, G. & Kosina, H. Carrier concentration dependence of the mobility in organic semiconductors. *Synthetic Metals* **157**, 243-246(2007).

10. Kawasaki, N. et al. An investigation of correlation between transport characteristics and trap states in n-channel organic field-effect transistors. *Appl. Phys. Lett.* **92**, 163307-3(2008).
11. Chesterfield, R.J. et al. Organic Thin Film Transistors Based on N-Alkyl Perylene Diimides: Charge Transport Kinetics as a Function of Gate Voltage and Temperature. *The Journal of Physical Chemistry B* **108**, 19281-19292(2004).
12. Roichman, Y., Preezant, Y. & Tessler, N. Analysis and modeling of organic devices. *physica status solidi (a)* **201**, 1246-1262(2004).
13. Goldstein, J. et al. *Scanning Electron Microscopy and X-ray Microanalysis*. (Springer: 2003).
14. Meyer, E., Hug, H.J. & Bennewitz, R. *Scanning Probe Microscopy: The Lab on a Tip*. (Springer: 2003).
15. Fultz, B. & Howe, J. *Transmission Electron Microscopy and Diffractometry of Materials*. (Springer: 2007).
16. Fritz, S.E. et al. Structural Characterization of a Pentacene Monolayer on an Amorphous SiO2 Substrate with Grazing Incidence X-ray Diffraction. *Journal of the American Chemical Society* **126**, 4084-4085(2004).
17. Bouchoms, I. et al. Morphology identification of the thin film phases of vacuum evaporated pentacene on SIO2 substrates. *SYNTHETIC METALS* **104**, 175-178(1999).

3 The Pentacene Precursor Reaction

3.1 Background

The pentacene precursor from IBM (13,6-N-Sulfinylacetamidopentacene or SAP) has been successfully used for fully printed organic TFTs,[1] showing mobility in the $0.1 cm^2/Vs$ range. Due to the success of this material, it is important to have a proper understanding of the chemistry of this material. The reaction rate of SAP to pentacene has not yet been measured, and the knowledge of the reaction is imperative to properly characterize the conversion of the SAP into pentacene.

The reaction rate is measured by measuring the time it takes for SAP to convert to pentacene at different temperatures, and the data is fit to an Arrhenius equation which would give activation energy and a temperature independent reaction rate. Whereas the Arrhenius equation is overall merely an empirical fitting tool, in simple chemical reactions such as the degradation of SAP, the Arrhenius equation takes on a physical meaning.

Tracing the completion of solid-state chemical reactions can easily be measured using a thermogravimetric analysis (TGA) and differential scanning calorimetry (DSC). These two methods many times are combined into one machine and the TGA and DSC measurements are done in parallel. Using this technique, a solid sample is placed in a small container and heated at a fixed temperature until the sample fully reacts. The mass

of the sample is traced as a function of time, and the heat flow in and out of the sample is also traced as a function of time. Only one sample is needed for each temperature that is to be measured. From sample to sample, the precise amount of material does not have to be identical. Unfortunately, the machine cannot be brought to the reaction temperature instantaneously. It takes a few minutes before the machine heats up from room temperature to the reaction temperatures. This lag will give an inaccurate reading on the reaction rate of SAP to pentacene at higher reaction temperatures. In Afzali's original paper, TGA was merely used to find the temperature where SAP decomposition begins and also to find the reaction yield. It was found that SAP starts converting to pentacene at 120^0C, and the reaction yield is close to 100%.

In order to be able to properly trace the reaction completion of SAP conversion, UV-vis spectroscopy was used to measure the reaction of the pentacene precursor instead. The downside to this technique is that a large number of samples needs to be prepared for this technique as compared to TGA-DSC. The preparation of each sample needs to be identical otherwise the absorbance measurements would be meaningless. With UV-vis, SAP is first deposited onto glass slides and then reacted on a hotplate. The hotplate is set to the reaction temperature and samples are placed onto the preheated hotplate. Since the slides are small and thin, the time lag to heat samples from room temperature to the reaction temperature is short, so this method is more accurate than TGA-DSC. In order to properly trace the reaction for each reaction temperature many samples need to be prepared, with each sample reacted to various stages of reaction completion. In order to trace a chemical reaction from beginning to end many samples are needed so that the complete reaction can be captured.

3.2 Experimental Procedures

Solid-state UV-vis absorbance spectroscopy (UV-vis) was used to find the reaction rate of pentacene precursor. UV-vis samples were prepared by spinning SAP onto glass substrates. SAP was made by the method described in the Appendix. Glass substrates were 22mm by 22mm glass microscope cover slips from Fisher Scientific. Solutions were prepared by dissolving 12mg of SAP into 1mL of 99% anhydrous chloroform stabilized with amylenes purchased from Aldrich. Solutions were deposited onto the glass microscope cover slips at 0rpm (200μl per cover slip). Once solutions were deposited onto the glass substrates, the substrates were quickly ramped up to 4000rpm (within 2s) and spun at 4000rpm for 30s.

Each sample was then heated at a specific for a fixed amount of time. All samples were heated in a dry nitrogen glovebox. Using the results of from Alfazi *et al*,[2] it was determined that the decomposition temperature starts at ~120^0C. The temperature range used for sample heat should at least be 120^0C. For each reaction temperature multiple samples were used each being heated at different durations. For the lower temperature points, more samples and longer total times were used in order to trace the reaction rate more accurately. For the higher temperature points fewer samples were used and shorter reaction times were used. The shortest sample heating times was 1s, since placing samples on and off hotplates could not be accurately measured at times shorter than 1s. Table 3.1 shows all the different heating conditions used.

Temperature	Heating times
125	2.5m, 5m, 10m, 20m, 40m, 80m
130	15s, 30s, 45s, 1m, 2m, 4m, 8m, 16m, 32m, 64m, 128m
140	15s, 30s, 45s,1m, 2m, 4m, 8m, 16m, 32m
150	1m, 2m, 4, 8m, 16m, 32m
160	1s, 2s, 4s, 8s, 16s, 32s, 64s, 128s
170	1s, 2s, 4s, 8s, 16s, 32s, 64s, 128s
180	1s, 2s, 4s, 8s, 16s, 64s
190	1s, 2s, 4s, 8s
200	1s, 2, 4s, 8s
220	1s, 3s

Table 3-1: List of all the temperature time conditions used for UV-vis anaylsis

All samples were scanned with a UV-vis spectrophotometer at wavelengths ranging from 800nm to 400nm. Pentacene should have a strong absorbance been below 400nm,[2] however the glass slides used as substrates are not transparent below 400nm. No peaks were found above 800nm, so those regions were truncated.

By using the prescribed method described earlier, the reaction rate of the SAP to pentacene was extracted for each temperature and an Arrhenius relationship was fit to the reaction rate.

3.3 Experimental Results

First a pentacene precursor baseline was measured. Between 400nm and 800nm there were no distinct peaks that can be identified by UV-vis. A sample heated at 140^0C for 1hr had five distinct peaks can be easily identified in the 400nm to 800nm range, as shown in figure 3.1. It was assumed that this sample was fully reacted. The most pronounced peak is the peak is approximately at 667nm. There is clearly no peak at 667nm for an unreacted pentacene precursor film, so for reaction rate measurements, reactions will be followed by watching the 667nm peak.

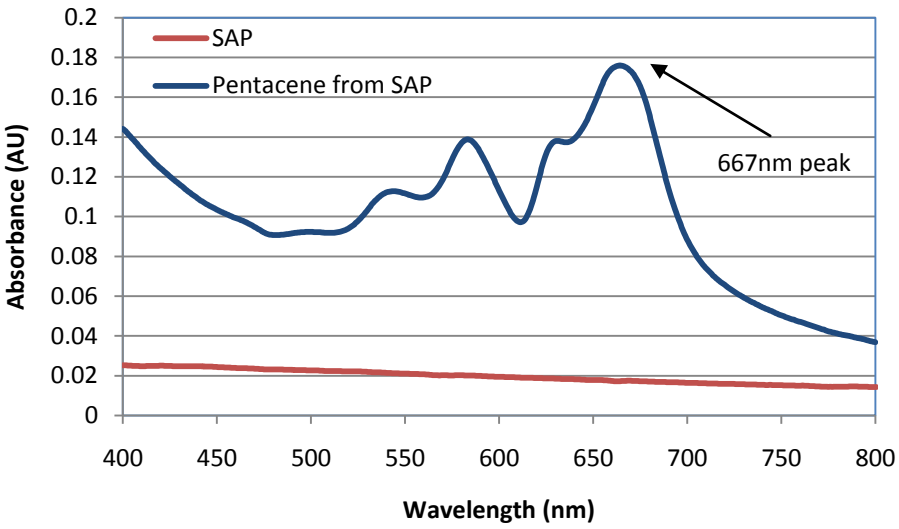

Figure 3-1: UV-vis absorption spectrum of pentacene precursor and pentacene thin-film on glass. The precursor sample was an unreacted sample of pentacene precursor. The Pentacene sample was a sample pentacene precursor reacted at 140^{0}C for 1hr.

Since every sample was prepared using the solution concentration and deposited with the same spin speed, every sample should have the same amount of starting material and therefore it is valid to trace the peak height in order to determine the fraction of reacted material.

The absorbance value of an unreacted sample at 667nm was found be approximately 0.012. When the absorbance value at 667nm of a particular sample was the same as the 667nm absorbance of another sample both heated at the same temperature but at different times, it was assumed that the two films are fully reaction and 100% of the SAP had turned to pentacene. It was determined that for all temperature points the absorbance of a fully reacted film was approximately 0.15. Figure 3.2, shows how the absorbance of the 667nm peak increases as the reaction proceeds at 130^{0}C. The increase

of absorbance at 667nm peak indicates that pentacene is being created and SAP is disappearing.

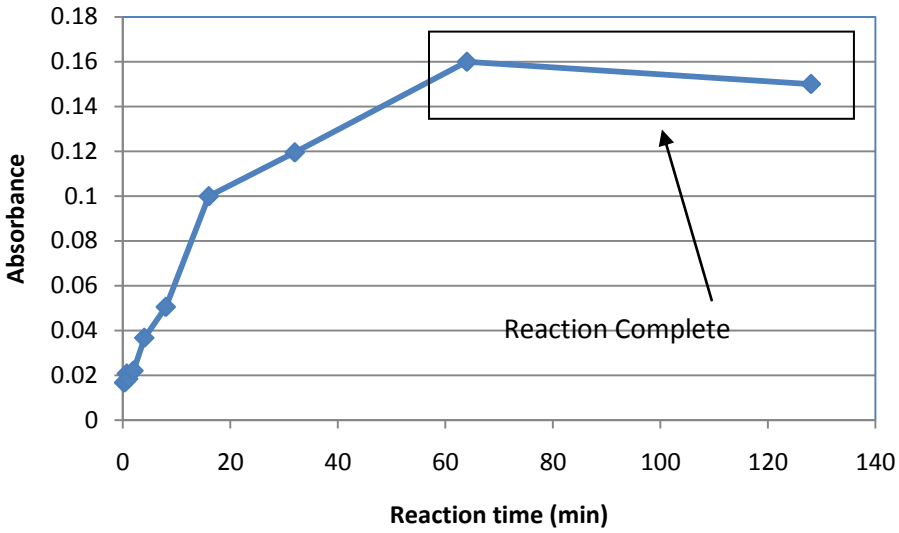

Figure 3-2: The change of absorbance as the SAP reaction proceeds.

Using the absorbance data in figure 3.2, figure 3.3 was created using the using the methods prescribed in chapter 2 in the section in UV-vis analysis. In Figure 3.3 aborbance values was converted to SAP concentration and show how SAP disappears over time when reacted at 130^0C.

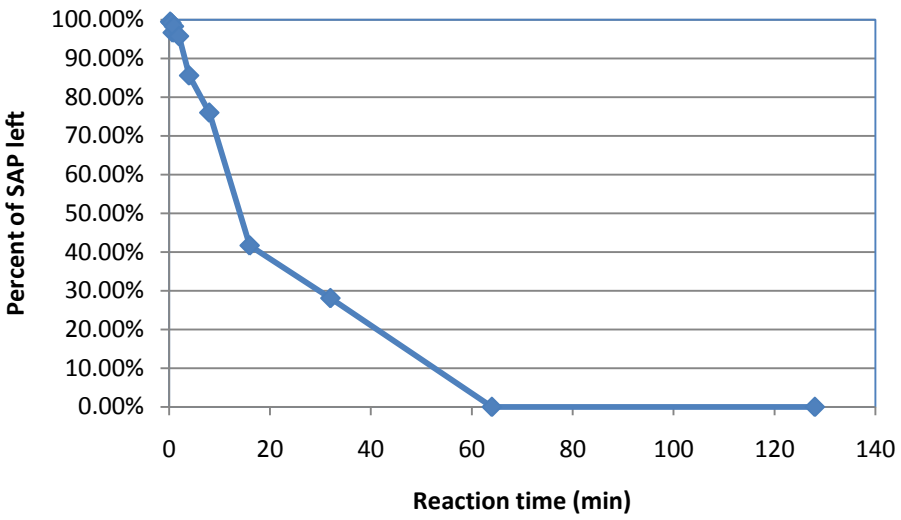

Figure 3-3: Disappearance of SAP at 130^{0}C traced by UV-vis.

The decomposition of SAP to pentacene can be described by the general reaction A → B + C, where A is the starting material SAP and B and C is the resulting product, pentacene and the NSO adduct. This reaction is a first order reaction, where disappearance of A can be described by:

$$\frac{dA}{dt} = k[A]$$

Equation 3-1

Where k is the rection rate, and the solution of this differential equation is:

$$A(t) = C_0 e^{-kt}$$

Equation 3-2

Where C_0 is the starting concentration of the reactant A. Equation 3.2 can be rewritten into linear form:

$$\ln[A(t)] = -kt + const.$$

Equation 3-3

In Figure 3.4, figure 3.1 is replotted as a log(y) vs. linear(x) plot, and the slope of line gives the reaction rate k. The data points more or less fall on a straight line showing that using the first order degradation reaction is a valid assumption.

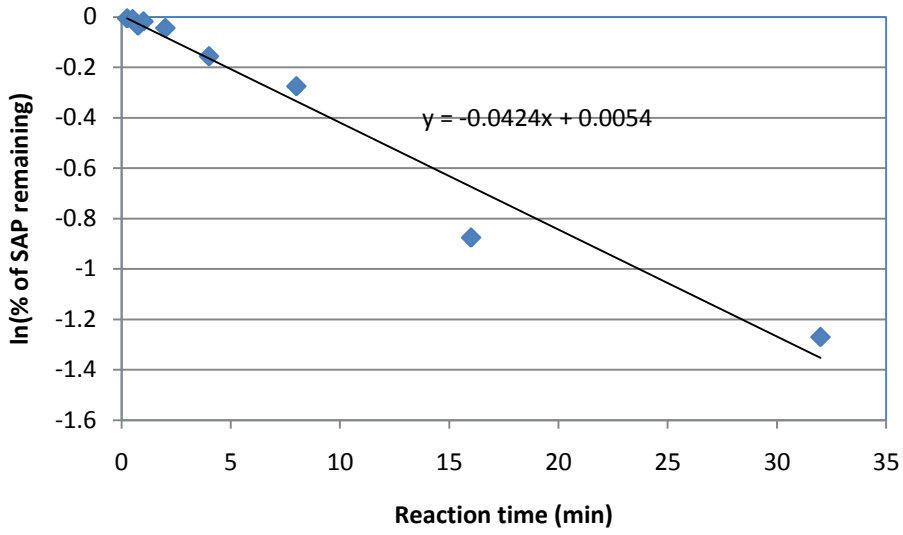

Figure 3-4: *log-linear plot of SAP disappearance at 130^{0}C in order to extract reaction rate.*

The same figures were reproduced for every reaction temperature. As expected, reactions occur much faster at higher temperature than lower temperatures. Due to the high reaction rates at higher temperatures, films are fully converted to pentacene within a few seconds at 190^{0}C. The reaction rate extractions for these data points may not be accurate, because of sample heating issues. Figure 3.5 shows the same graphs plot for the SAP decomposition reaction at 160^{0}C. Notice the compress x-axis showing that the

reaction procedures faster at higher temperatures. Here the decaying exponential still works quite well to describe the disappearance of SAP.

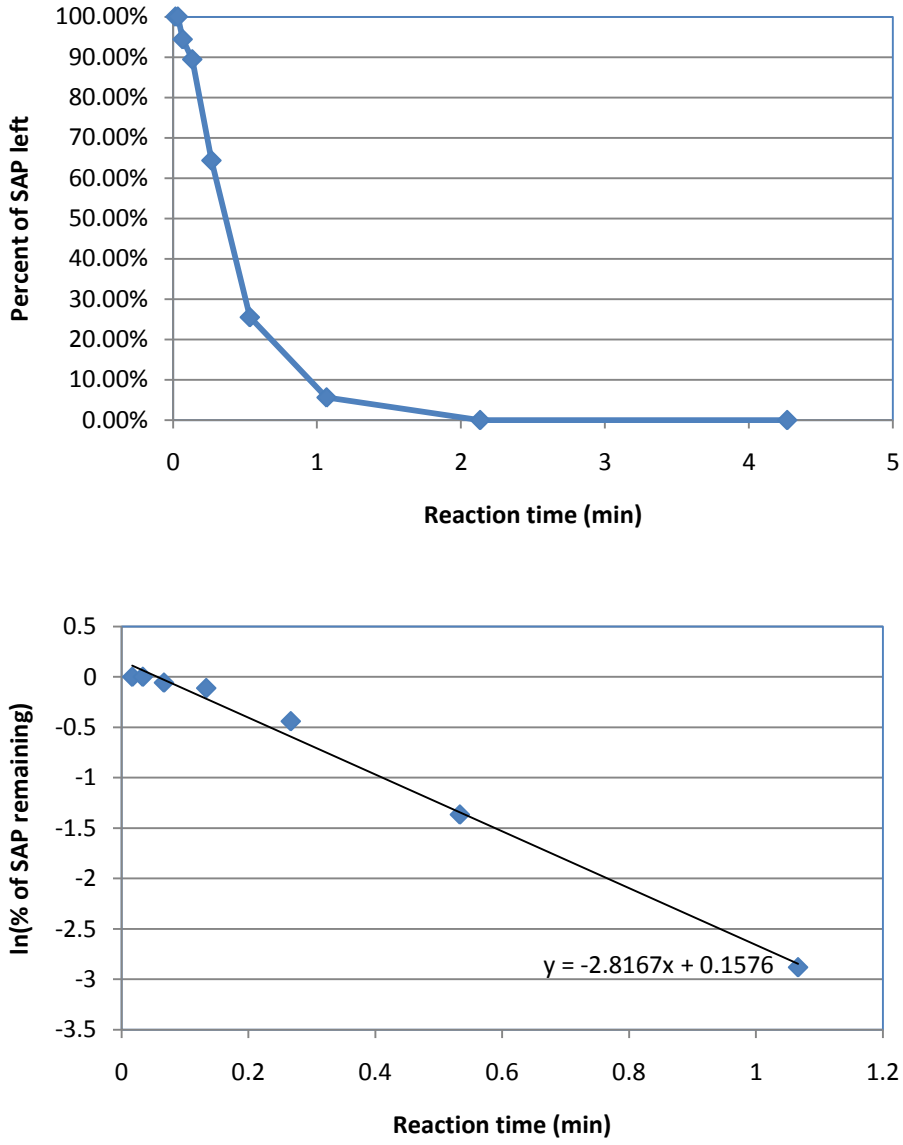

Figure 3-5: *(top) Linear-linear plot of SAP disappearance at 160^{0}C. (bottom) Log-linear version of SAP disappearance at 160^{0}C.*

It roughly takes 2-3 seconds for the glass coverslip to go from room temperature to 90% of hotplate temperature once the sample is placed on the hotplate. At low

temperatures where the reaction requires up to 1 hr for reactions to fully occur this 2-3 transient is not a problem. At high temperatures where reactions start before the sample reaches the final temperature, we will get an underestimation of the reaction rate. Figure 3.6 shows the disappearance of SAP when reacted at 190^0C. This figure clearly demonstrates the pitfalls of the experimental setup. The first three points shows little disappearance of SAP as the glass coverslip slowly heats up. Between the third and fourth data point, the SAP concentration suddenly drops to 0, so the shape of the decaying exponential is not captured. For these two reasons, the reaction rate extractions at high temperature is clearly inaccurate.

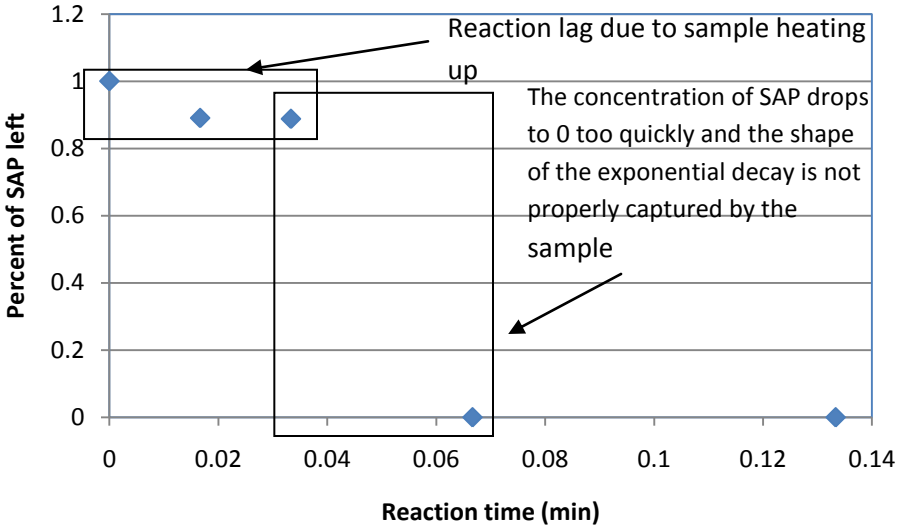

Figure 3-6: linear-linear plot of SAP disappearance at 190^0C

Table 3.2 shows the extracted reaction rates for each reaction temperature. This data can be plotted according to the Arrhenius relationship:

$$k = k_0 e^{-E_a / RT}$$

Equation 3-4

Here, k is the reaction rate of reaction, k_0 is the reaction rate constant, E_a is the activation energy and R is the gas constant. Figure 3.7 shows the reaction rates plotted in a log-linear fashion to extract the activation energy. The activation energy was estimated to be 123.2kJ/mol.

Temperature	Reaction rate (min^{-1})
125	0.037533
130	0.042407
140	0.063045
150	0.597243
160	2.773099
170	1.785336
180	11.79519
190	6.975172
200	28.81501
220	13.69029

Table 3-2: Reaction rates for different temperatures

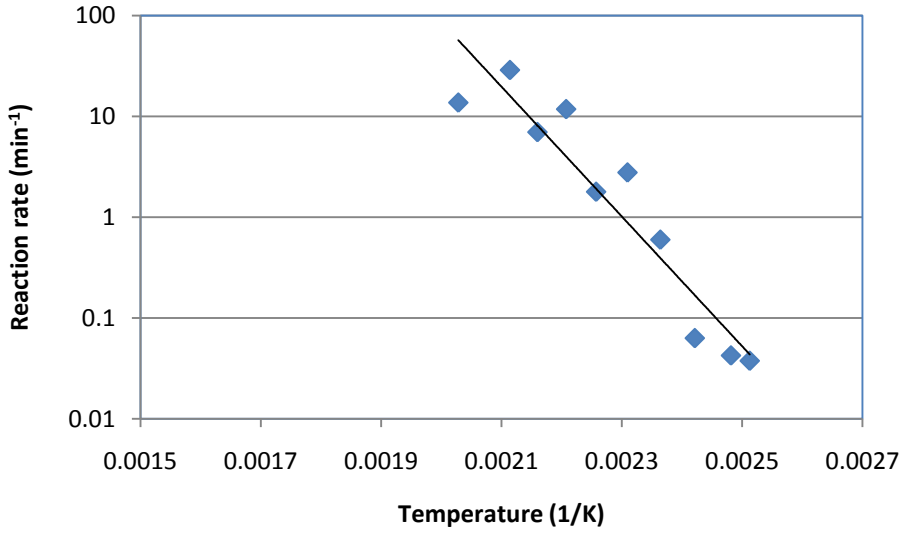

Figure 3-7: Reaction rates were fitted to an Arrhenius relationship in order to estimate activation energy.

3.4 Discussion

Using UV-vis the product of SAP decomposition has been confirmed to be pentacene, since the UV-vis spectrum matches properly to the reported UV-vis spectrum of evaporated pentacene as well as pentacene from SAP as seen in literature. Further more the reaction rate of SAP degradation has been extacted using UV-vis absorbance. The degradation of SAP was modeled using a 1^{st} order reaction. The data fit well with the 1^{st} order reaction as predicted based on the chemical equation of SAP decomposition. Finally the reaction rates were fit to the Arrhenius equation for the extraction of the activation energy.

A chemical reaction in the form of a first order equation is only required to take the form of a decaying exponential when the reaction takes place in gas phase. In liquid phase the decaying exponential also occurs when the reactants are in low concentrations. For a solid-state reaction which is the case of a pentacene thin film from SAP, the decaying exponential does not necessarily take place. In solid state reactions, energy is necessary not only to cause a transformation either in phase or to cause a chemical reaction to take place, but energy also needs to be placed into nucleation and crystal growth, therefore a simple exponential decay may not necessarily describe a solid-state reaction.

Typically in a solid-state phase transformation or chemical reaction, the transformation can be described with a sigmoidal curve which is described using the Avarmi equation.

$$1 - F(t) = \exp\left(-Kt^n\right)$$

Equation 3-5: Avrami equation, where F(t) is the fraction of starting material reacted, n and K determine film growth mechanisms.

When the data point from 125^0C to 160^0C is fit to the Avarmi equation, n = 1. When n = 1, the Avrami equation is precisely an exponential decay. Only these five temperature were used in the extraction, because these five points have the least measurement errors. This extraction indicates that the use of using the exponential decay is valid.

The fact the data fits nicely using a decaying exponential and the follows the Arrhenius equation nicely is probably due to the simplicity of the reaction. The reactant only needs "fall apart," and does not need to collide with another reactant, therefore even though the reactant is in the solid state the mechanism for the chemical reaction to take place is extremely simple. Most likely the most energetically costly step in the formation of pentacene is the decomposition of SAP. The appearance of pentacene is apparently not hindered by nucleation or crystal growth, this may be another reason for a simple exponential decomposition.

After calculating the reaction rate the formation of pentacene from SAP needs to be looked at in more detail. How exactly does pentacene nucleate to form pentacene films? This is the subject of the next chapter. Knowing the reaction rate is important when looking at the formation of pentacene films, so that it can be determined the amount of pentacene and SAP present at any given time.

3.5 Conclusion

Using UV-vis the retro Diels-Alder reaction rates was measured. Measuring the reaction rate of the pentacene precursor allows for proper control of reaction times. It has been suggested that the greatest energetic step in pentacene formation is the SAP to pentacene retro Diels-Alder reaction and not the formation of pentacene crystals and nuclei. More experiments still need to be done in order to gain more insight on pentacene formation through SAP.

3.6 References

1. Molesa, S. et al. A high-performance all-inkjetted organic transistor technology. *Electron Devices Meeting, 2004. IEDM Technical Digest. IEEE International* 1072-1074(2004).doi:10.1109/IEDM.2004.1419384

2. Afzali, A., Dimitrakopoulos, C. & Breen, T. High-performance, solution-processed organic thin film transistors from a novel pentacene precursor. *JOURNAL OF THE AMERICAN CHEMICAL SOCIETY* **124**, 8812-8813(2002).

4 The Pentacene Thin-film growth on SiO_2 from Pentacene precursor

4.1 Background

Pentacene TFTs have been made and tested quite extensively. Even though one of the goals of pentacene is for flexible electronics, the most typical substrate pentacene is deposited on is still amorphous SiO_2 (*a*-SiO_2). The backgated TFT is the easiest test bed for testing organic materials. Thermal evaporation is the most common and the easiest way to deposit pentacene onto silicon dioxide. One of the major points of study these past years in organic electronics is pentacene thin-film growth on SiO_2. At this point the thin-film growth mechanism of pentacene on a-SiO_2 is very well known. This knowledge has aided in understanding the electrical properties of pentacene TFTs on SiO_2. The focus of this chapter is on the thin film growth of pentacene through thermal degradation of SAP on *a*-SiO_2. A simple review of the growth of pentacene through evaporation serves as a model and point of comparison for pentacene growth through solution methods.

4.2 Growth of Pentacene on SiO_2 through Evaporation

It is known that bulk pentacene packs in the herring-bone structure creating a triclinic unit cell.[1] Pentacene films grown on *a*-SiO_2 are textured perpendicular to the

substrate and exist in three polymorphs.[2] The herring-bone packing is present in each of these polymorphs; however, lattice constants and angles between the pentacene molecules and pentacene to substrate change with the energetic interaction between pentacene and the oxide substrate.

The different polymorphs of thin-film pentacene are thickness dependent. The first monolayer of pentacene deposited stands nearly perpendicular to the oxide substrate, taking an orthorhombic crystal structure. This is the monolayer phase of pentacene.[2,3]

After a second layer of pentacene is formed on top of the first monolayer, the first monolayer relaxes and now the two monolayer film both become triclinic. The lattice constants and angles, however, are not same as bulk triclinic pentacene. This polymorph of pentacene is referred to as the thin-film phase of pentacene.[2-4] Each monolayer of pentacene is approximately 16Å. The thin-film phase of pentacene persists for approximately 10 monolayers of pentacene or a total of approximately 16nm. Both of the monolayer and thin-film phase of pentacene are textured perpendicularly to the substrate.

After approximately 20nm of pentacene is deposited, the third polymorph of pentacene appears. This phase of penatcene is called the bulk-like phase, because it is the most the most relaxed phased and most similar to bulk pentacene. The bulk-like phase of pentacene forms islands on top of the ~10 monolayer of thin-film pentacene. This is classic Stranski-Krastonov film growth. The S-K islands are textured perpendicular to the thin-film phase of pentacene. The textured island growth of bulk-like pentacene continues until a total film thickness of approximately 40nm.[2-4]

After growing an approximately 60nm film of pentacene, texturing of the bulk-like phase stops, and untextured bulk-like pentacene crystals start growing on top of the

well textured film.[3-6] This thickness dependent film growth of pentacene is summarized in figure 4.1.

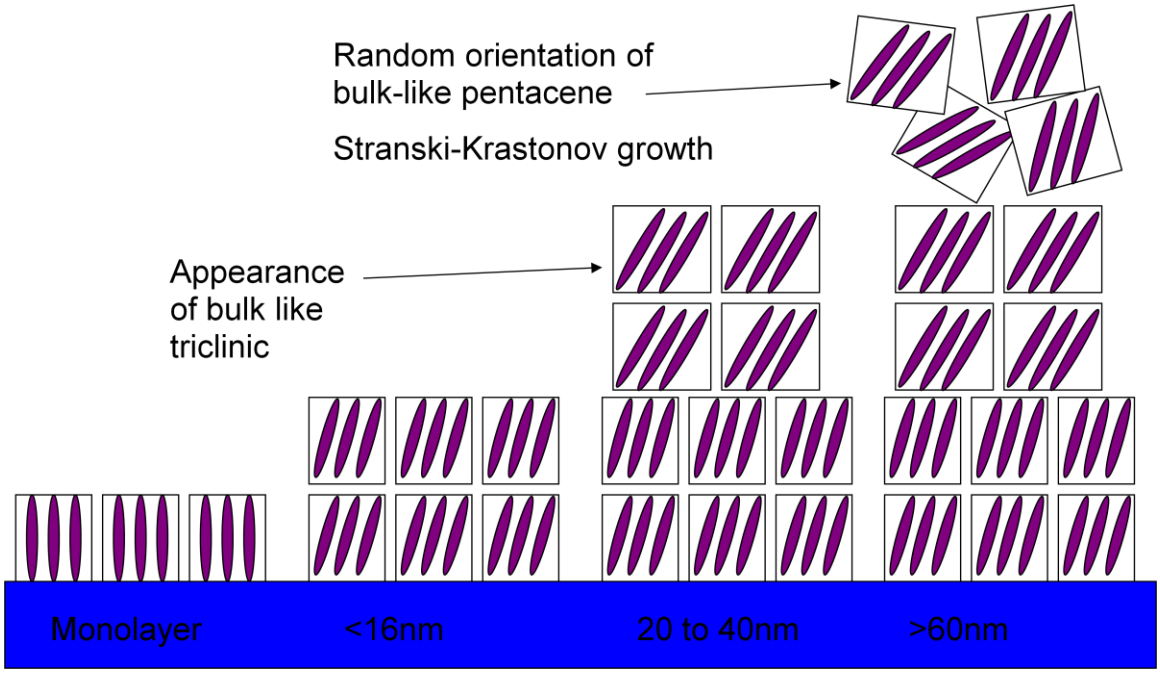

Figure 4-1: Summary of thickness dependent thin film growth of pentacene on oxide

The bulk triclinic phase of pentacene is the thermodynamically stable polymorph of pentacene. The orthorhombic monolayer of pentacene is the least stable phase of pentacene. The first monolayer takes the orthorhombic configuration because it matches the substrate energetically. Pentacene thin film growth is a good example of the Ostwald principle of thin-film growth. The Ostwald principle states that in thin-film growth the unstable phase condenses first before a more stable phase forms.

For high performance pentacene TFTs it is important to have large highly textured pentacene films with large crystallite sizes.[7] Mobility has also been shown to be higher in the thin-film polymorph versus the bulk-like polymorph.[8] Therefore, thermal evaporation of pentacene for pentacene-TFTs on a-SiO_2 is always evaporated slowly, at ~10Å/min, in order to encourage proper crystal ordering. Invariably slow evaporation is

coupled with substrate heating at ~70^{0}C to aid in pentacene molecular mobility and allow for grain growth.[9,10]

Currently, little is known about the growth of pentacene thin films using SAP. Solution processed pentacene TFT been made using this precursor is usually deposited onto the substrate drop-by-drop through inkjet printing or spinning. The deposited film is then heated on a hotplate at a fixed temperature anywhere from 120^{0}C to 200^{0}C for an arbitrary time. Little is known about the reaction rates of this precursor degradation. Neither is the film formation mechanism of this solid-state reaction known.

Currently very few studies have been performed to look at pentacene film from SAP. One study looked at the initial stages of film development using a Langmuir-Bloggett films of SAP two different substrates. It was found that a Volmer-Weber island growth was favored on the substrate with a lower surface free-energy, and a Stranksi-Krastonov growth was favored on the substrate with higher surface free-energy.[11] An X-ray study has been performed on the crystal structure of pentacene from SAP films,[12] however film development was not explored and a detailed study of film was not performed. Pentacene-TFTs from have been found to have the highest mobility the pentacene precursor is heated at 160^{0}C for approximately 5 minutes. The reason for the high mobility was not known.[13,14]

From the previous chapters the reaction rate has finally been measured using UV-vis. This information is useful to determine the minimum heating time to fully transform the precursor to pentacene. This chapter focuses to understand the growth of pentacene thin films on *a*-SiO_2 using SAP. The formation of pentacene thin films is traced using

SEM. AFM is used to look at the topology of these films and finally GIXD is used to identify the different pentacene phases.

Even though a fully solution processed organics TFT would never use *a*-SiO_2, however, *a*-SiO_2 is still the most commonly used gate dielectric material for pentacene TFT testing. Since, the growth of pentacene thin films through thermal evaporation onto *a*-SiO_2 is well understood and serves as a good reference point for comparison for pentacene thin-films through pentacene precursor.

4.3 Experimental Procedures

4.3.1 Preparing Pentacene precursor on Oxide

SAP was spun on standard undoped oxidized wafers. SAP solutions were prepared by dissolving the precursor into anhydrous chloroform stabilized with amylene from Aldrich (12mg/mL). SAP was prepared according to the methods in Appendix A,. Solutions were vortexed in a vortexer until the solute was fully dissolved. The solution has a clear to a light orange color. 1mL of solution was dispensed onto each wafer. Solutions were dispensed at 0 rpm. After dispensing the solution, the wafer was ramped up to 4000 rpm within 2s and spun at 4000 rpm for 30s. Finally, the wafer is diced into 1cm×1cm pieces.

4.3.2 Heating of conditions of samples to trace pentacene growth

Each sample was heated on a hotplate in a glovebox under dry nitrogen ambient. Table 4.1 shows all the time-temperature conditions which samples were heated at. Each sample was placed on a preheated hotplate and heated for the prescribed time. Once the

prescribed time is reached, samples are removed from the hotplate and placed ontop of a metal plate for cooling.

Temperature	Heating time
125	30s, 1m, 5m, 10m, 15m, 20m, 30m, 40m, 90m, 180m
130	15s, 30s, 45s, 1m, 2m 4m, 8m, 16m, 32m, 64m, 128m
140	15s, 30s, 45s, 1m, 2m 4m, 8m, 16m, 32m
150	15s, 30s, 45s, 1.5m, 4m, 8m, 16m, 32m
160	1s, 2s, 8s, 16s, 32s, 64s, 128s, 4m
170	1s, 2s, 4s, 8s, 16s, 32s, 64s, 2m
180	1s, 2s, 4s, 8s, 16s, 32s, 64s
190	1s, 2s, 4s, 8s, 16s, 32s
200	1s, 2s, 4s, 8s, 16s, 32s
220	1s, 2s, 4s, 8s, 16s, 32s
240	1s, 2s, 4s, 8s, 16s
260	1s, 2s, 4s, 8s, 16s

Table 4-1: Sample conditions for SEM

4.3.3 SEM imaging

SEM images were imaged at 5kV. Images process through the open source software The GIMP. Images were checked for number of pentacene nucleation sites. Crystal growth was monitored and measured by finding the characteristic length of pentacene islands. The characteristic length reported is the average value of multiple islands. The pentacene islands were measured by the scheme in figure 4.2. Finally, dewetting of films from the substrate was noted.

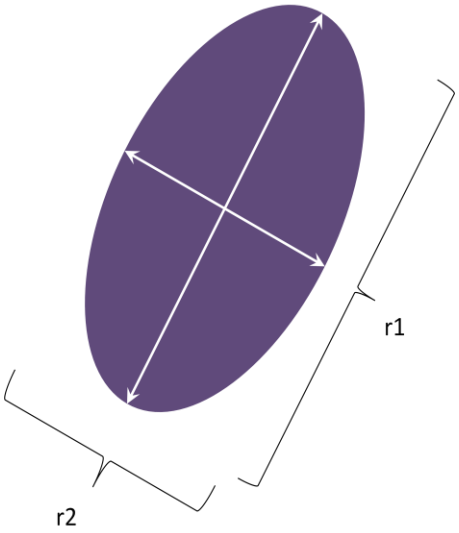

Figure 4-2: Calculation of characteristic length. $L_c = \sqrt{r1 \cdot r2}$

4.3.4 AFM imaging

On select samples, a surface topological image was taken using an AFM. All AFM images were taken through tapping mode surface contour measurements. Images were processed through the open source software Gwiddyon.

4.3.5 GIXD

GIXD was performed on another set of samples prepared the same way as noted above. Each sample was made into a 2cm × 2cm pieces. The heating conditions were according to table 4.2. Times were chosen to ensure that reactions have gone to completion.

Temperature	Heating times
125	180m
140	16m
160	2m
180	64s

Table 4-2: Sample conditions for GIXD

4.4 Results

4.4.1 Qualitative SEM results

There appear to be two temperature regimes of pentacene film growth, a low temperature regime (120^0C to 140^0C), and a high temperature regime (160^0C to 200^0C). At intermediate temperatures, there appears to be a mixed film growth resembling both high and low temperature film growth. At temperatures above 200^0C, there is rapid pentacene film formation and a large amount of film dewetting from the substrate.

4.4.1.1 Qualitative description of low-temperature film growth

For low temperature film development at 125^0C, white pentacene crystals islands are clearly visible after heating the precursor for 30s (figure 4.3). At this point, most of the film is still unreacted pentacene precursor, this seen as the dark parts around the white islands. Each island indicates a nucleation sites. The islands all have approximately the same size. With continued heating, the islands continue to grow and are clearly polycrystalline (figure 4.4). The polycrystalline islands clearly look like a group of triclinic crystals merged together. This is expected because pentacene usually takes a triclinic crystal structure.[6] After more time, the polycrystalline islands stop growing in size, even though the film has not fully reacted. Around the poly crystalline island, there is clear growth of a pentacene thin film.

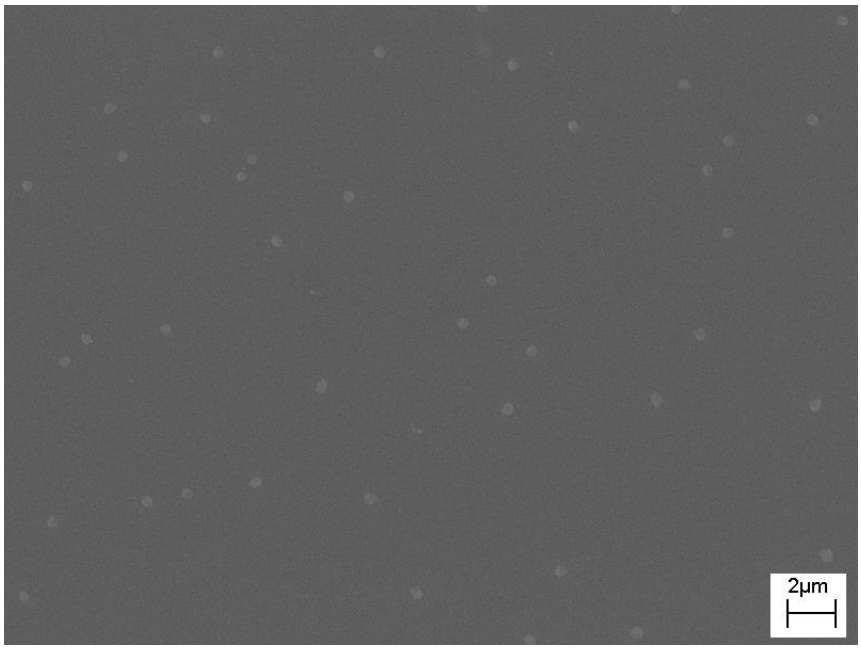

Figure 4-3: Nucleation of pentacene (125^{0}C, 30s)

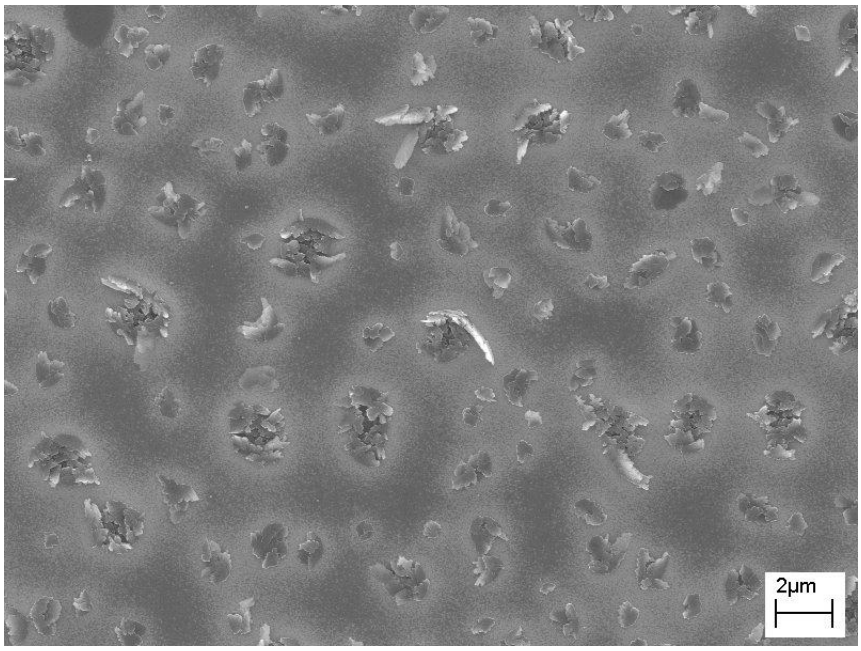

Figure 4-4: The initial nucleation sites have become polycrystalline islands. The light gray around the islands is a thin film of pentacene. The smaller islands are SK islands on top of the thin film. (125^{0}C,30min)

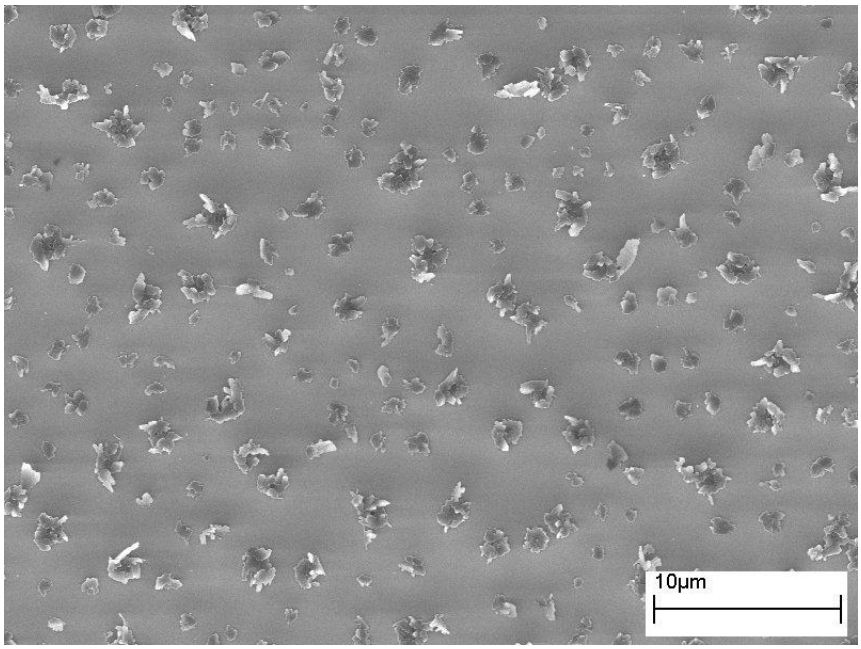

Figure 4-5: fully reacted pentacene film (125^{0}C, 3hr)

As the pentacene thin film grows and covers the regions around the polycrystalline islands with pentacene, small pentacene islands grow on top of the pentacene thin film. Again these islands have the characteristics of a triclinic crystal (figure 4.4). These small islands are seen starting after 10 minutes of reaction time.

After three hours of heating, the pentacene precursor should be fully reacted; all three aforementioned features are clearly visible, the polycrystalline islands, pentacene thin-film around the islands, and smaller islands on top of the thin film (figure 4.5). Small pentacene islands growing on top of a pentacene film matches the description of typical Stranski-Krastonov film growth. This is again expected, because pentacene grows in S-K mode when evaporated on top of oxide.[2,15]

4.4.1.2 Qualitative description of high temperature film growth

For films processed at 160^{0}C to 200^{0}C, the formation of a pentacene thin-film looks completely different than the formation of a pentacene thin-film below 130^{0}C.

There does not appear to be any of the low temperature island nucleation sites. Instead there are large black spots which appear during the early parts of the precursor reaction (figure 4.6). The spots are blurry and difficult to focus with SEM. These spots are located at the interface between pentacene precursor and the oxide and not in the precursor matrix.

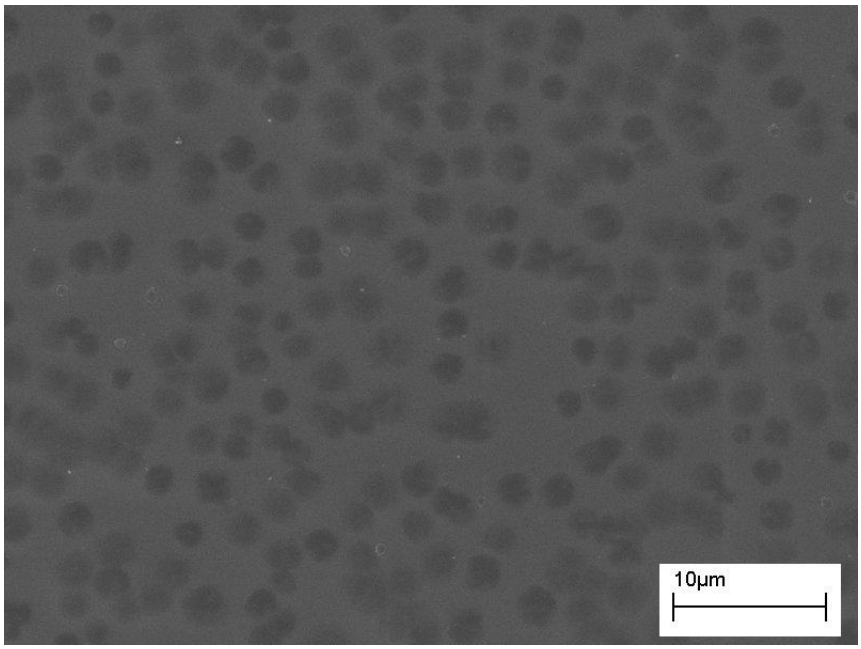

Figure 4-6: High temperature nucleation. (150^0C, 15s)

As heating time is increased, the spots become larger, but the size quickly becomes fixed. After more heating, the spots become more visible and easier to focus, crystallines edges characteristic of a triclinic crystal lattice once again start appearing (figure 4.7). Instead of large islands, these spots end up looking like flat plateaus. The boundaries of the islands are distinct and only a little bit larger than the original black spots which appeared early in film formation.

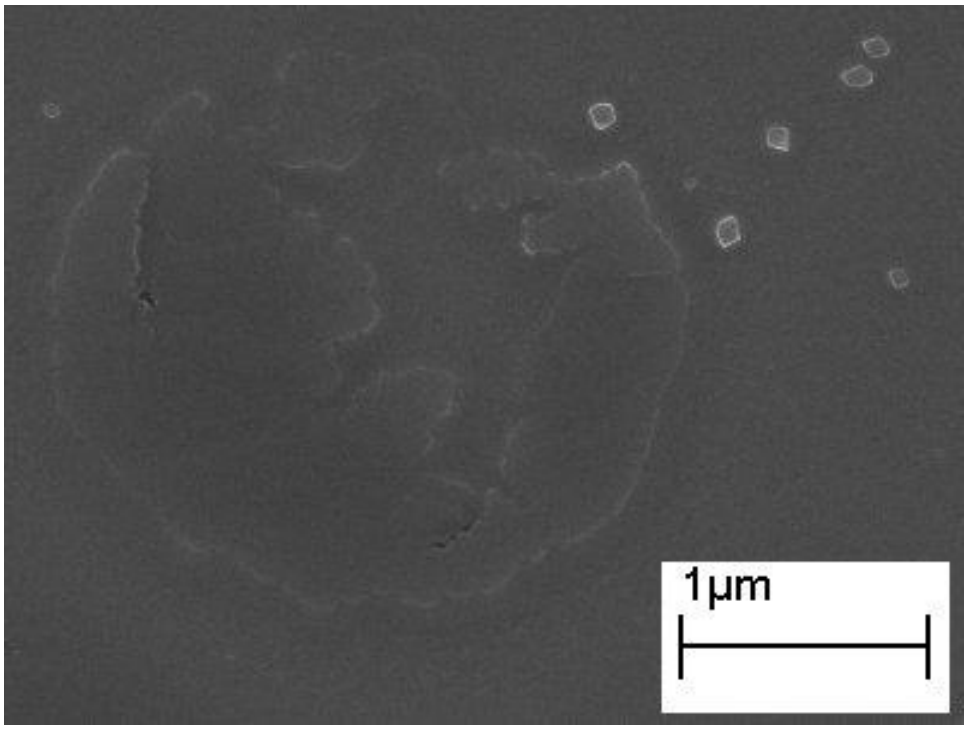

Figure 4-7: Crystal grown on the high temperature nucleation. (150^{0}C, 45s)

Once the reaction is complete, around the plateaus there is dewetting (figure 4.8), which is highly visible for films processed above 180^{0}C. For films processed at a lower temperature there is less dewetting, and a thin film of pentacene is formed in between the plateaus instead. On top of the thin film, smaller pentacene islands also grow, once again showing typical Stranski-Krastonov film growth.

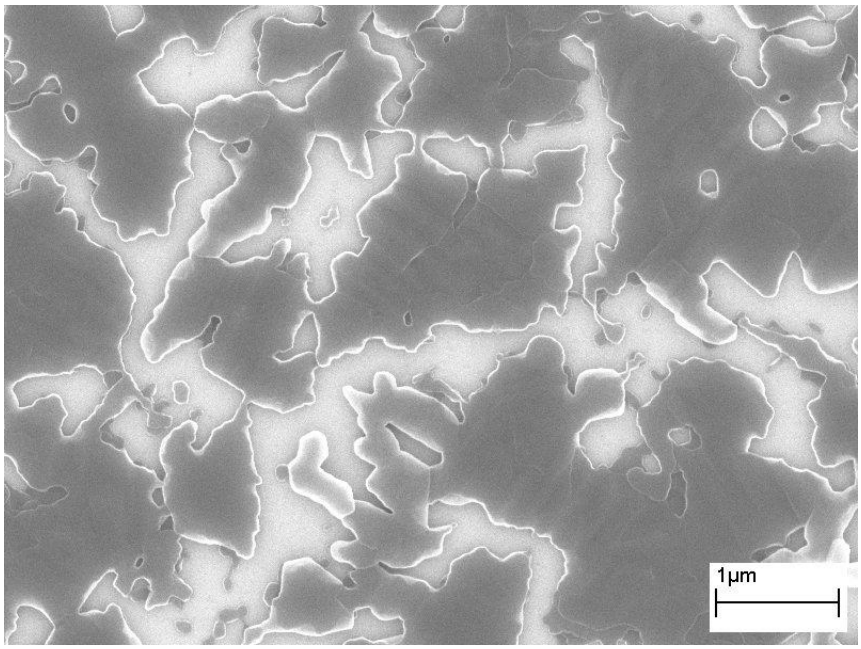

Figure 4-8: Dewetting on fully develop films. (180^{0}C,1min)

4.4.1.3 Qualitative description of film grow at intermediate temperatures

At intermediate temperatures (140^{0}C - 160^{0}C), a mixed film growth occurs. After 15 seconds of heating at 140^{0}C, both the low temperature islands appear as well as high temperature black nucleation spots (figure 4.9). As the reaction proceeds the size of the low temperature islands grow slightly. It appears that material preferentially goes to the high-temperature black nucleation spots instead of the low temperature nucleation sites(figure 4.10). After 4 minute of heating at 140^{0}C crystalline edges appear on the black nucleation spots (figure 4.10).

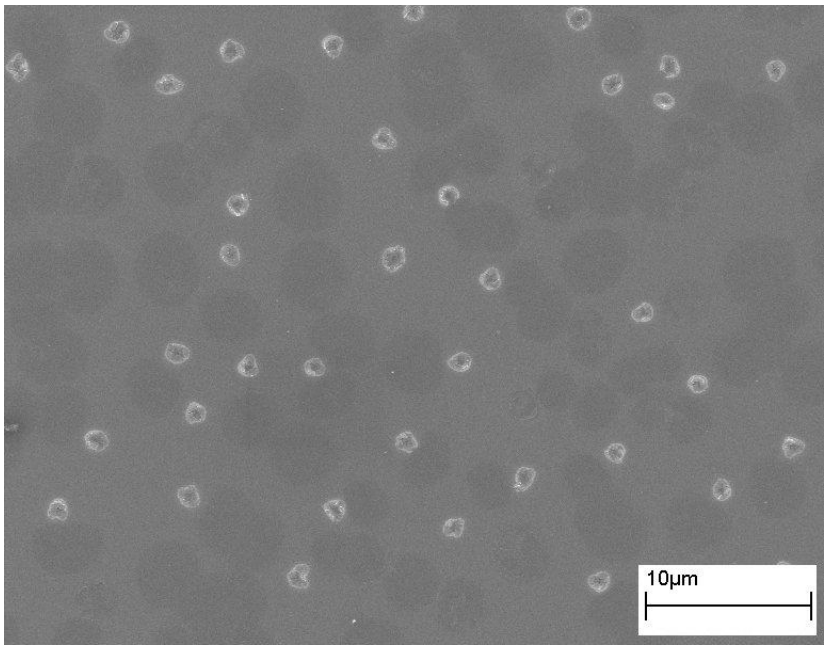

Figure 4-9: Mixed nuclation (140^{0}C, 1min)

After 4 minutes of heating, a thin film of pentacene has formed around the low temperature islands. Once again small islands developed on top of the thin film. The high temperature spots develop as it would at high temperatures, however, are not as "complete" as at high temperatures. Instead of forming a flat plateau, a "crescent" shape is formed instead (figure 4.10).

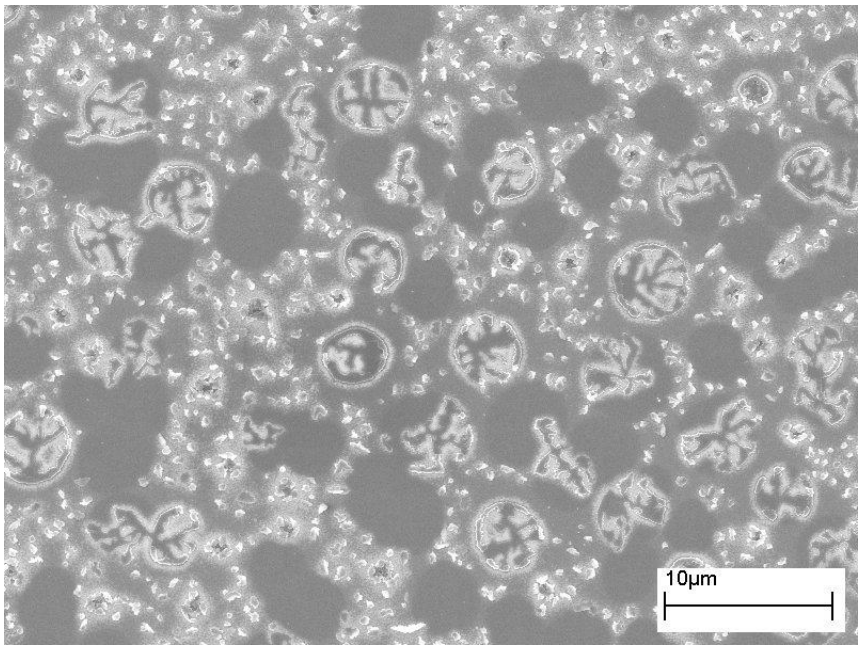

Figure 4-10: Crystal grown on mixed nucleation (140^0C, 4min).

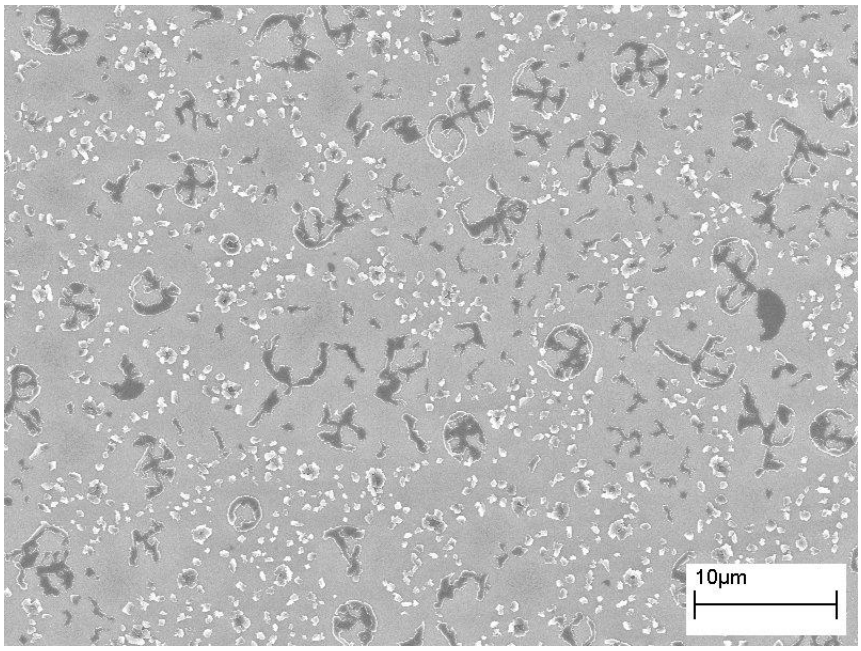

Figure 4-11: Fully reacted pentacene film (140^0C, 32min).

At 150^0C, the low temperature islands grow significantly less than the black high temperature nucleation. The final fate of the low temperature islands is difficult to determine because there were very few low temperature islands formed. From the

conception of the low temperature islands to the time the film fully develops, little growth occurs with the low temperature islands, so the islands are difficult to identify after the film is fully developed. The black high temperature islands once again becomes crescents once films are fully developed (figure 4.12). As usual, small S-K islands growing on top of the thin film in between the crescents. The small S-K islands are smaller and become more numerous at 150^0C in size versus 140^0C.

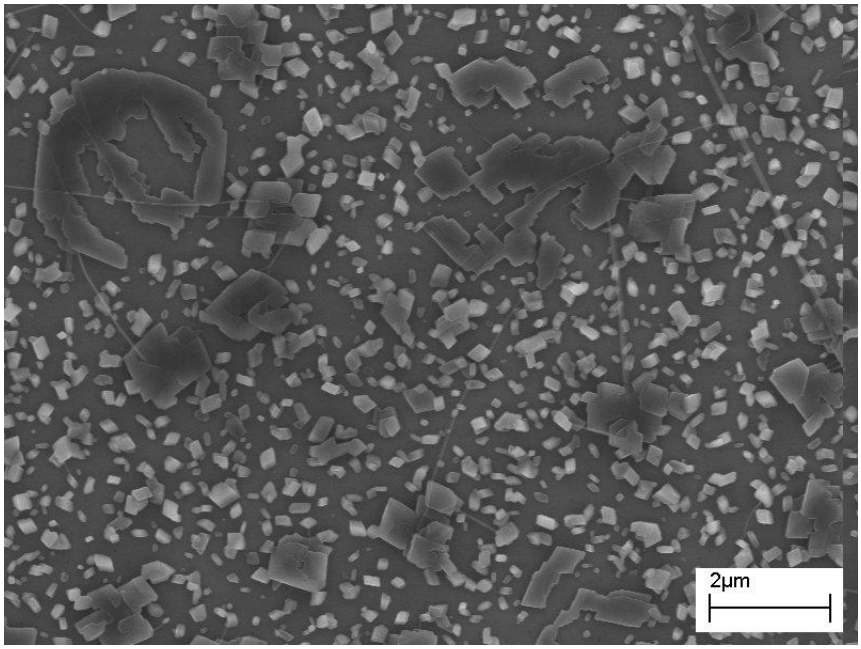

Figure 4-12 Fully reacted pentacene film (150^0C, 16 min). Note that the SK-islands are more numerous than compared to 140^0C.

4.4.2 Quantitative SEM results

For each SEM image, the size and density of both low temperature islands and high temperature black spots were counted and the characteristic lengths were measured.

4.4.2.1 Nucleation sites

Both the high temperature and low temperature nucleation density remain relatively constant throughout film formation. In other words from beginning to end of film formation there does not seem to be an increase or decrease of nucleation sites for both types of nuclei (figure 4.13 and 4.14). However, as processing temperature increases the number of low temperature nuclei decrease while the number of high temperature islands increase. Figure 4.14, summarizes the interplay between low temperature nuclei and high temperature nuclei. Low temperature islands were observed in films process from 125^0C to 150^0C. High temperature nucleation spots were observed starting at 140^0C. At temperatures above 160^0C, low temperature islands are no longer observed. The formation of low temperature islands becomes less favorable as temperature increases and the high temperature nuclei become more favorable.

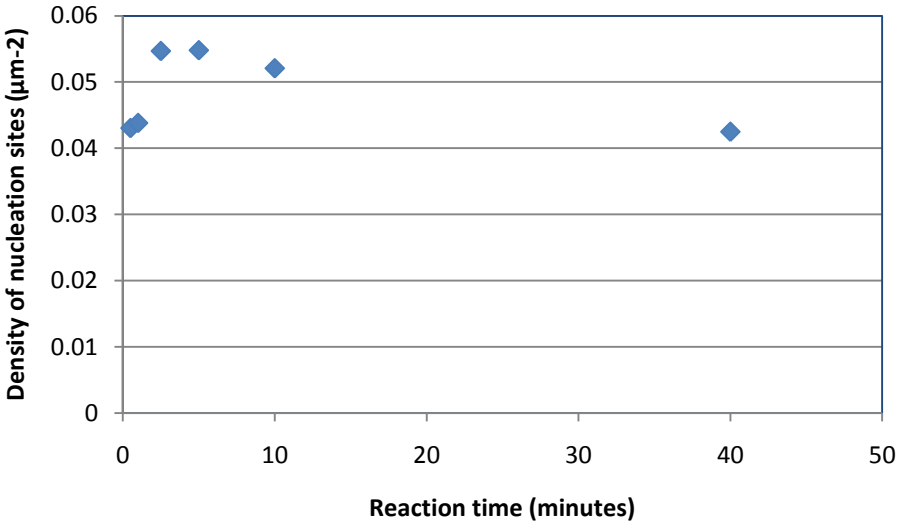

Figure 4-13: Density of nucleation sites stays constant throughout film development at 125^0C. This is true for all films at low temperatures.

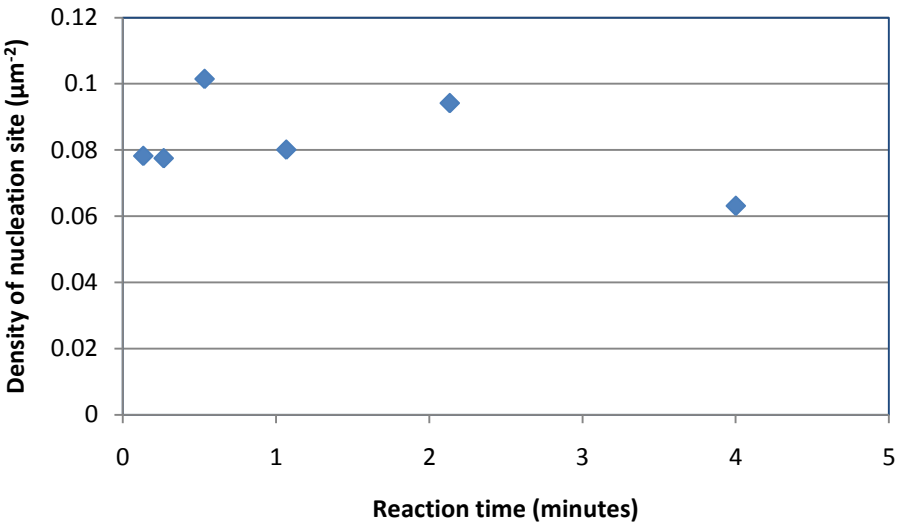

Figure 4-14: Density of nucleation sites stays constant throughout film development at 160^{0}C. This is true for all films at high temperatures.

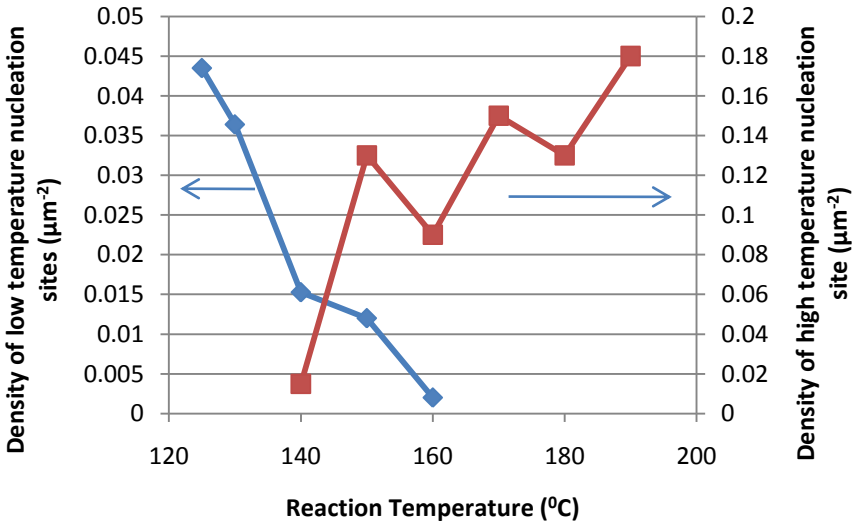

Figure 4-15: Temperature interaction between high and low temperature nucleation sites.

Not only does the density of low temperature islands decrease with increased temperature, but the final characteristic length of the low temperature islands also decreases with increased temperature. The high temperature plateaus increase in density with increased reaction temperature and decrease in characteristic length with increased temperature (figure 4.16).

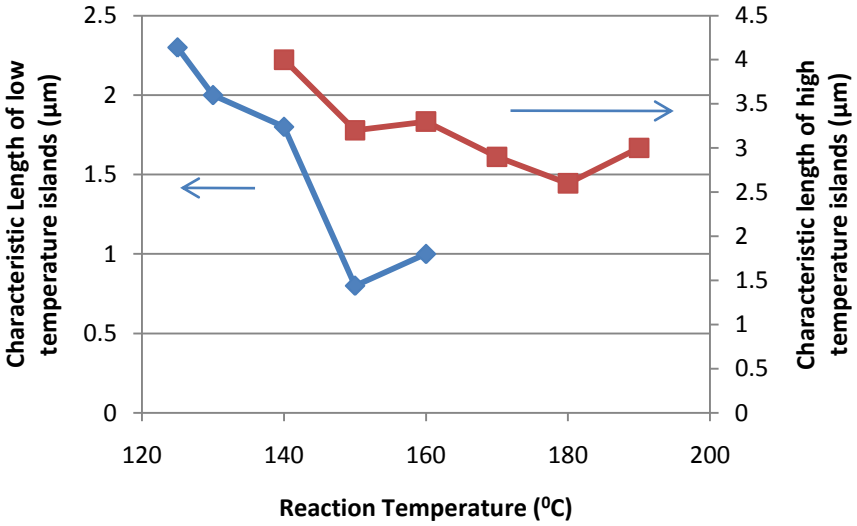

Figure 4-16: The effect of temperature on the final size of both high and low temperature islands.

4.4.2.2 Crystal Growth

Absolute time cannot be used to compare samples reacted on temperature, because from one temperature to another, reaction rates differ, so the amount of pentacene available for film formation is different for each sample. When comparing between samples processed at different reaction temperatures, instead of using absolute time, time was normalized to the reaction rate (real time×reaction rate). This way, samples with different reaction temperatures can be compared to each other. Normalized

time (τ) indicates the percentage of starting material that reacted. For example, at τ of 0.69 shows that 50% of the starting material has finished reacting.

Figure 4.17, indicates that lateral low temperature islands growth ceases at a later τ than at higher temperatures. In terms of reaction completion, this means that as the reaction temperature is increased the supply of pentacene to low temperature islands stops at an earlier stage of reaction, but instead pentacene is supplied to the high temperature nuclei, therefore low temperature island growth is stunted, and high temperature features dominate.

Figure 4.17 also shows the τ when high temperature plateaus stops lateral growth. The plot shows some fluctuations, however is probably actually constant. Unfortunately, the samples were not created such that each reaction temperature has the same exact number of samples and with each the corresponding τ for each temperature. Hence the fluctuation in the data is from lack of data points.

In the intermediate temperature range, where high temperature and low temperature nuclei form, the τ where lateral growth stopped is approximately the same τ for both high temperature plateaus and low temperature islands.

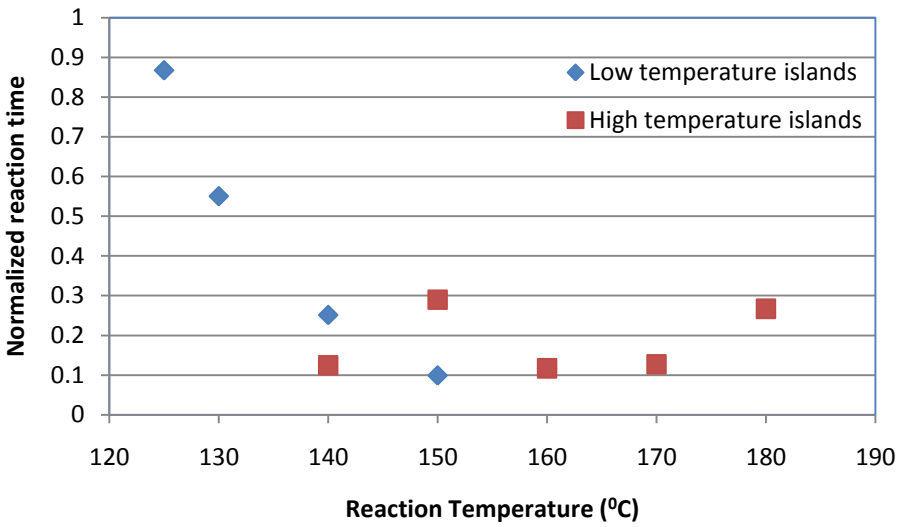

Figure 4-17: The effect of temperature on the time of lateral island growth stops.

4.4.3 AFM results

AFM was used to find the topology of SAP films at various phases of film development. By looking for defects in unreacted films of pentacene precursor, it was found that the spun-on pentacene precursor films on oxide were approximately 25-40nm in thickness.

4.4.3.1 AFM images for films processed at 125^0C

AFM images for film processed at 125^0C for only 5 minutes were taken (figure 4.18). The image shows a valley at the base of low temperature islands showing the consumption of pentacene precursor around islands. The cross-section of an island, shows that the valley is approximately 40 nm deep, which is the thickness of the precursor film.

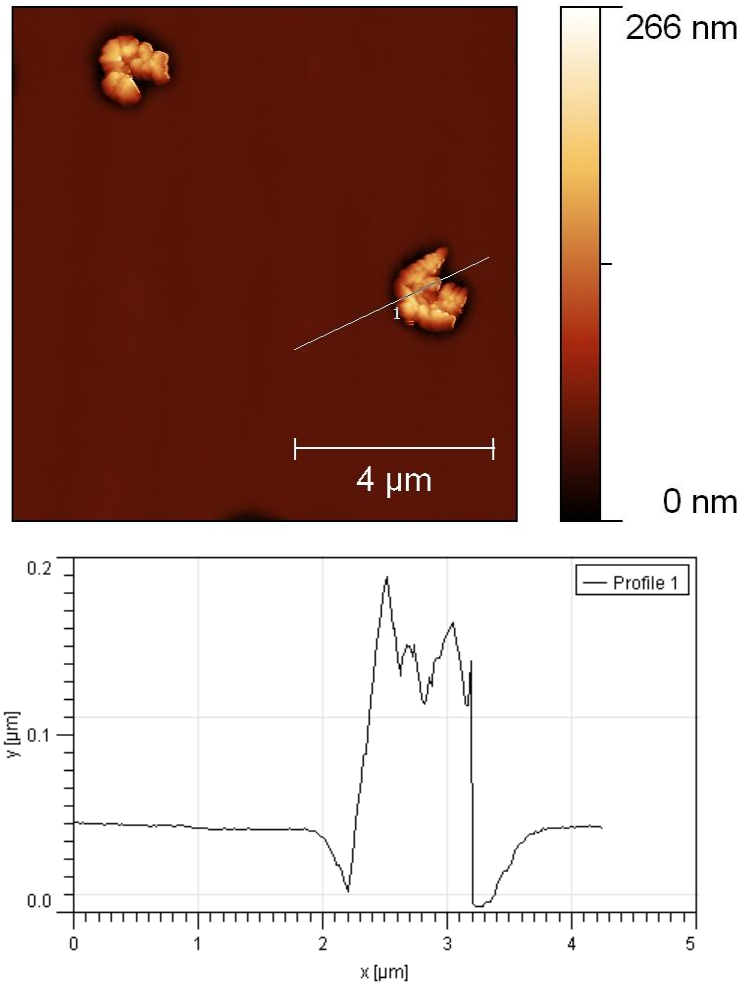

Figure 4-18: AFM of low temperature islands. Pentacene precursor consumption around the islands is quite apparent. (125^{0}C, 5min)

4.4.3.2 AFM images for films processed at 160^{0}C

An AFM images taken of SAP films processed at 160^{0}C for 4 seconds showed the the early stages of pentacene film development (figure 4.19). This was to specifically image the high temperature nuclei. The thickness of these spots were measured to be anywhere from 1.5nm to 3nm. This corresponds to 1 to 2 monolayers of pentacene respectively. This is strong evidence that at high temperatures nucleation of pentacene forms monolayers of pentacene on top of the oxide, instead of forming islands as seen at

low temperatures. It should be noted that because these monolayers form at the interface of the oxide to the pentacene precursor. AFM measurements are not actually in contact with the pentacene itself, but with the unreacted precursor instead. The formation of the pentacene monolayers create a bump in the top surface of the uncreated precursor on top of the monolayer, therefore the actual thickness of these pentacene monolayers are merely an estimate.

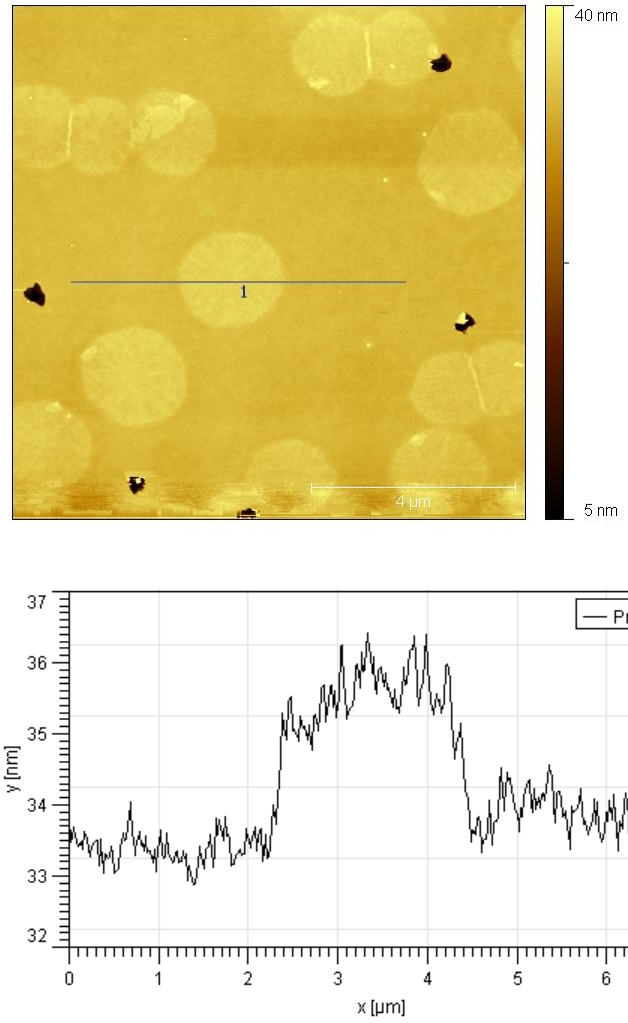

Figure 4-19: AFM of a high temperature nucleus. The thickness of nucleus corresponds to approximately 1 monolayer of pentacene. (160^0C, 4s)

4.4.3.3 AFM images of fully developed films at different temperatures

AFM images of fully reacted films processed at 125^0C and one processed at 180^0C (figure 4.20) were used to find the rms roughness of films. The rms roughness of both films was found (table 4.3). The film at high temperatures was much smoother than low temperature films. This makes sense from what was has already been deduced from SEM and AFM. Pentacene formation at low temperatures creates islands, while pentacene formations at high temperatures is formed layer by layer. Based on the roughness values at 180^0C, this roughness is very much a result of dewetting of the pentacene from the substrate. Without dewetting, high temperature pentacene films would be quite smooth. Pentacene formed at low temperatures initially start with island formation, so the final film consists of many large islands, hence making the final film extremely rough due to many valleys and peaks.

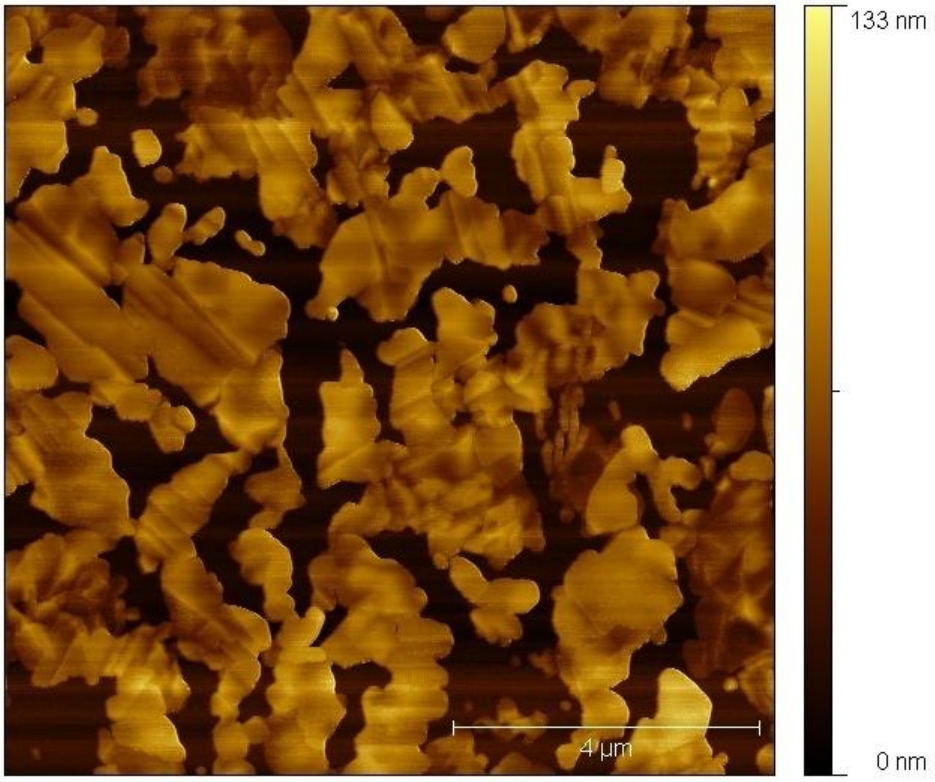

Figure 4-20: AFM a fully reacted film showing dewetting. (180^{0}C, 1min)

Temperature	125	180
RMS roughness (nm)	127	25.5

Table 4-3: Roughness of films

4.4.4 GIXD Results

Texturing was the most prominent at 160^{0}C (figure 4.23), where the mixed reflections are clearly seen, and the arcing is the least. As temperature is decreased from 160^{0}C, the spots blur and large arcs are seen instead. Moving from 160^{0}C to a higher temperature, the arcing is also larger compared to arcing at 160^{0}C. This indicates that surface texturing is maximized at 160^{0}C. However, comparing the degree of texturing at 180^{0}C (figure 4.24) vs. 125^{0}C (figure 4.21), it is still much more textured at 180^{0}C than at

125^0C. Low temperature films are more disordered versus higher temperature films. This shows that the low temperature crystals grow independent of the substrate and the crystal orientation is random. The high temperature islands are textured perpendicular to the substrate showing that the substrate plays a role in high temperature crystals.Only bulk-like pentacene was found on the low temperature samples (figure 4.21). Both thin-film and bulk-like phase was found on pentacene films processed at higher temperatures. The thin-film phase is seen through the doubling of peaks in the 300 planes (figure 4.22-24). The double peaks show that there are two 300 planes in existence, showing two morphotypes coexisting. The peak doubling is only seen in higher temperatures and not lower temperatures.

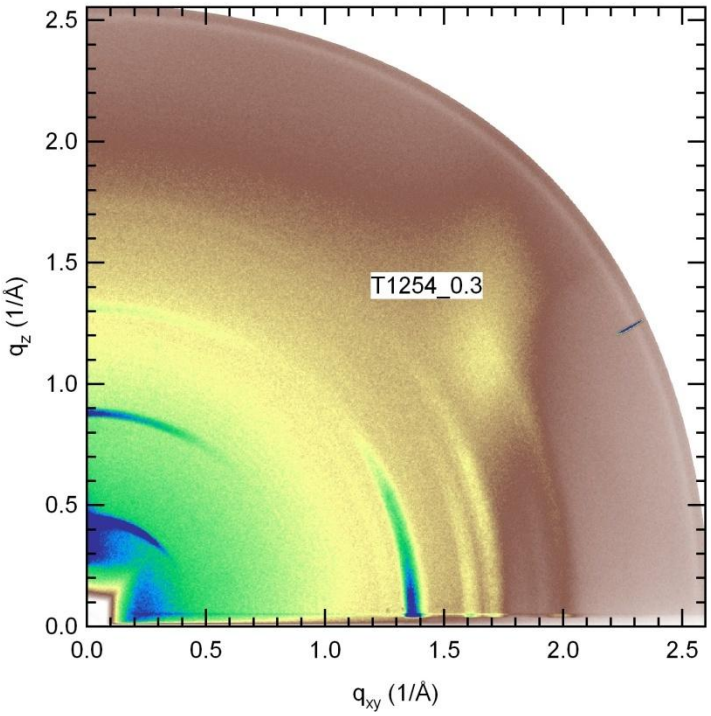

Figure 4-21: 2D GIXD plot for a film processed at 125^0C

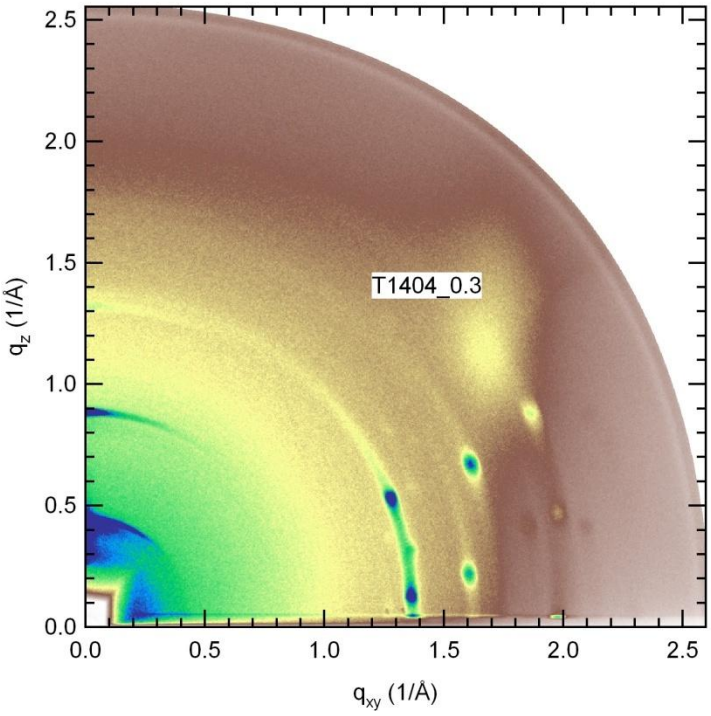

Figure 4-22: 2D GIXD plot for a film processed at 140^0C

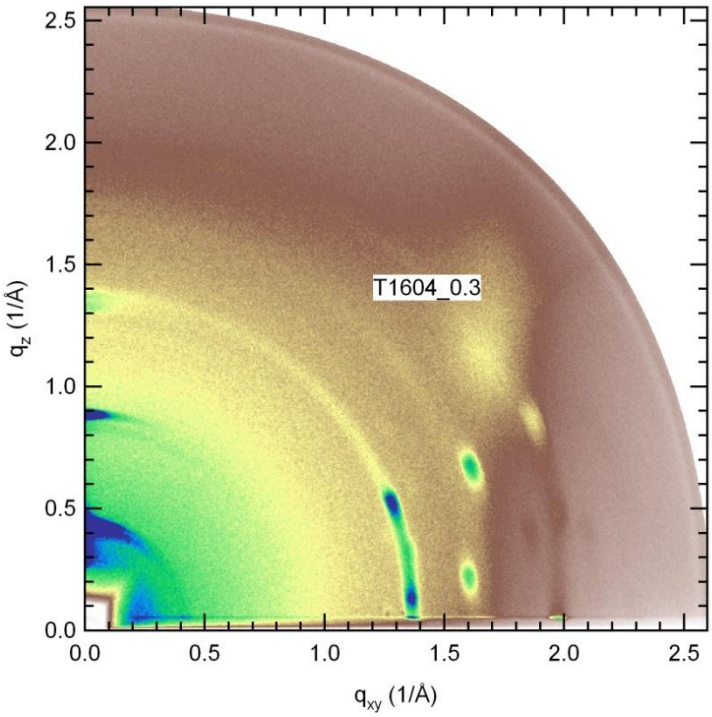

Figure 4-23: 2D GIXD plot for a film processed at 160^0C

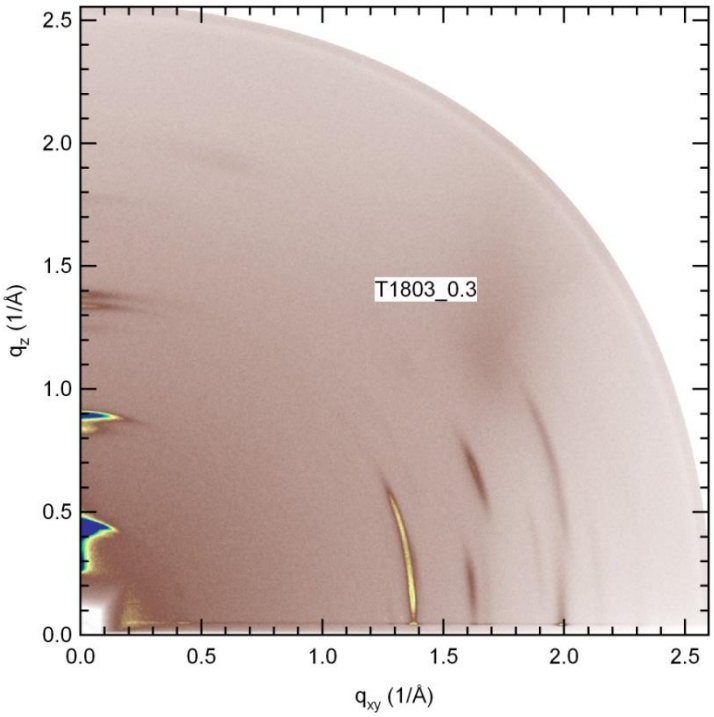

Figure 4-24: 2D GIXD plot for a film processed at 180^0C

The 100 peak was measured in higher resolution using the 7-2 beam line. By measuring the 100 peaks width the comparison of crystallite size can be calculated. For simplicity the crystals were assumed to take on a cubic structure, hence the extracted crystal size is merely an estimated (figure 4.25). The diffraction patterns suggest that at low temperatures the crystallite sizes are largest since the peaks the narrowest. As temperature increases, the crystallite size decrease since the peaks are more spread out. This shows that at low temperatures, slow crystal growth promotes the increase of crystallite size, whereas at high temperatures fast growth of crystal promotes nucleation of pentacene crystals but decreases the crystallite size. Unfortunately, there was not enough time to use the high resolution diffraction to obtain the crystallite size of at 125^0C. However, from the 2-D low resolution plots, it can be seen that the 100 peak at

125^0C is much narrower than the other processing temperature, indicating a larger crystallite size.

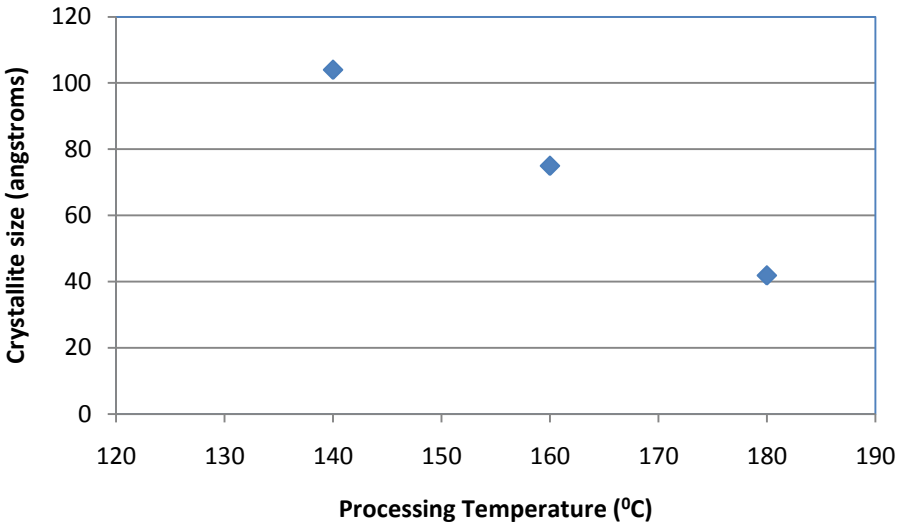

Figure 4-25: Crystallize size due to processing temperature

4.5 Discussion

From the SEM images, the existence of two modes of pentacene nucleation can be seen; one at low temperatures (120^0C-130^0C) and one at high temperatures (160^0C+). Both modes of nucleation showed a constant density with respect to reaction time. However, there is a change in nucleation density with respect to temperature. Previously, it was suggested that this indicates a heterogeneous mode of nucleation, where defects on the substrate helps catalyze nucleation of pentacene. However, the increase of nucleation density from temperature may indicate that the nucleation density affected by the precursor more than the substrate, and that the formation of nuclei is homogenous and not heterogeneous. The formation of pentacene nuclei in the precursor can be thought of as inclusion forming in a matrix, and the temperature changes the density of inclusions

which are formed, homogenously. The thought of inclusions in a matrix parts from the paradigm of thin film formation where the substrate plays an important role in crystallization. The appearance of two types of nuclei, where one seems to be substrate dependent shows that thin-film ideas are definitely at play. Therefore, there is both thin-film mechanism as well as bulk solid crystallization mechanisms at work.

At low temperatures, the reaction is extremely slow. Therefore the supply of the pentacene for film formation is very slow. Due to the slow reaction pentacene molecules have time to arrange themselves slowly. With the help of the matrix to stabilize pentacene crystals along with the slow crystal growth the thermodynamic product (bulk-like phase) is formed at low temperatures. This explains why no texturing is seen at low temperatures. Since the bulk-like phase is unstable on top of oxide, the bulk-like phase has no regards for the substrate and grows in arbitrary orientations. The exclusive growth of the bulk-like phase is not seen in thermal evaporation. This results because during evaporation, the supply of pentacene to the substrate is much faster than the supply of pentacene to the substrate from SAP reaction at low temperatures. Also with thermal evaporation, there is not a stabilizing matrix to help the bulk-like phase to grow.

The low temperature nuclei eventually form large polycrystalline islands. This further indicates the unfavorable interactions between the pentacene and oxide. An upward growth in lieu of a lateral growth is an attempt to minimize substrate interactions with pentacene. The vertical growth of islands is stopped as SAP around islands is consumed. The size of pentacene islands is limited by SAP film thickness.

Due to the low molecular mobility of pentacene at the low temperatures, not all pentacene molecules are able to travel to islands and aid in islands growth, instead a thin

film of pentacene also grows between islands. Once the thin film of pentacene grows, small pentacene islands nucleate on top of the thin film. Due to the slow reaction rate of the pentacene at low temperatures, crystallites are allowed to grow much larger. For the same reasons, these islands are larger at lower temperatures vs. higher temperatures.

At high temperature the appearance of pentacene is quite rapid, creating a different type of pentacene nuclei and the less stable thin-film phase forms. Here the growth looks more like pentacene growth through evaporation layer-by-layer. Pentacene nucleation starts as thin film phase monolayers of pentacene instead of islands. The formation of the thin-film phase is caused by a substrate interaction. The fact that the thin-film phase forms at higher temperature shows that as reaction temperature increases, the energetic effect of the substrate also increases, and the matrix plays a smaller energetic role in nucleus formation. Physically what may be happening is that an increased in processing temperature increases the reaction rate of pentacene conversion. This translates to an increased rate of pentacene appearance. Kinetic products are usually favored in lieu of the thermodynamic product during rapid reactions, so the thin-film phase is favored.

Since the substrate plays a role in the film formation, texturing perpendicular to the substrate is observed; similar to what is seen in evaporated pentacene. With the help the SAP matrix, after the formation of a few layers of the thin-film phase the bulk-like phase starts to grow. Due to the help of the matrix, pentacene is able to relax much faster than on evaporated film. This explains why so little thin-film phase of pentacene is formed. Due to the negative interactions between the pentacene and oxide, pentacene preferentially grows upward instead of laterally and causes dewetting on the substrate.

When the temperature is raised even higher, the reaction rate increases and nucleation sites became extremely numerous. Crystal growth also become even more rapid. Both these factors create small pentacene crystals. Furthermore texturing is slowly lost from rapid nucleation and crystal growth.

At intermediate temperatures, both types the high temperature and low temperature nuclei are formed. The ratio of high:low temperature nuclei depends on the reaction temperature. At higher temperatures, the high temperatures nuclei dominate and become more numerous. When the high temperature nuclei coexist with the low temperature nuclei, crystal growth from the high temperature nuclei is preferential over the low temperature nuclei. Since the high temperature nuclei are large flat spots, these nuclei formed a stable surface for pentacene crystals to grow on top of. The growth of low temperature islands require pentacene molecule to grow laterally as well as vertically, lateral growth is always unfavorable because it requires an unfavorable interaction with the substrate.

Also, at intermediate temperatures pentacene does not dewetting from the substrate, instead a thin film of pentacene grows between both the high temperature plateaus and low temperature islands. SK islands form on top of pentacene thin film. At high temperatures, the SK islands are smaller and more numerous due to the rapid supply of pentacene. At lower temperatures there are larger but fewer SK islands, because of the slow supply of pentacene. Figure 4.26 summarizes the effects of time and temperature on growing pentacene films on oxide.

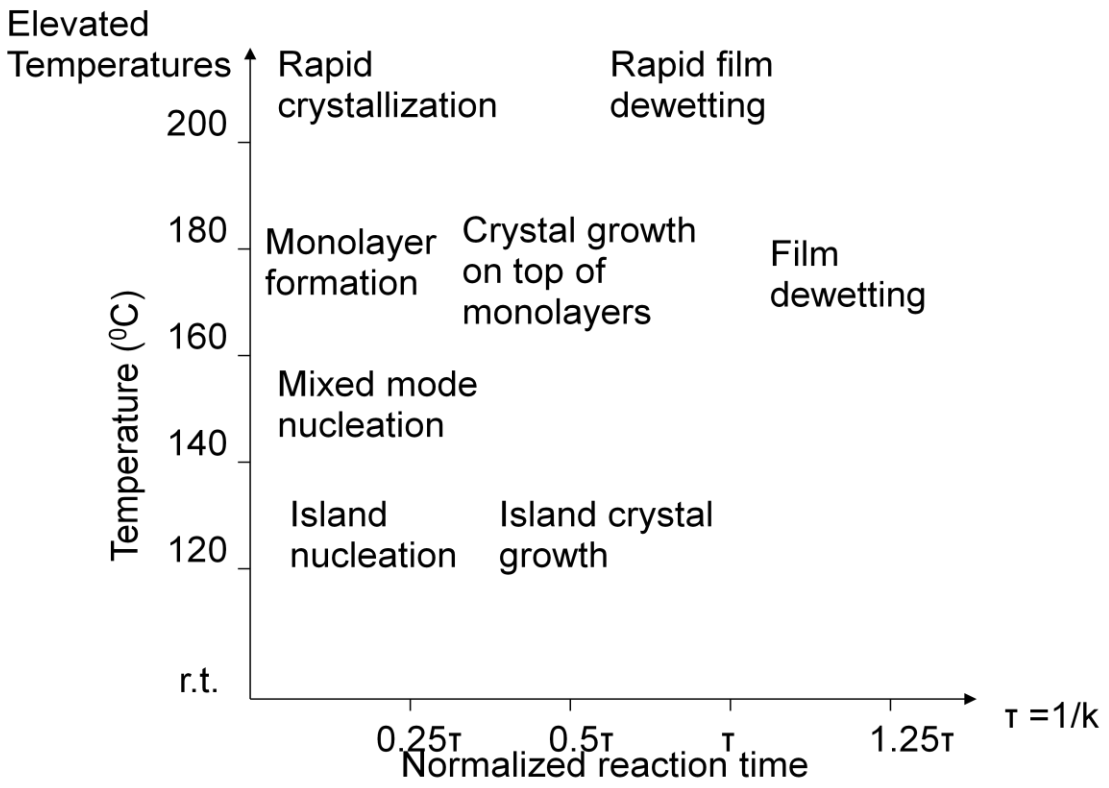

Figure 4-26: Time-temperature dependency on pentacene film growth from SAP.

The trends previously observed in TFT measurements can now be explained from the knowledge gleamed from pentacene film formation. The highest mobility is reported at intermediate temperatures.[14] The peak mobility falls between 150^0C and 160^0C. GIXD data show that there is the highest amount texturing in that particular temperature range. The thin-film phase of pentacene is also present in that temperature range. The high texturing and existence of the thin-film phase helps to give high mobility. Texturing is extremely low at 125^0C, and only the bulk-phase of pentacene is observed and gives low mobility. At 180^0C, the mobility should also be low compared to intermediate temperatures.

Even though at this temperature there is the thin-film phase and some texturing, however, the texturing at this temperature is lower than at intermediate temperatures. At

high temperature the rapid growth of films causes disorder, so texturing is lost. The rapid growth of crystals also decreases the crystal size. Finally, dewetting is pronounced at 180^0C. Decreased texturing, small crystal size and dewetting all contribute to the low mobility at high temperatures.

Regarding on/off ratios, at high temperatures the on/off ratio is the highest. Films processed at high temperatures have the fewest defects as well as miscellaneous byproducts from the precursor degradation giving the highest on/off ratio. The amount of byproducts and defects at lower temperatures keeps the on/off ratio relatively low.

As a final note, it is interesting that the thin-film phase persists in the high temperature film. All pentcene films in this study were processed above 120^0C in order for the reverse Diels-Alder reaction tp proceed. Literature reports that the thin-film phase relaxes to the bulk-like phase at when pentacene films are heated above 90^0C showing lower mobility.[12] Luckily, the thin-film phase still persists and the possibility of high performacen SAP-pentacene TFT may be possible.

4.6 Conclusion

The film growth of pentacene on oxide through thermal degradation of SAP has been reported. It has been shown that the film morphology is temperature dependent and reaction rate limited. Two different two types of nuclei can form depending on the processing temperature. At low temperatures an island-like nucleation occurs. Crystallite are large and highly disordered. Only the bulk-like polymorph of pentacene can be identified. At high temperatures, the film growth is more similar to pentacene film growth through thermal evaporation. Initial film growth is through layer by layer growth forming the thin-film phase. After a few monolayers the bulk-like phase forms.

These films have smaller crystallites, but are highly textured. At 160^0C, the film morphology is the most conducive for high mobilites, which explains why processing SAP at this temperature has been able to give the highest mobilites on TFTs made in the past.

4.7 References

1. CAMPBELL, R., TROTTER, J. & ROBERTSON, J. CRYSTAL AND MOLECULAR STRUCTURE OF PENTACENE. *ACTA CRYSTALLOGRAPHICA* **14**, 705-&(1961).
2. Fritz, S.E. et al. Structural Characterization of a Pentacene Monolayer on an Amorphous SiO2 Substrate with Grazing Incidence X-ray Diffraction. *Journal of the American Chemical Society* **126**, 4084-4085(2004).
3. Cheng, H. et al. Thickness-dependent structural evolutions and growth models in relation to carrier transport properties in polycrystalline pentacene thin films. *ADVANCED FUNCTIONAL MATERIALS* **17**, 3639-3649(2007).
4. Bouchoms, I. et al. Morphology identification of the thin film phases of vacuum evaporated pentacene on SIO2 substrates. *SYNTHETIC METALS* **104**, 175-178(1999).
5. Puigdollers, J. et al. Pentacene thin-films obtained by thermal evaporation in high vacuum. *THIN SOLID FILMS* **427**, 367-370(2003).
6. Endres, R. et al. Structural and electronic properties of pentacene molecule and molecular pentacene solid. *COMPUTATIONAL MATERIALS SCIENCE* **29**, 362-370(2004).
7. Kang, G.-. et al. The electrical characteristics of pentacene-based organic field-effect transistors with polymer gate insulators. *Current Applied Physics* **5**, 297-301(2005).
8. Ji, T., Jung, S. & Varadan, V.K. On the correlation of postannealing induced phase transition in pentacene with carrier transport. *Organic Electronics* **9**, 895-898(2008).

9. Salih, A. et al. Improved thin films of pentacene via pulsed laser deposition at elevated substrate temperatures. *APPLIED PHYSICS LETTERS* **69**, 2231-2233(1996).
10. Gundlach, D. et al. Pentacene organic thin-film transistors - Molecular ordering and mobility. *IEEE ELECTRON DEVICE LETTERS* **18**, 87-89(1997).
11. Musumeci, C. et al. Surface effects on the growth of solution processed pentacene thin films. *SURFACE SCIENCE* **602**, 993-1005(2008).
12. Akinaga, T. et al. Analysis of molecular aggregation states in pentacene thin films prepared from soluble precursor. *CHEMISTRY LETTERS* **35**, 1162-1163(2006).
13. Molesa, S. et al. A high-performance all-inkjetted organic transistor technology. *Electron Devices Meeting, 2004. IEDM Technical Digest. IEEE International* 1072-1074(2004).doi:10.1109/IEDM.2004.1419384
14. Volkman, S. et al. Inkjetted organic transistors using a novel pentacene precursor. *MRS Proceedings* H11.7(2003).
15. Ruiz, R. et al. Pentacene Thin Film Growth. *Chemistry of Materials* **16**, 4497-4508(2004).
16. Lin, Y. et al. Stacked pentacene layer organic thin-film transistors with improved characteristics. *Electron Device Letters, IEEE* **18**, 606-608(1997).

5 Pentacene Precursor Growth on other Substrates

5.1 Background

The growth of pentacene on *a*-SiO_2 through evaporation is a well studied system mainly because of the vast number of studies on back-gated pentacene TFTs that have been made. The previous chapter has reviewed this system already, as well as film growth of pentacene on *a*-SiO_2 through SAP processing. The back-gated SiO_2 dielectric test bed is a practical test bed for many organic semiconducting materials, either thermally grown or solution deposited. However, for an OTFT to eventually be used in a useful circuit, such as a RFID tag, the gate dielectric would most likely a solution processed inorganic or organic dielectric in order to cut out the expensive high vacuum steps. Using *a*-SiO_2 on a solution processed circuit does not seem plausible, nor is it optimal. There are many studies which show that a HMDS monolayer on top of *a*-SiO_2 helps the ordering of pentacene, and increase the mobility of pentacene TFTs.[1] This implies that, pentacene orders better on top of organic materials than on top of inorganic films. There have been many studies looking at the growth and mobility of pentacene on top of organic monolayers.[2-4,1]

One of the most common gate dielectrics used for pentacene TFTs is polyvinylphenol (PVP). It has been shown that pentacene forms large grains and exhibits high mobility when PVP is used as a gate material.[5,6] The growth of pentacene on PVP

has not been well studied as thoroughly as on a-SiO_2, most studies have only been on the performance of pentacene TFTs using PVP as dielectric material.

Depending on whether or not an organic TFT is a top contact or bottom contact device, the film growth of pentacene on the metal source drain is also of importance. One of the most widely used metals for metal source drains is gold because the work function of gold is well matched to many organic semiconductors. In recent years, there has been momentum to use silver as a source drain material, due to its high conductivity and relative low-cost. Silver is not as well match in work function to organic semiconductors as gold is matched, however, silver S/D created from silver nanoparticles have been found to form ohmic contacts to organic semiconductors.[7-11]

There is great interest in being able to create an organic Schottky diode, which can be used for rectification in RFID tags. In the case of the Schottky diode, *a*-SiO_2 will never be used, since an organic RFID is merely a three layer device, where the semiconductor is sandwiched between two metals. A typical pentacene diode is formed by sandwiching pentacene between an aluminum and gold contact, where aluminum and pentacene forms a Schottky contact and gold to pentacene form an ohmic contact.[7-11] Evaporated silver has been tested for use as a Schottky contact to pentacene as well,[12] however is not used as often as aluminum.

One more material of interest, especially for making diodes is PEDOT:PSS. The hole injection from gold into pentacene has been shown to increase by adding the conductive organic polymer, PEDOT:PSS, between pentacene and the gold contact.[13] The band structure of PEDOT:PSS matches pentacene more closely than gold, and hence has a more efficient transfer of holes. By using a hole injection layer in between gold an

pentacene, the Al-pentacene-Au Schottky diodes was found to have an order of magnitude increase in on current, as well as an increase in rectification cutoff frequency.[14]

For fully solution processed organic circuits it would be important to understand how SAP-pentacene grows on different materials other than *a*-SiO_2, especially the materials discussed above; silver, gold, PVP and PEDOT:PSS. Aluminum is unfortunately not included, due to the high reactivity of aluminum to oxygen, forming its oxide. No aluminum nanoparticles have been reported possibly for that particular reason. Currently there are no known ways to solution process aluminum.

Growth of pentacene through evaporation has been tested on all these materials;[13,15-18] however, growth of pentacene on these materials using SAP has not. In the previous chapter, the growth of pentacene on *a*-SiO_2 through thermal degradation of SAP has been explored in detail. In this chapter, the growth of pentacene through SAP is described on PVP, PEDOT:PSS, gold, silver, *a*-SiO_2+HMDS monolayer and *a*-SiO_2. The growth of pentacene on each of these materials is compared to the growth of pentacene on *a*-SiO_2. Dewetting, roughness of films, and nucleation density are looked at in the most detail when comparing film growth on the different substrates.

5.2 Theory (Comparison of Substrates)

In order to properly compare the growth of pentacene on different substrates, the substrates themselves need to be properly compared with each other and "ranked." One of the standard ways is to look at hydrophobicity and hydrophilicity and measure the contact angle of different liquids on top of the substrate. Assuming the capillarity model of thin film growth is valid for pentacene; it would be more useful to find the free-energy

of each substrate and its interaction with pentacene. Unfortunately, the free-energy between materials cannot be easily measured.

Since pentacene films from SAP show dewetting from the surface when processed at high temperatures, a method of finding relative film stability on pentacene can be found as follows.

Assumptions:

1. The capillarity theory of film formation is what governs the formation of pentacene thin films.
2. Pentacene molecules are mobile and able to rearrange to minimize the free-energy of the system, such that the final configuration reaches thermal equilibrium.
3. The substrate can only take on one of two states. Either the substrate is covered by pentacene, or it is exposed and not covered by pentacene.
4. There is no free-energy change from pentacene movement and rearrangement within itself. Free-energy changes only there is change in the number of pentacene molecules exposed to the substrate or air.
5. As an approximation only two monolayers of pentacene contributes to energetic changes, all other molecules of pentacene moves around between these two monolayers and therefore does not contribute to free-energy change.
6. As an approximation, one pentacene molecules takes up a volume of approximately $0.33nm^3$[22]. For simplicity the volume is assumed to be cubic, so the aerial density of pentacene molecules is assumed to be 4.78×10^{17} molecules/m^2.

Using traditional thermodynamics free energy changes moving from one substrate to another can now used to compare films. The equilibrium constant can be defined as the ratio of the area exposed (without pentacene) to the area covered (with pentacene). The free-energy change of the system is 0J when the 50% of the film is exposed, this is when the ratio of exposed to unexposed is equal to one. The governing equations are:

$$K_{eq} = \frac{A_1}{A_2}$$

Equation 5-1: Definition of the equilibrium constant

$$\Delta G = -NkT\ln(K_{eq})$$

Equation 5-2: Equation for Gibb's free energy

ΔG = free-energy change, K_{eq} = equilibrium constant , A_1 = uncovered, A_2 =exposed, N = number of molecules involved in the process, k = Boltzmann constant

The standard free-energy is defined at 0J for pentacene SiO_2, and all the other substrates will be ranked according to this standard for comparison. Negative free energies indicate that pentacene is more stable on the substrate stability compared to pentacene on SiO_2. More positive results indicate that pentacene is less stabile on the substrate as compared to SiO_2. Higher stability means, that pentacene likes to wet the substrate more and lower stability means that pentacene would rather stick to itself and dewet from the substrate.

Clearly, based upon the assumptions above, these numbers are clearly estimations and the absolute numbers are inaccurate. The aerial density of pentacene is probably an under estimation, because a cubic volume was assumed for the pentacene molecule, this assumption makes the packing of pentacene less density than it should be. Second, it is assumed that only two monolayers of pentacene plays in change of free-energy. It is

assumed that these two monolayers are perfectly flat. This is clearly another under estimation of free-energy. Even though this model is clearly flawed, however, it serves a good model in order to give a relative order in which to compare films.

5.3 Experimental

5.3.1 Preparation of substrates

All substrates were prepared on top of standard 4 inch undoped silicon wafers with 1000Å of wet oxide.

5.3.1.1 HMDS substrates

HMDS was deposited onto oxide wafers by standard methods

5.3.1.2 Gold and silver substrates

Gold and silver substrates are made by standard thermal evaporation conditions for each respective material on top of oxide substrates. As described previously a 15Å chrome adhesion layer was evaporated before evaporating the gold and silver on to substrates. The final thickness of both gold and silver substrates were approximately 1000Å

5.3.1.3 PEDOT:PSS substrates

High conductivity grade PEDOT:PSS was purchased from Aldrich and used with no further processing or purification. PEDOT was spun on top of gold substrates at 6000 rpm for 60s.

5.3.1.4 PVP substrates

PVP substrates were made by spinning PVP directly onto oxide wafers. PVP solution was made by dissolving 1.08g of PVP and 0.1mL of PMFA in 15mL of propylene glycol methyl ether acetate (PGMEA) and using a vortexer. All materials were purchased from Aldrich and used without further purification. The solution is poured on to oxide wafers spun at 500rpm, afterwards, the wafer is ramped up to 4000rpm and spun for 1 minute. The wafer is then heated on a hot plate in air at 100^0C for 1 minute, and then heated at 200^0C for 5minutes. This process creates cross-linked PVP film with a thickness of approximately 200nm.

5.3.1.5 Pentacene precursor

Pentacene was deposited using the same method as in chapter 4. The solvents, concentrations and spin speeds were all identical. The thickness was checked for each substrate, and was found to be identical to SiO_2 in all cases. SEM samples were created from these samples.

Each sample was created according to the heating temperatures and times in table 5.1. Samples were heating in a dry nitrogen glovebox.

Temperature	Heating times
125	1m, 5m, 10m, 20m, 45m, 90, 180m
140	1m, 2m, 5m, 11m, 22m, 44m
160	5s, 10s, 15s, 30s, 1m, 2, 4m
180	2s, 4s, 8s, 16s, 30s, 1m, 2m

Table 5-1: Heating conditions for all samples

5.3.1.6 Analysis Techniques

SEM and AFM were utilized in the same ways as in the previous chapter.

5.4 Results and Discussion

5.4.1 Qualitative SEM results

In this particular experiment, fewer samples were created than in the previous chapter. Once again there clearly exists the two types of nucleation, the high temperature and low temperature types of nucleation. The low temperature nuclei, which lead to large islands, and the high temperature nuclei which becomes large flat plateaus. Both these types of nuclei are shown in figure 5.1.

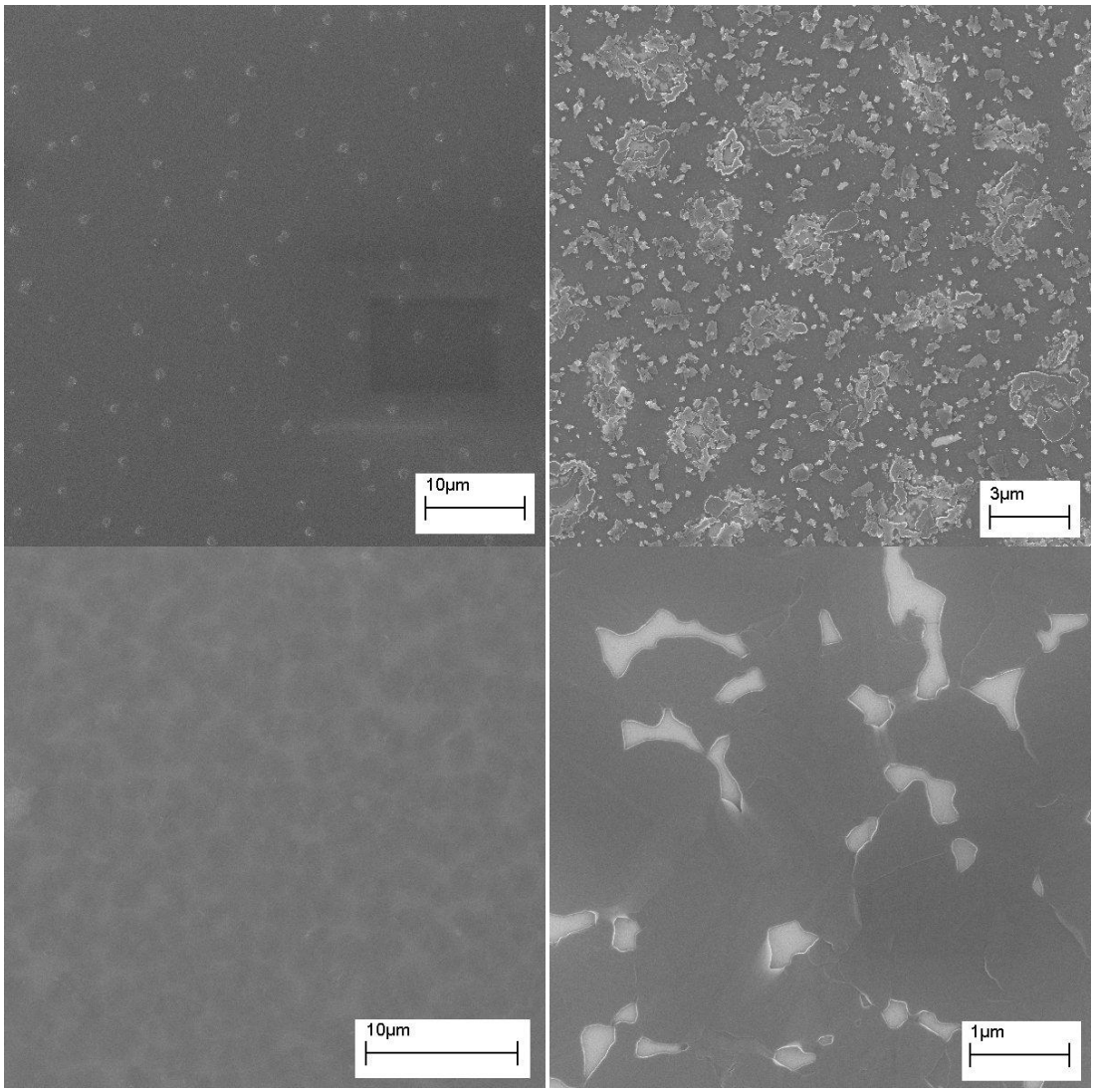

Figure 5-1: (top left) Low temperature nuclei after 1 minute of processing at 125^{0}C. (top right) The final result of the low temperature islands, as well as S-K islands. (bottom left) High temperature nuclei after 2 seconds of processing at 180^{0}C. (bottom right) High temperature plateaus. All these films were processed on HMDS substrates.

All of the different substrates showed, the same types of growth and growth mechanism as seen the pentacene growth through SAP on oxide. There was clear dewetting in both the silver and gold substrate even on films processed even at low

temperature (figure 5.2), which was not seen in the other samples. In high temperature samples, all samples clearly showed pentacene dewetting from the surface (figure 5.3).

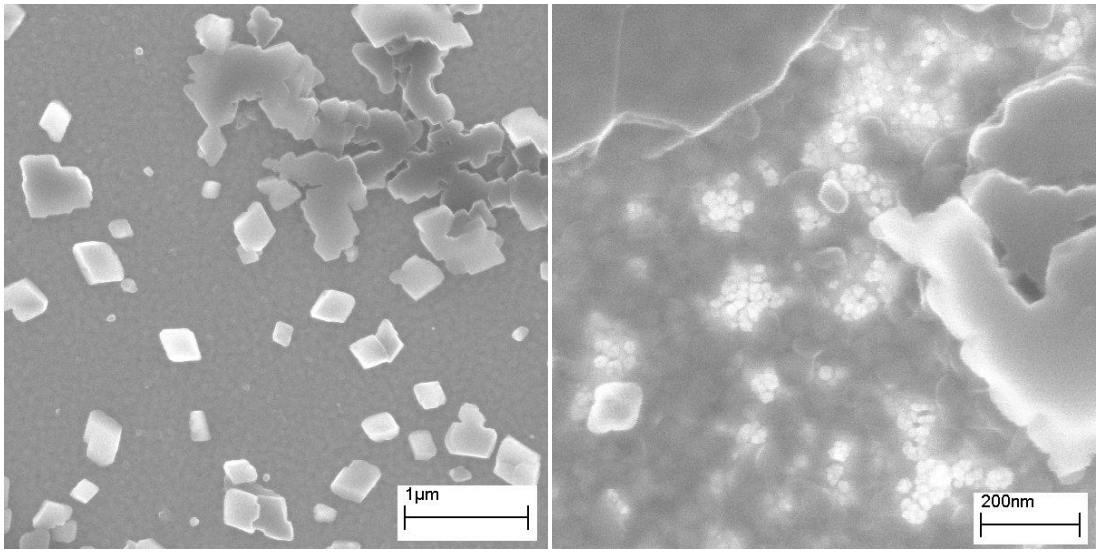

Figure 5-2: (left) Pentacene processed on PVP at 125^{0}C. (right) Pentacene processed on silver at 125^{0}C. There is no visible dewetting on the pentacene on PVP, however there is clear dewetting the film processed on top of silver.

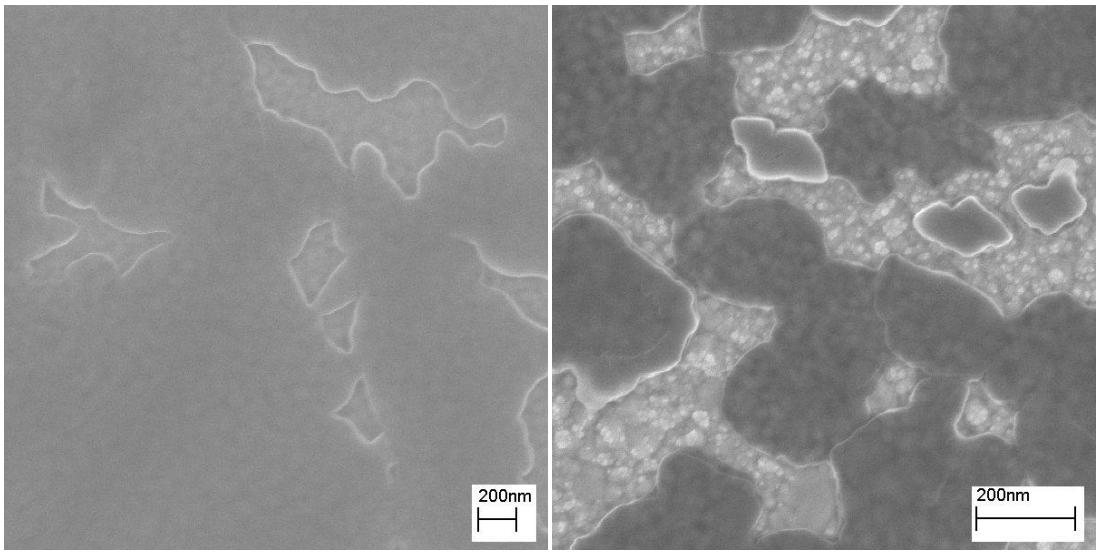

Figure 5-3: (left) Dewetting of pentacene on PVP. (right) Dewetting of pentacene on silver. Both films were processed at 180^{0}C.

5.4.2 Pentacene Stability Calculation

Dewetting was measured with SEM and was used to compare substrates based on the scheme previously derived. Dewetting was most pronounced and well defined at 180^0C and can only be accurately measured at 180^0C, therefore comparisons will still be plotted against the stability of pentacene to the substrate at 180^0C. It is known that the free-energy between a thin film and the substrates changes with temperature, however since dewetting was only accurately found at 180^0C, everything will still be plotted against the stability at 180^0C. Since the exact values calculated are not entirely accurate, trying to get the exact values of free-energy for each temperature is unnecessary. There is no reason why the relative order of pentacene stability should change when the temperature changes, therefore using the same order for all temperatures should still be valid.

Dewetting was measured only on the fully reacted films, results are shown in figure 5.5. Using the results of dewetting at 180^0C, the relative free-energy is calculated in figure 5.6. Table 5.2 shows the relative free energy proper ranked with oxide centered at 0J. The ranking of pentacene stability shows all of the organic substrates having a negative relative free-energy and the inorganic substrates with a positive relative-free energy. This is completely expected. Many studies have already confirmed that pentacene grown on top of PVP give relatively large grains,[5,6] indicating that pentacene growth well on top of PVP. Using this ranking system that has been derived, it is now possible to compare the growth of pentacene on each of these different substrates.

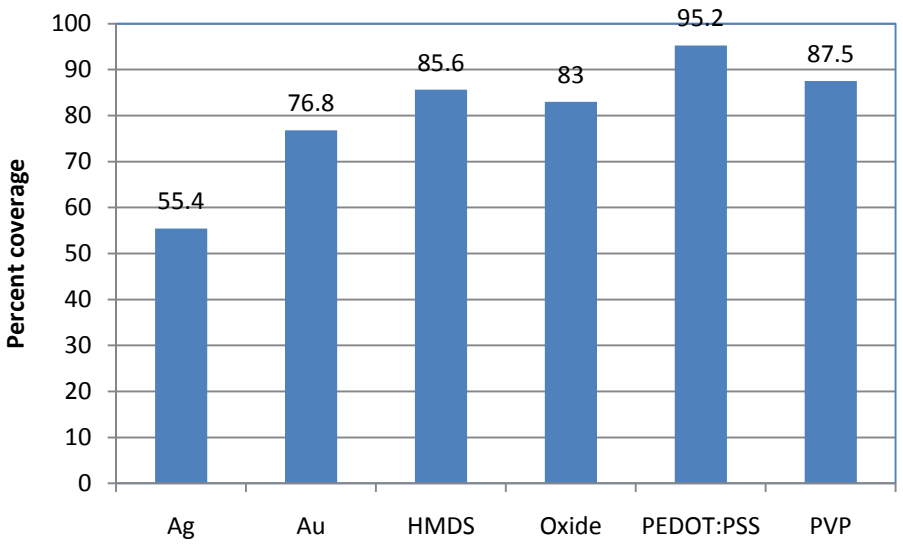

Figure 5-4: Film coverage by substrate at 180^0C

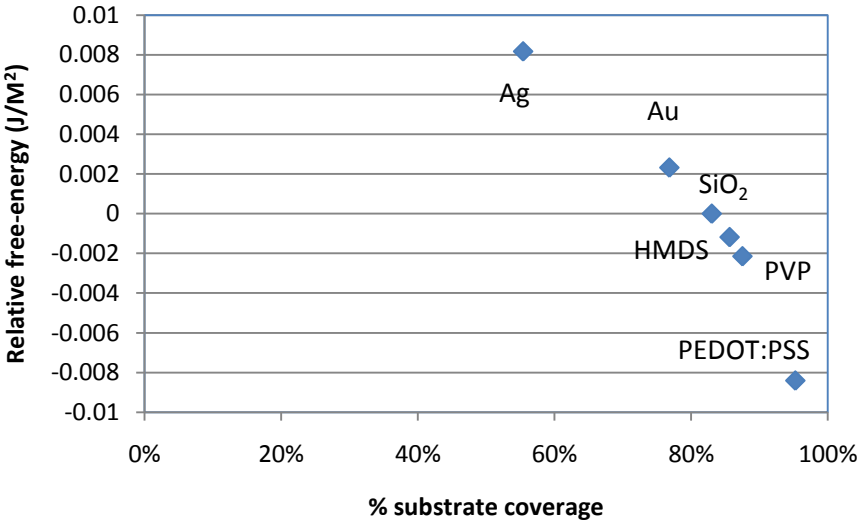

Figure 5-5: Calculation of relative free-energy based on dewetting

Substrate	Relative-Free energy (J/m^2)
PEDOT:PSS	-0.00841
PVP	-0.00215
HMDS	-0.00118
Oxide	0
Au	0.002322
Ag	0.008174

Table 5-2: Ranking of substrate relative free-energy compared to SiO_2.

5.4.3 Quantitative Results and Discussion

Once again the number of nucleation sites was determined for each temperature. Nucleation sites were not quantified for samples 160^0C or higher due to the difficulty in counting, because the high rate of nucleation causing overlapping nucleation sites, causing counting difficulties. Only the island-like nuclei were counted for processing at 125^0C and 140^0C samples. The characteristic lengths of the final low temperature islands were also measure. Using the free energy calculation from above each nucleation density, characteristic length, etc. are all plot in the order of stability.

Figure 5.6 and 5.7 shows the density of low-temperature islands grown at 125^0C and 140^0C respectively. There does not seem to be a change in the low-temperature island density as a function of the pentacene stability. The nucleation density at 125^0C seems relatively constant for all the different substrates. There seem to be more fluctuations in nucleation density at 140^0C, however this data can be thought of as relatively constant. A constant nucleation density across different substrates suggests that the formation of the nuclei is energetically affected more by the precursor matrix than by the substrate. The formation of nuclei can be thought of as the formation of an inclusion within a matrix, with the precursor being the matrix and the nucleus being the inclusion. Since the matrix is the same regardless of substrate, this shows that the energetics acting between the matrix and the forming nucleus plays a much greater role than the free-energy of the substrate to the forming nucleus.

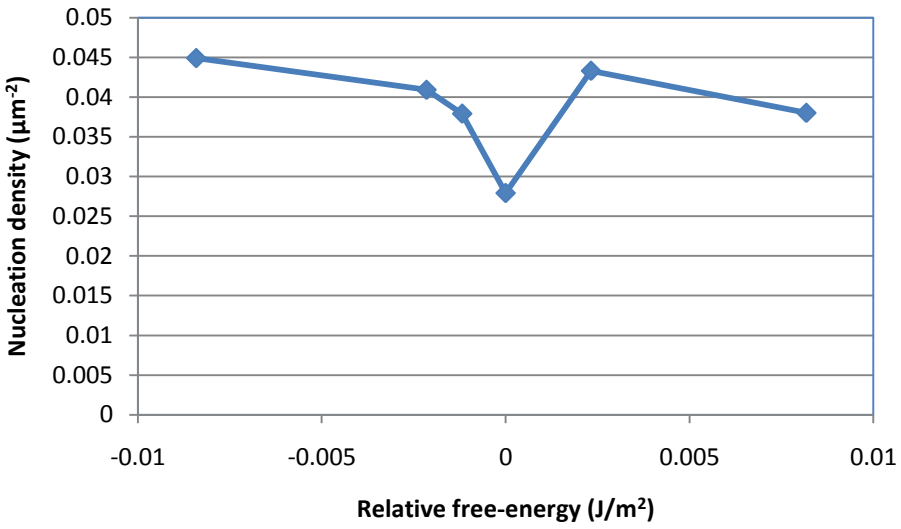

Figure 5-6: Nucleation density for films processed at 125^0C.

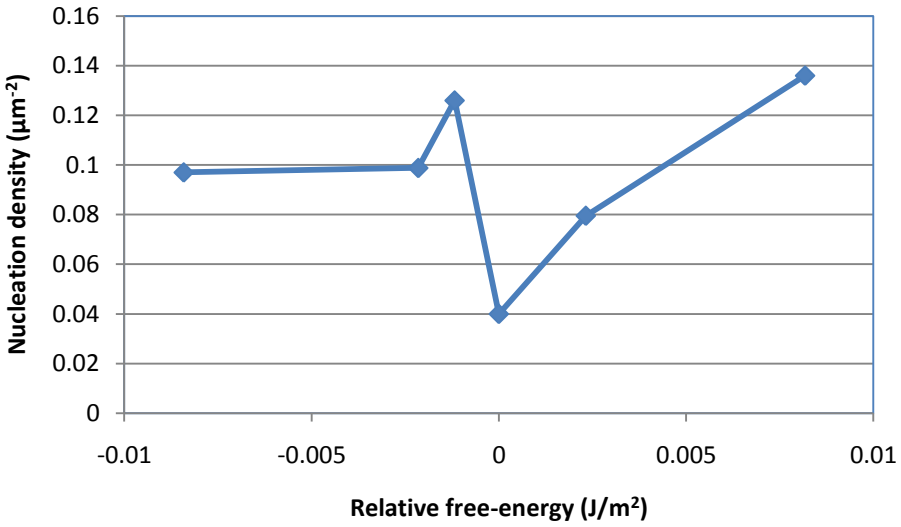

Figure 5-7: Nucleation density for films processed at 140^0C.

From figure 5.8 and 5.9, it can be seen that the final characteristic length of the low-temperature islands is constant across all the substrates. Data fluctuations are more or less hidden within the standard deviation of each data point. The size of the islands is determined by the thickness of the precursor film and the nucleation density. Thereby the constant characteristic length of the islands further confirms the previous assertion that

nucleation densities are not affect by the substrate. It can be concluded that especially in the early parts of film development, the substrate plays very little role in the formation of the film. This is confirmed by the SEM data, where the growth mechanism of pentacene looks the same on each substrate, and matches the observations of pentacene growth on oxide.

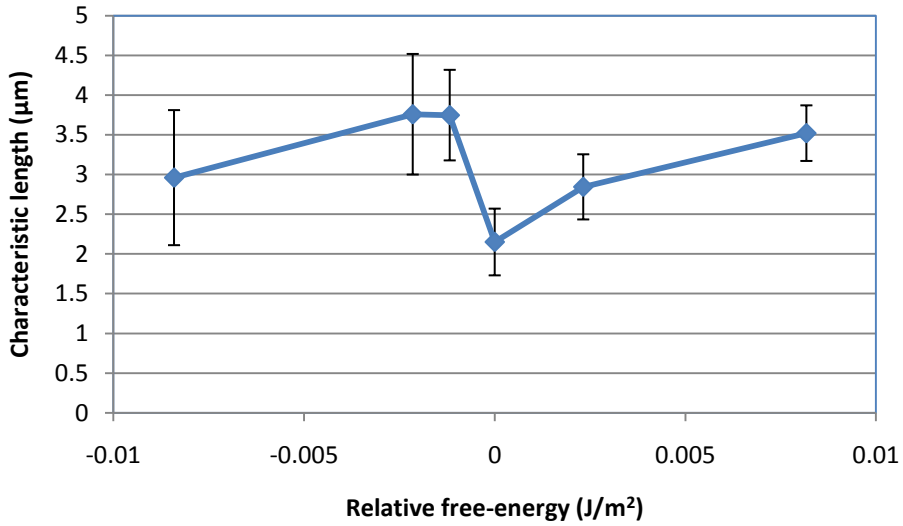

Figure 5-8: Characteristic length of islands on films processed at 125^{0}C.

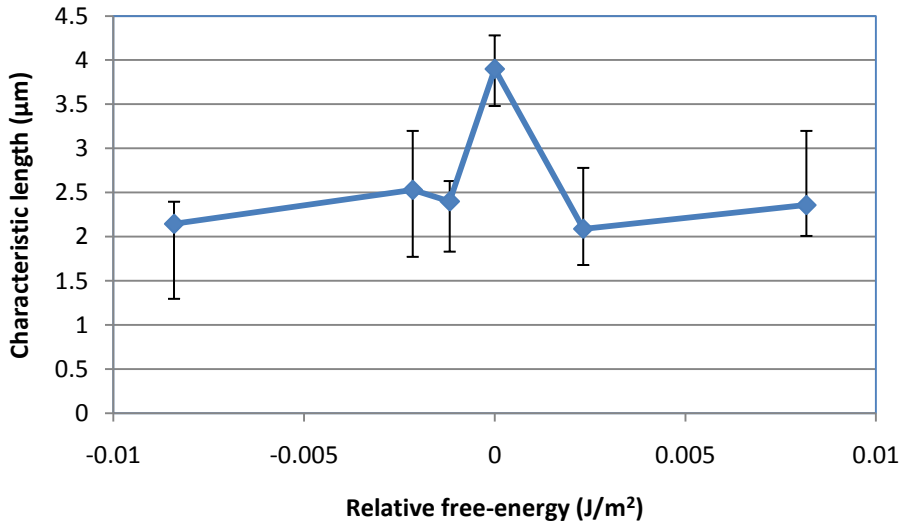

Figure 5-9: Characteristic length of islands on films processed at 140^{0}C.

What role does the substrate have on the growth of pentacene films? From figure 5.10 and 5.11 the rms roughness of pentacene films on different substrates is shown. The data suggests that as the stability of pentacene increases on a substrate, the roughness of the film decreases.

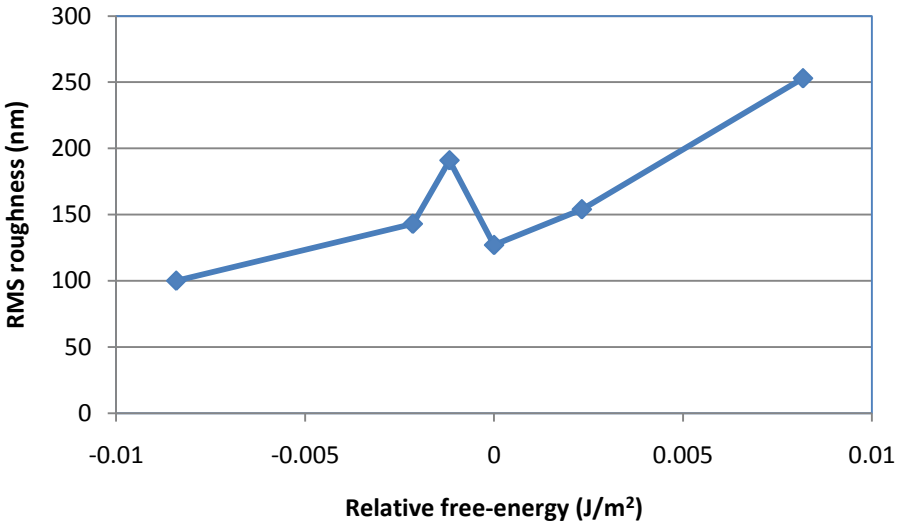

Figure 5-10: RMS roughness of films processed at 125^0C.

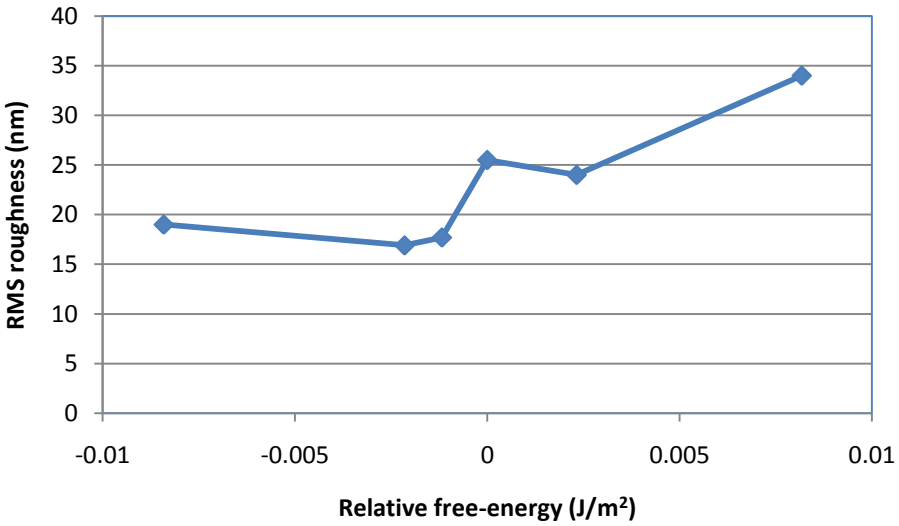

Figure 5-11: RMS roughness of films processed at 180^0C.

It can be argued that this data was forced to take this particular trend because the relative free-energy was calculated from pentacene dewetting data. It can be assumed that every film has the same amount of pentacene, since the initial precursor thickness was constant on all substrates. Therefore, if there is more dewetting off a substrate, then there must be more roughness of the film. However, the trend of roughness to free-energy still held true for the film processed at 125^0C. At 125^0C, there is very little to no dewetting on most substrates, except from the two metal substrates. This shows that at low temperatures, dewetting may not occur either because surface mobility is low, therefore pentacene is incapable of dewetting, or at low temperatures pentacene is more stable. Either way, at these lower temperature, even though pentacene does not necessarily dewet from the substrate, however pentacene is still trying to dewet. Pentacene would much rather be surround by other pentacene molecules than be exposed to the substrate. As seen the metal substrates, where pentacene is extremely unstable, dewetting already starts at these lower temperatures.

By using thinner precursor, it may be possible to start seeing dewetting of pentacene from the surfaces all the substrates even at low temperatures. By looking at the dewetting of pentacene at a range of temperatures, it may be possible to see how the stability of pentacene changes as a function of temperature.

The roughness data suggests that the substrate plays a role in the final film typology. Initially the formation of pentacene through a precursor is largely unaffected by the substrate. Nucleation of the pentacene crystals is more or less affected by the precursor matrix. As the precursor is consumed, the substrate starts to play a larger role in the film development. If the pentacene is stable on the substrate, then more molecules

of pentacene would be willing to grow over the substrate causing less dewetting. If the pentacene unstable on the substrate, then crystal growth would favor an upward growth of islands and plateaus and more dewetting would occur.

5.5 Conclusions

In this study, the growth of pentacene using SAP on different substrates has been shown. The growth mechanism of pentacene was found to be the same regardless of substrate. In fact the low-temperature nuclei density has been found to be constant regardless of substrate. The initial stages of film development is largely unaffected by the substrate.A simple way of comparing pentacene stability on different substrate has been demonstrated. It has been shown that stable films show less roughness than unstable films. As film development continues, the substrate starts to play a larger role in film development.In the future, the stability of pentacene needs to be found for a range of temperature, currently the stability of pentacene has only been extracted at one temperature. X-ray studies also need to be performed in the future in order to find the effect substrates on crystallite size.

5.6 References

1. Lim, S. et al. Surface-treatment effects on organic thin-film transistors. *SYNTHETIC METALS* **148**, 75-79(2005).
2. Kim, J. et al. An organic thin-film transistor of high mobility by dielectric surface modification with organic molecule. *Appl. Phys. Lett.* **85**, 6368-6370(2004).
3. Kymissis, I., Dimitrakopoulos, C. & Purushothaman, S. High-performance bottom electrode organic thin-film transistors. *Electron Devices, IEEE Transactions on* **48**, 1060-1064(2001).
4. McDowell, M. et al. Improved organic thin-film transistor performance using novel self-assembled monolayers. *Appl. Phys. Lett.* **88**, 073505-3(2006).
5. Kang, G.-. et al. The electrical characteristics of pentacene-based organic field-effect transistors with polymer gate insulators. *Current Applied Physics* **5**, 297-301(2005).
6. Klauk, H. et al. High-mobility polymer gate dielectric pentacene thin film transistors. *JOURNAL OF APPLIED PHYSICS* **92**, 5259-5263(2002).
7. Wu, Y., Li, Y. & Ong, B. A simple and efficient approach to a printable silver conductor for printed electronics. *JOURNAL OF THE AMERICAN CHEMICAL SOCIETY* **129**, 1862-+(2007).
8. Jeong, S. et al. Fabrication of the organic thin-film transistors based on ink-jet printed silver electrodes. *MOLECULAR CRYSTALS AND LIQUID CRYSTALS* **459**, 35-43(2006).
9. Xue, F. et al. Inkjet printed silver source/drain electrodes for low-cost polymer thin film transistors. *MICROELECTRONIC ENGINEERING* **83**, 298-302(2006).

10. Cai, X. et al. N- and P-channel transport behavior in thin film transistors based on tricyanovinyl-capped oligothiophenes. *JOURNAL OF PHYSICAL CHEMISTRY B* **110**, 14590-14597(2006).
11. Ando, M. et al. Self-aligned self-assembly process for fabricating organic thin-film transistors. *APPLIED PHYSICS LETTERS* **85**, 1849-1851(2004).
12. Diao, L. et al. Electrical characterization of metal/pentacene contacts. *JOURNAL OF APPLIED PHYSICS* **101**, (2007).
13. Koch, N. et al. Organic molecular films on gold versus conducting polymer: Influence of injection barrier height and morphology on current--voltage characteristics. *Appl. Phys. Lett.* **82**, 2281-2283(2003).
14. Steudel, S. et al. Comparison of organic diode structures regarding high-frequency rectification behavior in radio-frequency identification tags. *JOURNAL OF APPLIED PHYSICS* **99**, (2006).
15. Lim, S.C. et al. Surface-treatment effects on organic thin-film transistors. *Synthetic Metals* **148**, 75-79(2005).
16. Wang, Y. et al. Structural evolution of pentacene on a Ag(110) surface. *PHYSICAL REVIEW B* **69**, (2004).
17. Knipp, D. et al. Polycrystalline pentacene thin films for large area electronic applications. *JOURNAL OF NON-CRYSTALLINE SOLIDS* **299**, 1042-1046(2002).
18. Hu, W. et al. Molecular orientation of evaporated pentacene films on gold: Alignment effect of self-assembled monolayer. *LANGMUIR* **21**, 2260-2266(2005).

6 Heat Treatments of Pentacene Precursor for improving pentacene TFT performance

6.1 Background

Thus far most OTFTs have been processed using only simple thermal processing. Since many organic semiconducting layers are deposited by thermal evaporation. The knobs used to tune the final morphology are more or less limited to the controls in thermal evaporation, including substrate surface energy[1-5], substrate heating[6,7] and evaporation rate[8-11] during evaporation. Typical OTFT evaporation rates are approximately 10Å/min[12-14] with 50-70^{0}C substrate heating[12,15]. This condition is to allow for slow growth of pentacene crystals to promote large ordered pentacene crystals. This potentially makes high mobility devices with minimal defects. In pentacene processing for diodes, the main problem is preventing a short between the top and bottom contact. As a result, standard evaporation conditions are 5 Å /min with no substrate heating[16,17]. This creates a smooth film with small crystals, making sure there are no pinholes in the semiconducting surface preventing any shorts between the two metal contacts. In both cases there are not any post film deposition heating steps.

There have been attempts to improve the mobility of OTFTs with post deposition thermal treatments[18-20]. Experiment shows that post deposition heating of pentacene films above 90^{0}C after deposition drops the mobility of the OTFT[20]. This can be

attributed to the film reordering, causing morphological changes in the film and relaxing the high mobility thin-film phase to the low mobility bulk-like phase. Post-deposition annealing of pentacene below 90^0C caused the mobility to increase,[18,19] which is attributed to promotion of grain growth the decreased defects.

For solution processed organic semiconductors. Post deposition heating is considered a standard process.[21,22] In solution processing, heating serves two purposes. One purpose of solution processing is to drive off solvents, which may interfere with transistor action. The other reason is because is to help order films. In the case of PBTTT, heating of films is required, because heating of the film causes a phase transition in the PBTTT film changing it form a nonconductive film to a semiconducting film[23].

In all the cases above, the processing of organic semiconductors utilizes relatively simple processing anneal steps and does not incorporate any short of complex heating and cooling steps which is quite common in metals processing[24]. In the case of metal processing, complex heat treatments allows allow the control of many different properties of the metal, such as hardness, crystal size and brittleness. Such processes have been used since antiquity for manufacturing of weapon, tools, etc. In the case of pentacene processing through a precursor where different crystal types are involved, there is no reason why multi-step heat treatments should not be used in order to improve the performance of the semiconductor. The tricks used in metals processing may become applicable for precursor systems. By using multi-step heating to process the pentacene precursor, final films should be different than processed only at a single temperature.

This chapter focuses on the usage of two step heating for pentacene processing from SAP. Four heating processes are explored. One-step heating, the standard heating

method, which only uses a single temperature to process the SAP film from beginning to end. Step-down heating, starts with a short higher temperature heating step to form high temperature nuclei, then the temperature is dropped to a lower temperature for crystal growth. . Step-up heating, is the exact opposite of step-down heating which starts with a low temperature step to form low temperature nuclei, and then stepped up to a longer higher temperature heating step for crystallization. Finally, post-processing annealing uses the standard one-step single temperature processing, but after the one-step film formation an extra short high temperature anneal is added. For each of these processes the films are inspected using SEM to look for visual difference in the films processed under the different heating conditions. Finally, TFTs are made with the pentacene processed with the same heat treatments described. The mobility and on/off ratios are compared between each of the different heating conditions.

6.2 Experimental

6.2.1 SEM sample preparation

The standard SAP concentration of 12mg/mL of chloroform was used to made precursor solutions. This time, due to availability, SAP was purchased from Aldrich. SEM comparison was made between the SAP synthesized in house as well as the SAP purchased from Aldrich. The solution from SAP made in house ranged anywhere from clear to yellow to orange. The SAP solutions from Aldrich were always colorless. Most likely, there are fewer contaminants in the chemicals from Aldrich compared to the chemicals purified in house. An SEM comparison between pentacene films made from the Aldrich precursor looked the same as the ones made from in house precursor.

Finally, TFT mobilities and trends were the same for TFT fabricated using either precursor. Therefore, it was concluded that the in house and Aldrich precursors are the same and have the same performance, with the exception of some slight impurities.

Again, the standard oxide wafers with HMDS treatment were used. HMDS oxides were used so that the growth of pentacene on the SEM samples would the same as the growth of pentacene on the TFTs. SEM samples were prepared on oxidized Si wafers, and then diced into smaller pieces. The annealing of the SEM samples, will be described later.

6.2.2 Pentacene TFT preparation

Pentacene TFTs were prepared using the standard process as described in chapter 2. The same concentration of SAP solutions used in the SEM samples was used to make TFTs. Samples were then diced into smaller pieces for all the different heating conditions. The different heating conditions of the TFT samples were identical to those used on SEM samples.

6.2.3 Heat treatment of TFT and SEM samples.

Four types of heating were tested. One-step heating, is the standard heating method which starts and ends pentacene film formation with only a single temperature. The previous chapters have explored the film growth of this type of heating in detail, however no TFT measurements have been describe. Since this is the standard type of pentacene film processing, it also serves as a control for comparison with the two-step films.

Step-down heating, starts with a short higher temperature heating step to form high temperature nuclei, and ends with a longer lower temperature step to promote large crystal growth and complete the solid-state reaction. High temperature processing creates smooth and textured films, however give small pentacene crystals. The hope of the step-down films is to form smooth and textured films with large pentacene grains.

Step-up heating, starts with a low temperature step to form low temperature nuclei, and ends with a long higher temperature step in order to complete film formation. This type of heating is used to contrast with step-down heating.

Finally, post-processing annealing uses the standard one-step film formation and ends with a short high temperature anneal. The hope is that mobility can be improved by a final high temperature anneal, by helping grain growth and reduction of defects.

In both step-up and step-down heating, the time chosen for the first heating step allowed for approximately 12% of the precursor to reaction, which is equivalent to 0.13 reaction time constants. The second heating step was chosen to allow for the reaction to reach completion, which corresponds to approximately 7 reaction time constants. For, the post-process anneal, the reverse conditions were used; 7 reaction time constants for the first heating step, and 0.13 reaction time constants for the second step. For different temperatures, different absolute reaction times were used. Each of the heating conditions is tabulated below in tables 6.1 and 6.2.

The samples were heated on a hotplate which does not reach the set temperature quickly, hence it was not possible to have sharp temperature changes. In order to simulate sharp temperature changes on this hotplate, the hotplate is first heated to the temperature 1 for heating step 1, the sample is then placed on the hotplate for the

prescribed time and then removed and placed on a metal plate at room temperature to quench the solid-state reaction. The hotplate is then brought to temperature 2, once temperature 2 is reached the sample is placed back onto the hotplate for the second heating step. Once the prescribed time for temperature 2 is reached, the sample is once again removed and cooled on a metal plate.

Since samples are removed from the hotplate and brought to room temperature between the heating step 1 and 2. The effects of the cooling in between step needs to be understood. Hence, a quench control was performed. The quench control consists of sample heated to 160^0C for 0.13 time reaction time constants, then the reaction is quenched to room temperature. Afterwards, the sample is placed back on to the hotplate to continue heating at 160^0C and heated for 7 reaction time constants. If the quenching step has no effect on the sample, then this control sample should be identical to a one-step sample formed at 160^0C.

In order to follow the reaction properly by SEM, intermediate samples were also made. For example for a step-down sample, processed first processed at 160^0C and then processed at 125^0C (160-125), an extra sample was made which was only processed with the first 160^0C step, without the final 125^0C step. This serves as a comparison for the fully processed film.

All these conditions were carried out separately, and classified as experiment 1 and 2. Experiment 1 tests one-step heating and step-down heating. The one-step samples (called C1) serves as an experimental control for the step-down samples. Experiment 2, tests, step-up heating, post-processing annealing and has its own set of one-step controls (C2.1). The quench control was tested with experiment 2. Along with the quench

control, the 160^0C step-down series was repeated (160-150, 160-140, 160-125). Collectively, this set of controls are referred to as C2.2.

Control (C1)	
Temperature	time (min)
125	168
140	42
150	18
160	8
170	3.7
180	1.8

Step-down			
Temperature 1	time (s)	Temperature 2	time (min)
180	2	150	18
180	2	140	42
180	2	125	168
170	4	150	18
170	4	140	42
170	4	125	168
160	9	150	18
160	9	140	42
160	9	125	168

Table 6-1*: Experiment 1. One-step heating and step-down heating is tested. One-step heating heats the samples for ~7 reaction time constants. Step-down heating heats the samples for 0.13 reaction time constant at temperature 1, then 7 reaction time constants at temperature 2.*

Control (C2.1)	
Temperature 1	time (s)
125	168
140	42
150	18
160	8
170	3.7
180	1.8
190	0.9
200	0.5

Quench Control (C2.2)			
Temperature 1	time (s)	Temperature 2	time (min)
160	9	160	8
160	9	150	18
160	9	140	42
160	9	125	168
Step-up			
Temperature 1	time(s)	Temperature 2	time (min)
125	180	160	8
125	180	170	3.7
125	180	180	1.8
140	47	160	8
140	47	170	3.7
140	47	180	1.8
150	20	160	8
150	20	170	3.7
150	20	180	1.8
Post-processing anneal			
Temperature 1	time (min)	Temperature 2	time (s)
125	168	160	9
125	168	170	4
125	168	180	2
140	42	160	9
140	42	170	4
140	42	180	2
150	18	160	9
150	18	170	4
150	18	180	2

Table 6-2: Experiment 2. One-step heating is repeated to serve as a control. Step-up heating and post-processing anneal is tested. The quenching control is also tested.

6.2.4 Sample Analysis

TFT IV measurements were taken. On/off ratio and mobility were extracted.

SEM images were taken using the standard conditions. Nuclei density and island sizes were not characterized.

6.3 Results and Discussion

6.3.1 One-step Heating (C1 and C2.1)

The one-step results seem consistent in both experiment 1 and experiment 2, and match the results in previous chapters. The films in experiment 2 appear to have a bit more roughness than in experiment 1. Figures 6.1 and 6.2 show SEM images of 125^0C and 140^0C films respectively. What appears to be dewetting in the 140^0C sample of experiment 2 (figure 6.2) is not dewetting, but merely thin regions of pentacene. ,Small pentacene islands only form if there is a film of pentacene underneath (S-K growth).

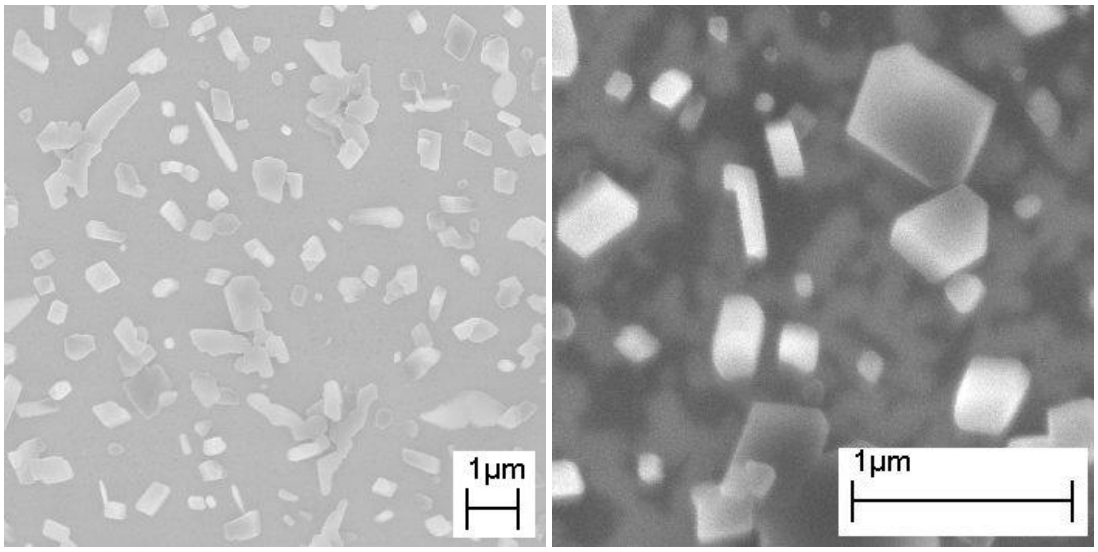

Figure 6-1: (left) one-step 125^{0}C from experiment 1. (right) one-step 125^{0}C from experiment 2. Both films are quite typical, however the film from experiment 2 show more roughness.

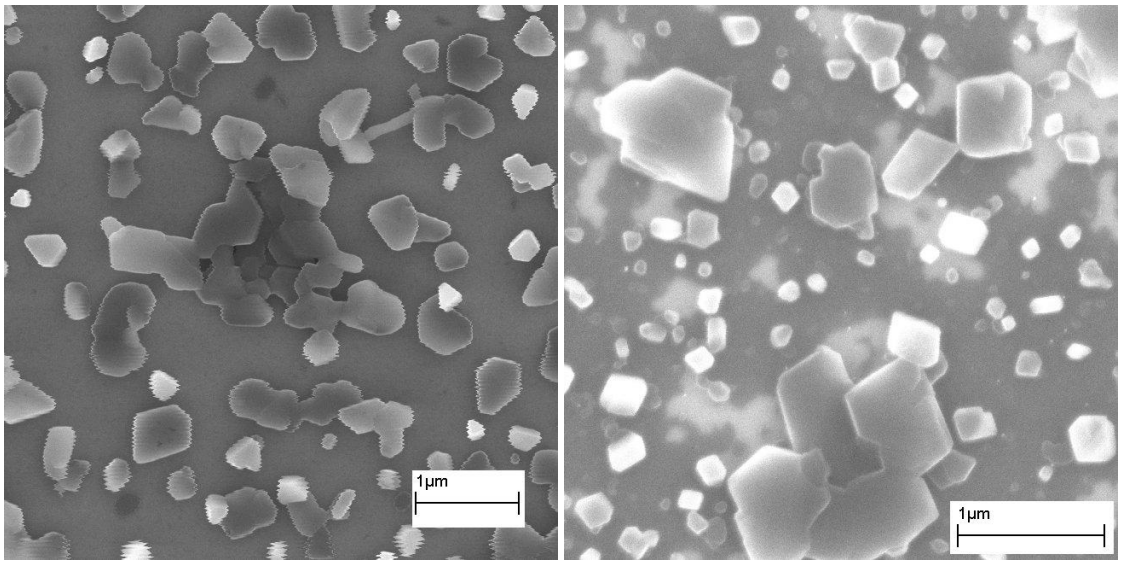

Figure 6-2: (left) one-step 140^{0}C from experiment 1. (right) one-step 140^{0}C from experiment 2. Again films are quite typical, however the film from experiment 2 show more roughness, what appear to be dewetting are areas where pentacene is thin.

The one-step TFT results are used as comparisons for the two-step results. C1 is used to compare with experiment 1 and C2.1 is used for experiment 2. The results in C1 (figure 6.3) are typical and extremely clean. There is a peak in the mobility at intermediate temperatures, and the mobility is the lowest at high temperatures. The trends for the on/off ratio are the exact opposite to the mobility trend. The on/off ratio was the highest at high temperatures and lowest at intermediate temperatures.

The results in C.2 (figure 6.4) had the same trends as C1, however the data is extremely noisy. The mobility peak is at 180^0C, instead of the typical 150-160^0C. The on/off ratio was unusually high at low and high temperatures.

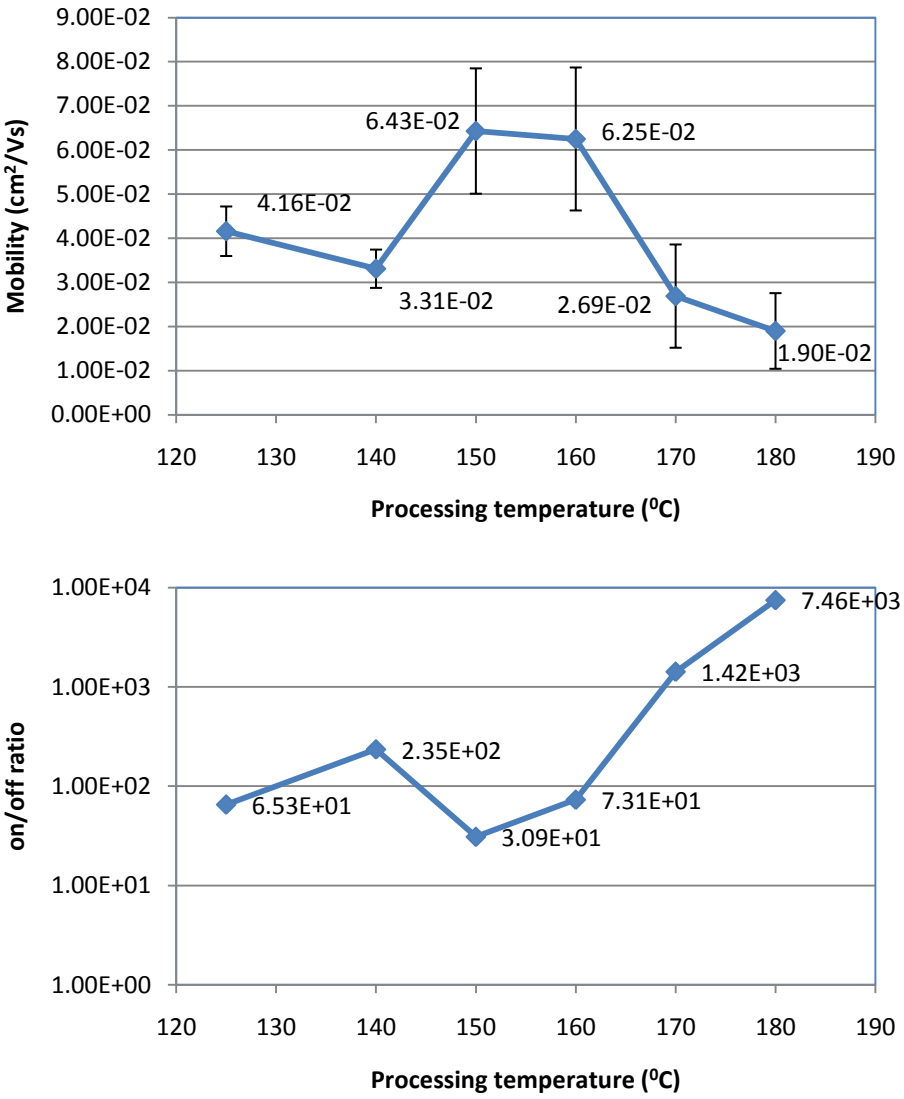

Figure 6-3: C1 TFT results (top) mobility (bottom) on/off ratio

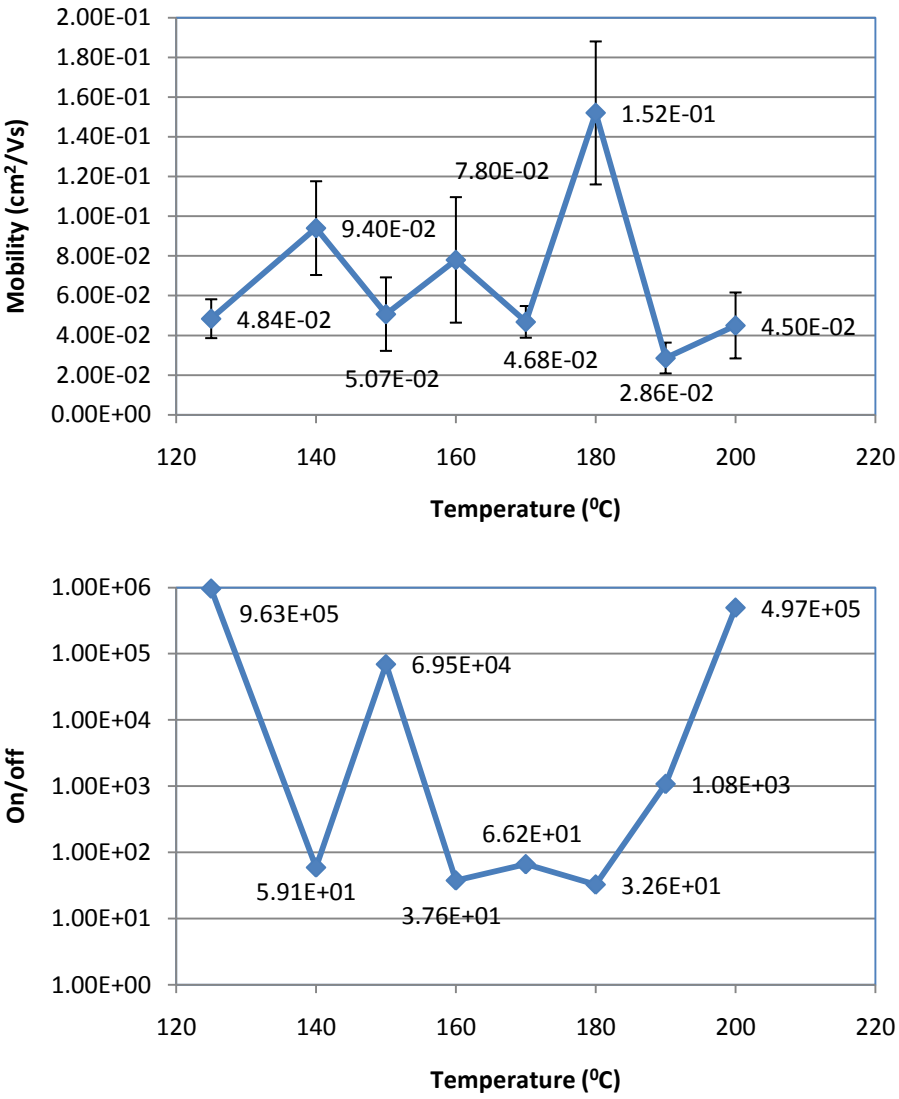

Figure 6-4: C.2 TFT results (top) mobility (bottom) on/off ratio

The one-step anneals followed the predictions from chapter 4. The trends in C1 were clean and showed the predicted trends, while C2.1 was quite noisy but still more or less followed the predictions. As predicted, the mobility should be the highest at intermediate temperatures. The peak mobility for C1 falls between 150^0C and 160^0C. From the previous GIXD data there is the highest amount texturing in that temperature range, which helps to give high mobilities. Texturing is extremely low at 125^0C as well

as at 180^0C, hence the mobility is lower as compared to the intermediate temperatures. The mobility at 125^0C is still higher than at 180^0C because once again from the GIXD results, the crystallite size is smaller at 180^0C as compared to 125^0C. From the SEM data there is little dewetting at low temperatures as compared to high temperatures. Dewetting causes the effective width of devices to decrease, causing an effective mobility drop.

From the data in C1 and C2.1, the on/off ratio and mobility seem to be inversely proportional from each other. The on/off ratio is the lowest where the mobility is the highest. At high temperatures the on/off ratio is the highest. Films processed at high temperatures have the fewest defects as well as miscellaneous byproducts from the precursor degradation giving the highest on/off ratio. In C1, the on/off ratio at low temperatures is not particularly larger than at intermediate temperatures. The amount of byproducts and defects at low temperatures keeps the on/off ratio relatively low. C2.1, shows that there is the potential for extremely high on/off ratios at low temperatures, however this data set is unusual. The high on/off at 125^0C and 150^0C are anomalies.

It should be noted that evaporated pentacene is able to have mobility of greater than $1cm^2/V{\cdot}s$.[25] However, none of the transistors tested above have been able to reach this high mobility. In fact no SAP -pentacene TFTs have been able to reach the high mobility of pentacene TFTs with evaporated films. This is probably due to the temperatures which are used to process SAP-pentacene films. Film must be heated above 120^0C in order for the reverse Diels-Alder reaction to occur. It has been shown pentacene films heated above 90^0C have lower mobility because the thin-film phase starts relaxing to the bulk-like phase.[26] As seen from the GIXD data in chapter 4, only a small amount of the little thin-film phase of pentacene if formed on the high temperature films,

and no thin-film phase of pentacene is even detected at the lower temperatures. The small amount of the thin-film phase is probably because since pentacene processing is above 90^0C, the formation of the thin-film phase is not favorable. Fortunately some thin-film phase is still present, to allow for the potential of high mobility.

Even though the formation of the high mobility thin-film phase is unfavorable, it may still be possible to optimize these SAP-pentacene films utilizing a final high temperature anneal is an attempt to fix defects and to drive off unwanted byproducts from the sample. This is the reason for utilizing the post-processing anneal.

6.3.2 Post-processing anneal

Figure 6.5 shows the post-processing anneal series for films processed at 125^0C (125+160, 125+170, 125+180). No visual differences were noticed between films that were processed with a final high temperature step versus films that were processed at only one temperature from beginning to end. The SEM suggests that the final high temperature anneal does not evoke large morphological changes. This makes sense, because the final high temperature anneal was after the SAP to pentacene reaction has already completed, there is no reason for anything drastic to happen after the film has formed. The only possibility for a big visible film change is for pentacene to sublimate away from the film, but this occurs at temperatures above 200^0C.

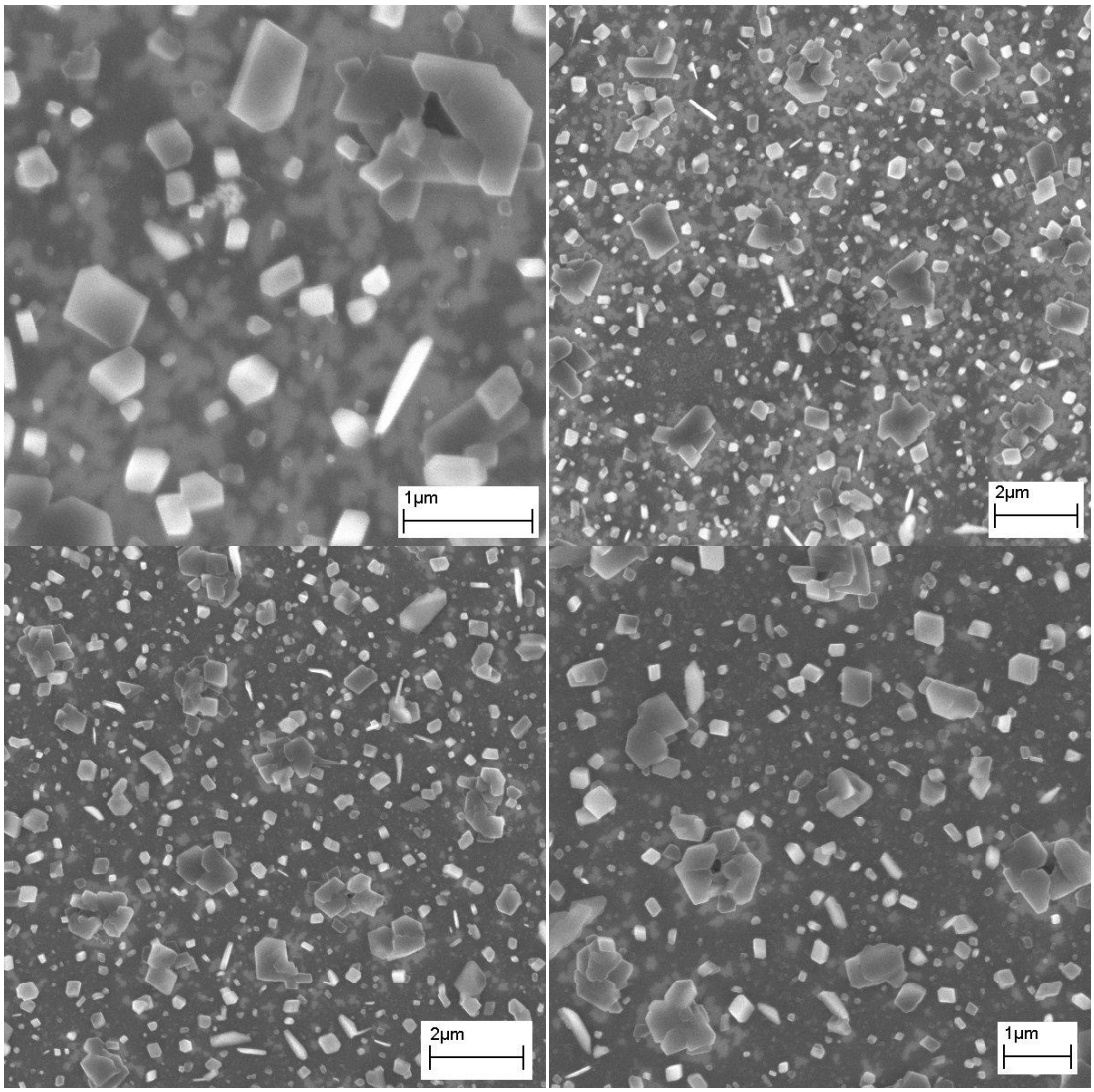

Figure 6-5: 125^{0}C films with post-processing anneal (top left) no anneal. (top right) 160^{0}C anneal. (bottom left) 170^{0}C anneal. (bottom right) 180^{0}C anneal.

Figure 6.6, shows the TFT results for the post-processing anneal. For both the mobility and the on/off ratio for films processed at 150^{0}C, the different final anneals do not produce statistically different results. In the 150^{0}C heating series a final high temperature anneal of any temperature does not change the performance of the pentacene TFT. This is largely corroborates with the SEM data, showing that a final does not

produce any change. However, SEM by itself cannot confirm possible changes in crystal structure and pentacene crystallite size. Only X-ray diffraction may be able to determine the changes in crystallite size. Compared to the control samples, annealed films still overall have a higher mobility, with no change in the on/off ratios.

For films processed at 140^0C and 150^0C, results suggest that using a final high temperature anneal also changes the mobility. The trend appears that a higher temperature final anneal decreases the mobility while a lower temperature final anneal increases the mobility. It is however, difficult to claim a statistical difference between the 125+180 and 125+160 samples. What can be state conclusively is that, the highest mobility devices in these two heating series have a higher mobility than the standard one-step TFTs processed without the final anneal. Unfortunately, once again, the data show an inverse relationship between mobility and on/off ratio. The good news is that the lowest on/off values in the TFTs with the post-processing anneal over all exhibits higher on/off than the one-step TFTs showing that the post-procesing anneal is able to improve leakage.

Even though, the data does not conclusively state the effect of the final anneal temperature, however it is clear that having a final anneal can give a boost in the final mobility and there is an overall improvement the on/off ratio. In these series of tests only short anneal times were tested, in the future, longer anneal times needs to be tested, and changes in crystallite size needs to be confirmed.

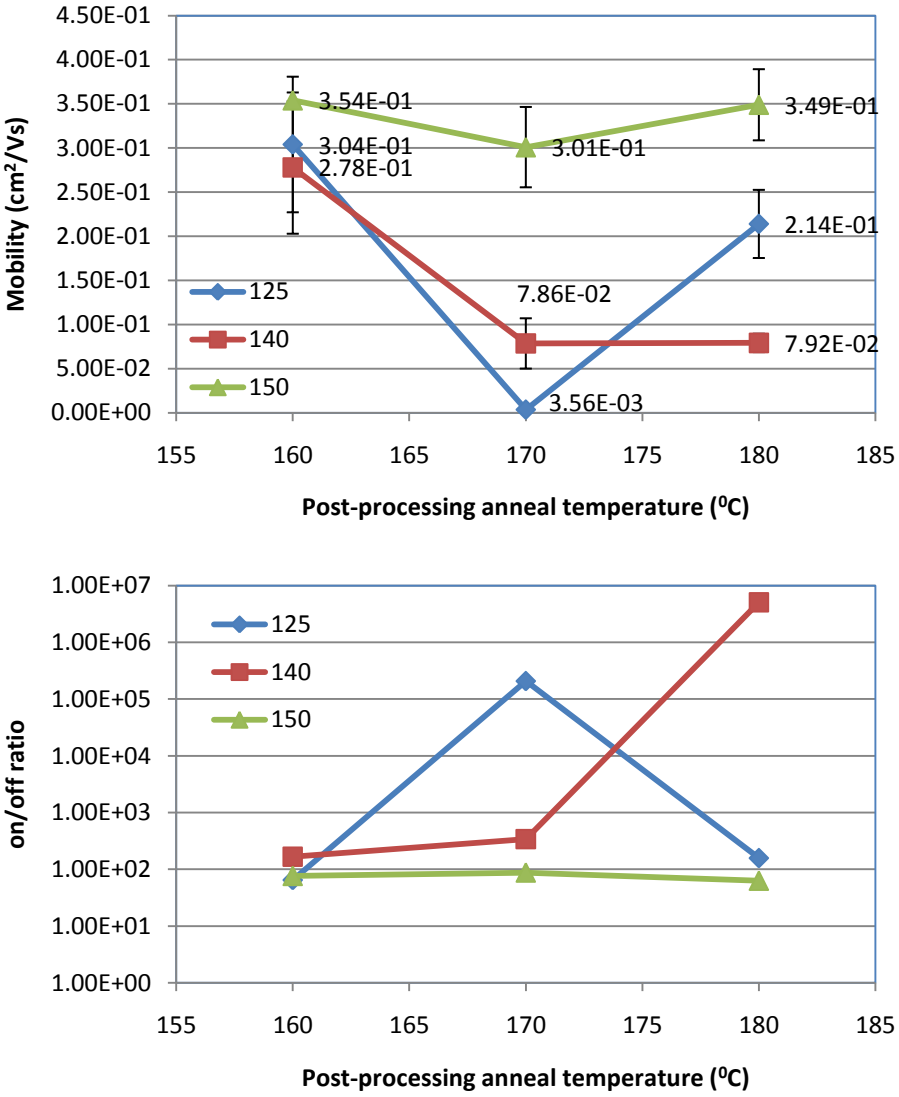

Figure 6-6: Post-processing anneal. Each series of lines represent one heating series (i.e. Samples with the same processing temperature, but different final anneal temperature). (top) mobility (bottom) on/off ratio

6.3.3 Step-down Heating

For two-step heating samples, intermediate samples were made to check for proper film development in between temperature steps. Figure 6.7 shows the formation

of high temperature nuclei after processing at 160^0C and 170^0C to form the high temperature nuclei. The SEM images show proper formation of high temperature nuclei.

A the samples are fully processed with the step-down conditions the final films, visually resemble one-step films which were processed at the higher temperature. For example, as seen in figure 6.8, the 160-150, 160-140 and 160-125 films visually resemble one-step 160^0C films. The plateaus which are characteristic of films processed above 150^0C were a defining feature in the entire step down films, showing that high temperature characteristics were created using the two-step process.

Even though the films more closely resemble the higher temperature one-step films, however, there were also some characteristics of low temperature processing. For example, when comparing between samples in the 160 series (160-150, 160-140 and 160-125), small pentacene islands between plateaus show up in samples 160-140 and 160-125 films. These small islands are typical of low temperature processing. There where more islands in the 160-140 film compared to the 160-125 film, which is also a trend seen in low temperature processing. Furthermore, the amount of dewetting decreases as the second heating step temperature decreases. As seen in figure 6.8, sample 160-125 had less dewetting than sample 160-150, this again followed the trends seen in chapter 4. All the trends decscribed for the160 series where true for all the other sample series as well.

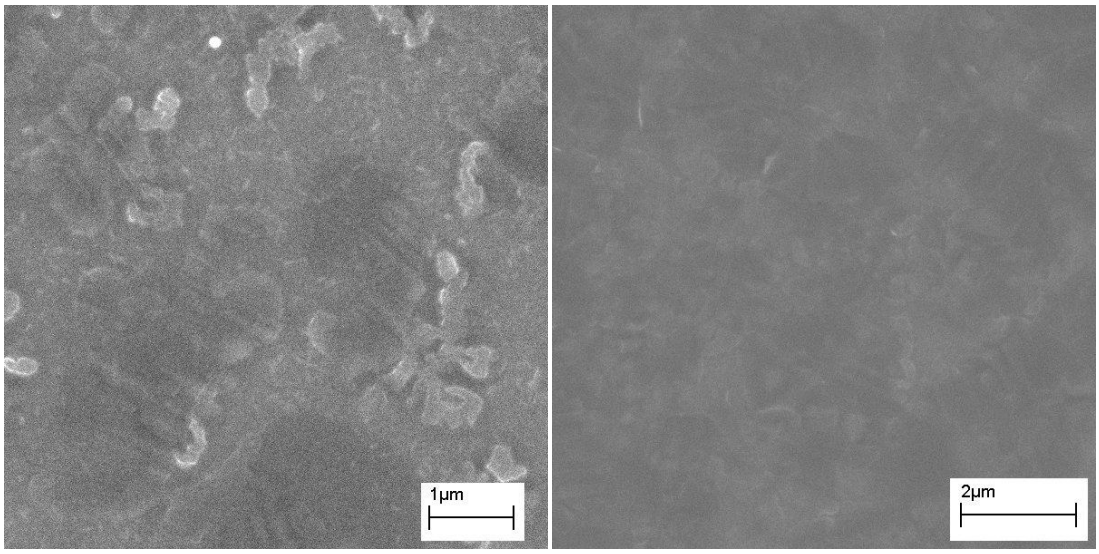

Figure 6-7: (left) Step-down film after 9s of processing at 160^0C, without processing at the lower temperature. (right) Step-down film after 4s of processing at 170^0C, without processing at the lower temperature. These films with high temperature nuclei show typical nucleation with some crystal growth.

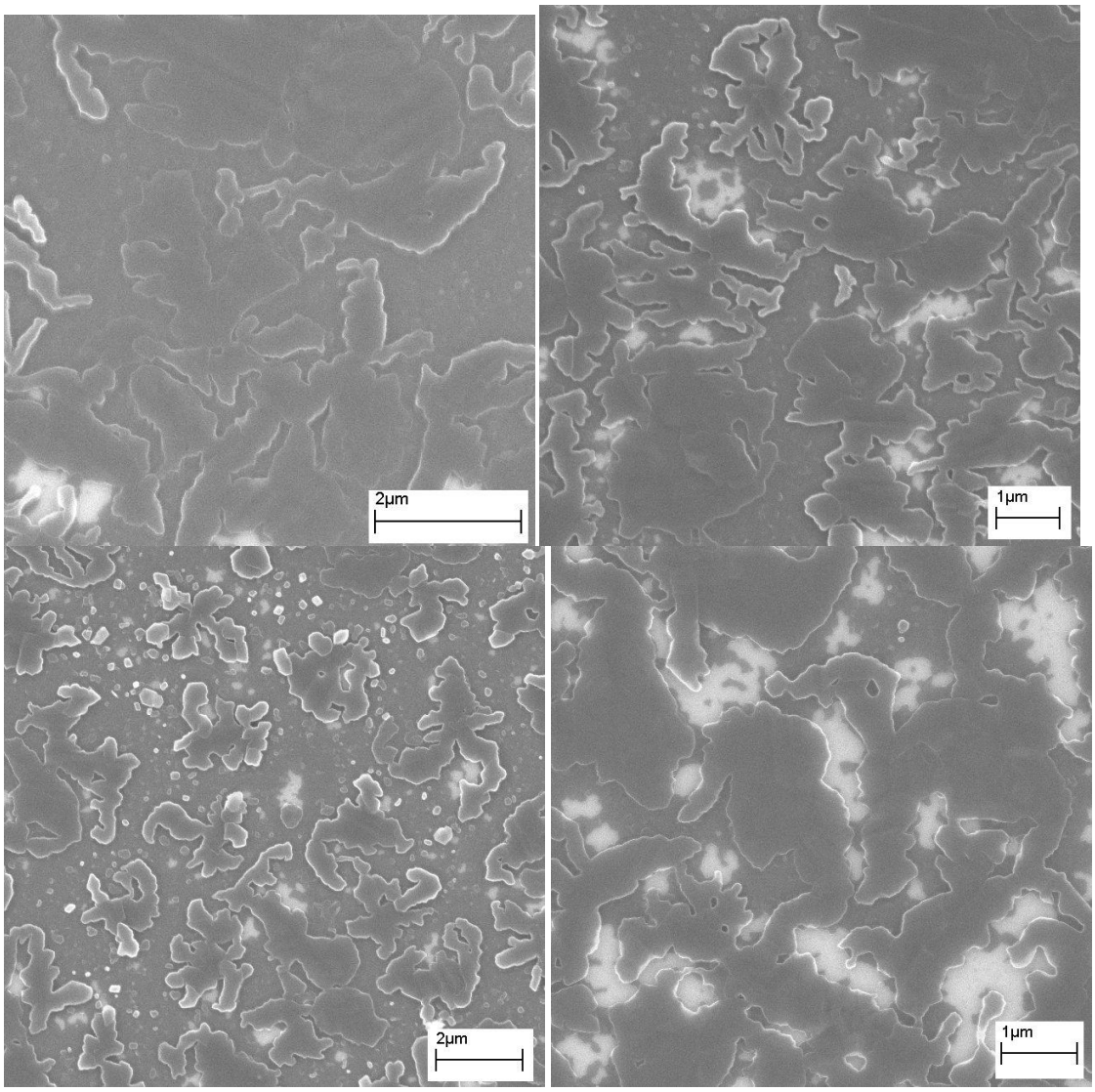

Figure 6-8: (top left) One-step 160^{0}C film. (top right) Step-down 160-125. (bottom left) Step-down 160-140. (bottom right) Step-down 160-150.

TFT measurements for step-down experiments showed a clear mobility trend (figure 6.9). For samples with the same nucleation temperature, the mobility increases with increasing crystal growth temperature. The mobility drop comes from the increased number of nuclei which forms when high nucleation temperatures are used. The increased number of nuclei decreases the pentacene crystal size and would account for a decrease in mobility.

On the other hand, when the nucleation temperature is fixed and the crystallization temperature changes, mobility increases for higher crystal growth temperatures. It was originally thought that the 160-125 sample would give the highest mobility, since at 160^0C the texturing is the highest, and the low crystal growth temperature would grow large pentacene crystals. However, using 125^0C consistently gave the lowest mobility for each heating series. The low mobility for the 125^0C crystal growth can probably be attributed to the loss of texturing when the low temperature crystallization is used. So even with the high temperature nuclei, the crystals which grow above the intial nuclei are probably still relatively disordered. A good guess would be that the step down films should be more textured than a film processed exclusively at a the low crystal grwth temperature, but less textured than a film processed exclusively at a the high nucleation temperature. Furthermore, even though a low temperature is used in order to promote crystal growth, the increased number of starting nuclei would probably make the final crystal size smaller than film growth exclusively at the low crystal growth temperature. These two factors contribute to the decreased mobility from a low crystallization temperature. However, when compared with single step films, the best step-down films are able to achieve higher mobility than one-step films.

The trends for on/off ratio were not quite as clear. For all heating series, using the highest crystal growth temperature (150^0C) gave the best on/off ratio. However, the on off ratio was higher when the crystal growth temperature was 125^0C versus 140^0C, albeit both at 125^0C and 140^0C, the on/off ratios were significantly lower than at 150^0C. When the nucleation temperature was reduced the the on/off ratio also decreased.

Again, just as with mobility, the highest step-down on/off ratio exceeded the one-step on/off ratios. Unlike the control set however, mobility and on/off ratio are not inversely proportional to each other.

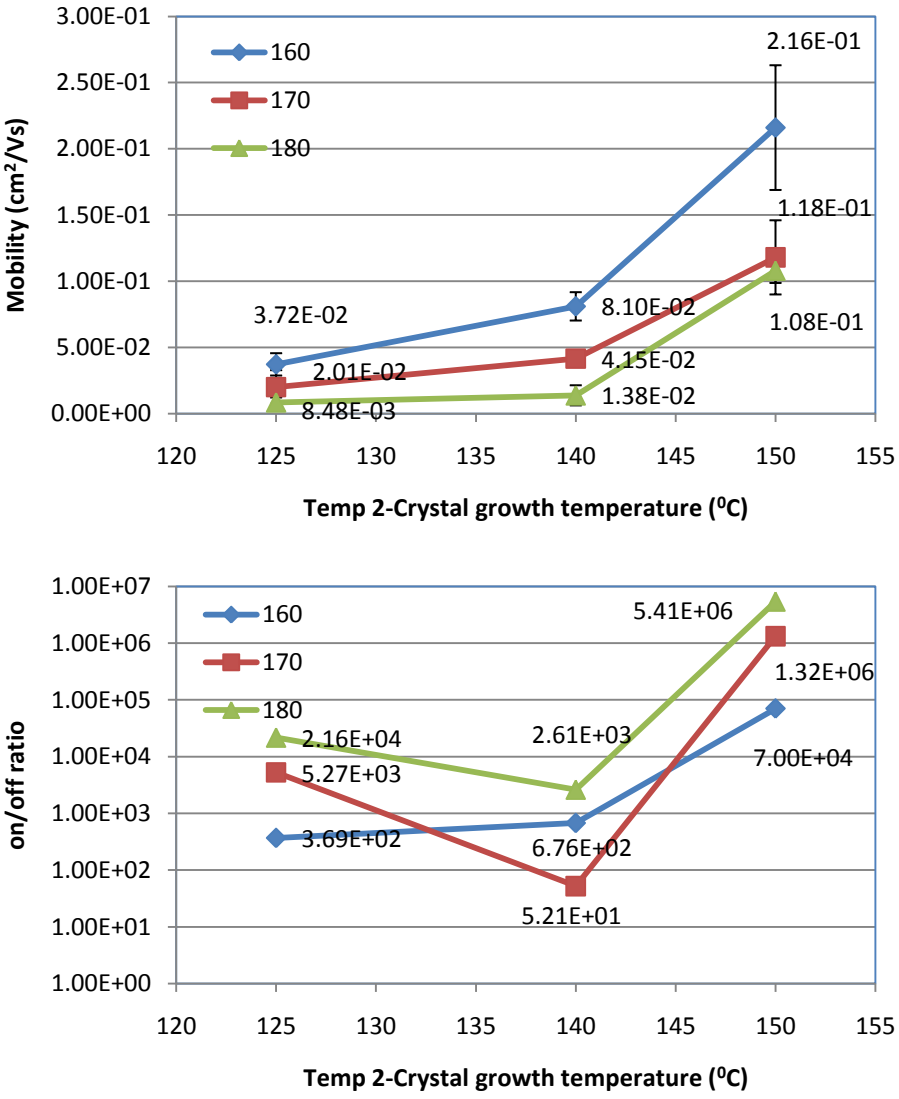

Figure 6-9: Step-down heating. Each series of lines represent one heating series (i.e. Samples with the same nucleation temperature). (top) mobility (bottom) on/off ratio

The goal of the step-down experiments was attempt to get the best of both worlds, by using a high temperature nucleation should leads to a textured film, but using a low

temperature for crystal growth should promote large crystallite sizes and decrease dewetting, all these factors should allow for films with higher mobility compared with one-step processed films. The greatest benefit seen in the step-down films is the high mobility along with high on/off ratios. These films give mobility higher than one-step films as well as on/off ratios larger than the one-step films. The previously seen inverse relationship between on/off ratios and mobility is broken. On again the sweet spot for high performance occurs in the 150^0C-160^0C. This can probably be explained by postulating that nucleating at 160^0C, allows for highly textured high temperature nucleation, but the crystal growth at 150^0C gives larger crystal than processing purely at 160^0C, however the crystals are still textured as compared to crystal growth at 125^0C lower temperature. This however needs to be tested with X-ray diffraction. Furthermore, only a limited set of step-down conditions have been tested, a wider range of step-down conditions also needs to be tested.

6.3.4 Step-up results

For step-up films there were no great visual differences between each series. Figure 6.10 shows, the step-up series for 125^0C. The step-up film more closely resembles a one-step film processed at the lower temperature.

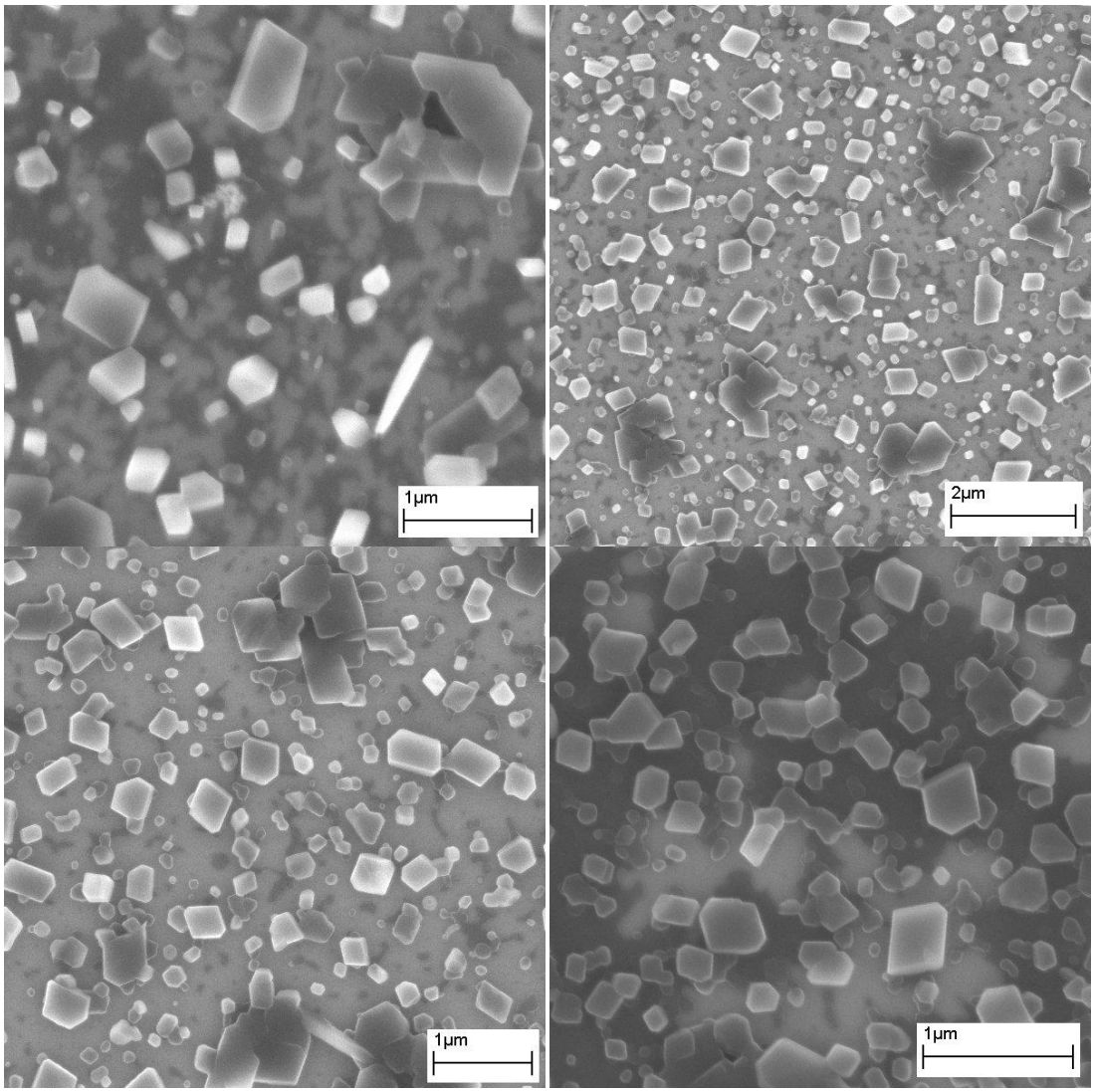

Figure 6-10: (top left) one-step 125^{0}C. (top right) step-up 125-160. (bottom left) step-up 125-170. (bottom right) step-up 125-180.

No clear trends can be seen in the step-up results (figure 6.11). This set of TFTs came from experiment 2, where there was a great deal of noise in the control, which indicates that there is great deal of noise in all the TFTs in experiment 2, therefore the results may be hidden in the noise. Nonetheless, the highest mobilities and on/off ratios in the step-up experiments exceed the highest mobilities and on/off ratios in C2.1. Unfortunately, high mobility also corresponded to low on/off ratios.

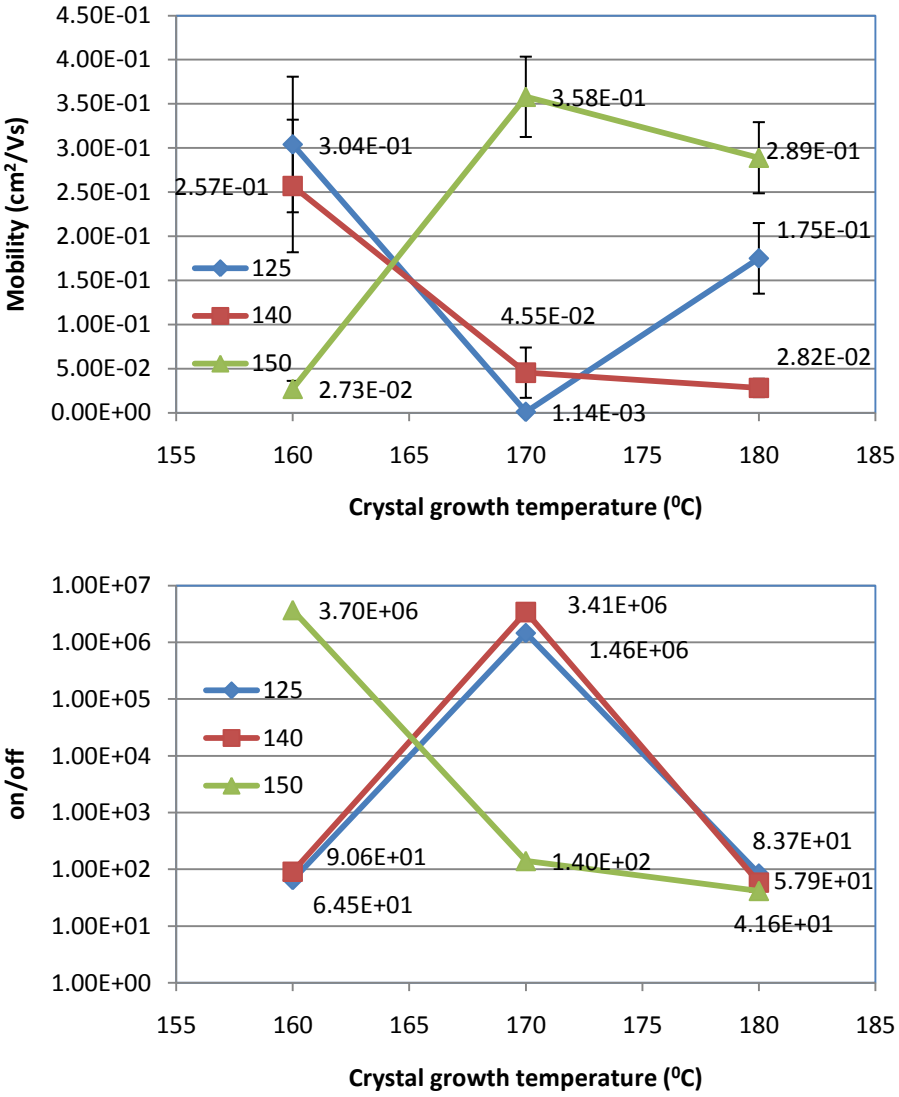

Figure 6-11: Step-up heating. Each series of lines represent one heating series (i.e. Samples with the same nucleation temperature). (top) mobility (bottom) on/off ratio

Step-up films, look like the one-step films processed at the lower temperature. However, the step-up films may have smaller crystallite sizes than one-step films. This still needs to be confirmed with x-ray diffraction.

TFTs with step-up processing, showed no clear trends. Overall, mobility were higher than the one-step TFTs. The step-up films being subject to a final high

temperature step may have received the same benefits as films with a post-processing anneal, overall giving s boost in mobility and the on/off ratio. The inverse proportionality between mobility and on/off however is still present.

6.3.5 Quenching Control (C2.2)

The results of C2.2 consists of a repeat of the 160^0C step-down series, as well as a step down, where the second temperature remains at 160^0C. The 160-150, 160-140 and 160-125 samples are consistent with the step-down result from experiment 1. The 160-160 control sample had the small pentacene islands between the pentacene plateaus, resembling the 160-140 film instead of the one-step 160^0C film. This shows that the 160-160 film is not identical to the one-step 160^0C. The cool down and reheat clearly has a significant effect to the processing of pentacene films.

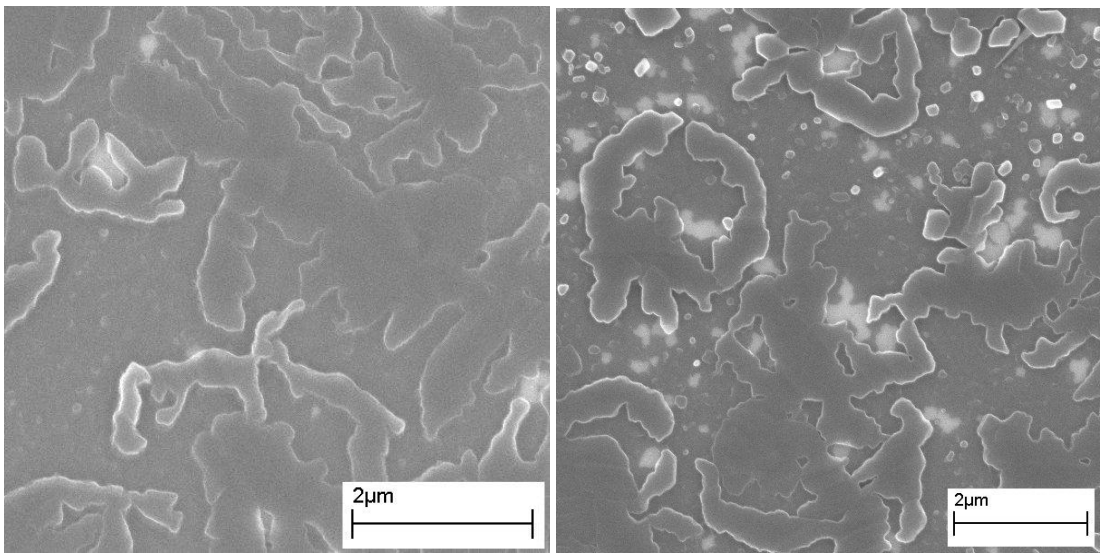

Figure 6-12: (left) One-step 160^0C film. (right) 160-160 film. The 160-160 film has small pentacene island characteristic of films processed at lower temperatures.

Figure 6.13 shows the results for the TFT quench control experiment. C2.2 was measured mainly to check the results the effects of cooling and reheating during pentacene film processing. The data point of most interest was the reheat back 160^0C. There seems to be a significant increase in mobility and on/off ratio as compared to the single step 160^0C measurement. For the rest of the data points were repeats of the 160^0C step-down heating series. The data follows the trend seen above in the full step-down data set. Mobility and on/off ratio both decreases as crystallization temperature decreases.

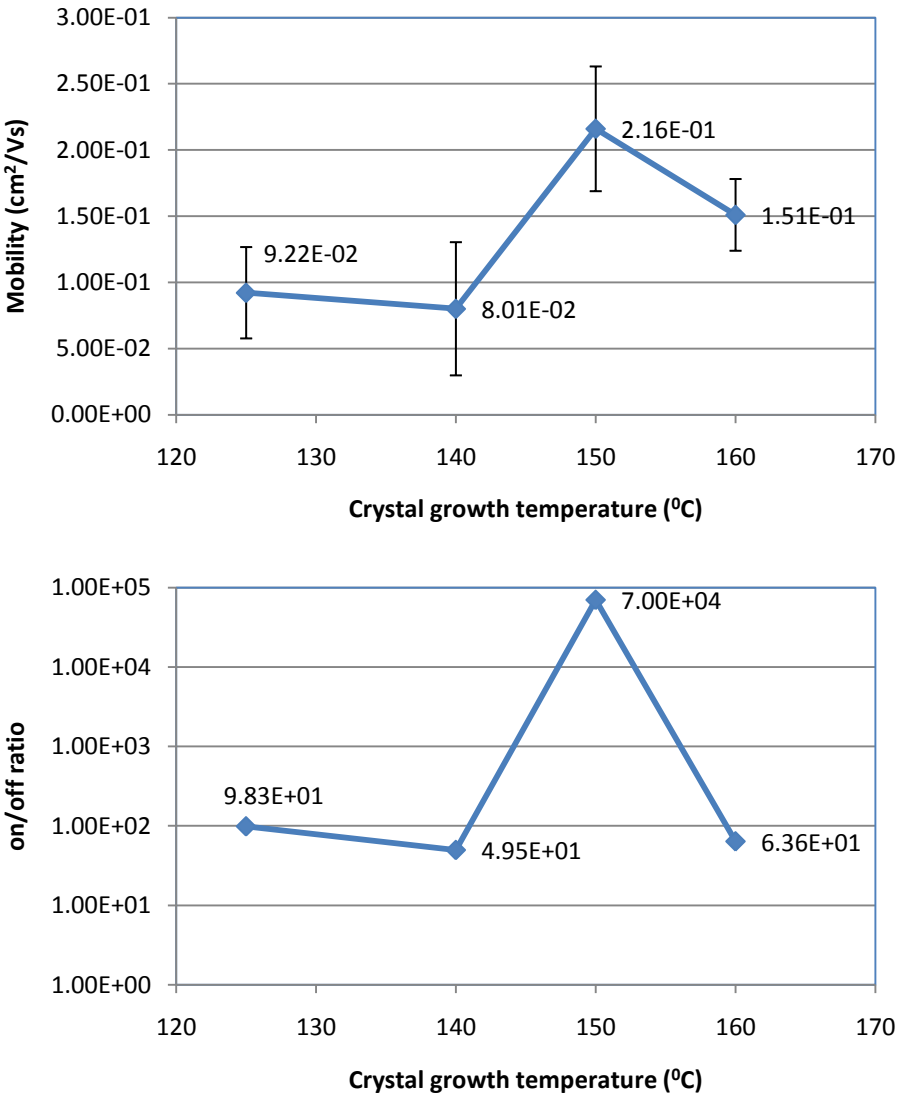

Figure 6-13: Quench control. (top) mobility (bottom) on/off ratio

The data from C2.2, is important in determining the effects of cool down and reheat in the step-up experiments. Clearly the cool down and reheating did not produce films identical to one-step 160^{0}C film. The final film visually resembles 160-140 films, showing that Diels-Alder reaction cannot be instantly quenched nor can it be instantly restarted at the high temperature. Instead, as the film reheats, there is crystal growth below the desired temperature, because films cannot instantly jump from one temperature

to another via the crude techniques employed. A few seconds pass before the film is reheated to the set temperature. Therefore, the 160-160 control sample is not the same as the one-step sample. This may not necessarily be an issue for the step-down films, however may be an issue for step up films

Considering the C2.2 data the cool down and reheat used for the step-up film may play a significant role in the final film. None of the step-up films may truly step-up films, since significant crystal growth takes place at temperatures lower than the desired crystal growth temperature. In order to prevent problems of cooling and reheating, a heating system with quick temperature response would be necessary for future experiments.

6.4 Conclusions

It is quite clear from the SEM result, that the appearance of the final film is largely determined by the type nuclei formed in the early parts of film development. The nuclei type is determined by the initial processing temperature, making the initial processing temperature the most important part of SAP-pentacene film formation. In both the step-up and step-down films, the film appearance is closer to a one step-film processed at the nucleation temperature of the two-step film. This indicates that, as expected, nucleation is more energetically intensive than crystal growth. As seen in chapter 4, the nucleation density does not increase as the Diels-Alder reaction proceeds. Once the nuclei are formed, it is more favorable for crystals to grow than for new nuclei to form.

Even though in two-step processing the films is most affected by the starting temperature, however in the case of the step-down film both high temperature and low

temperature features appear in the final film, with high temperature feature being the most dominant. The identification of pentacene morphotypes and crystallite size is unknown. This can only be determined through X-ray diffraction. Most likely, even though the final film resembles the one-step film, however, because crystal growth temperatures is different from the one-step film, the crystallite sizes are different. In the case of step-down films, the crystal sizes should larger than the one-step films because crystals are allowed to grow slowly. In the step-up films, the crystals should be smaller than one-step films because of the fast crystal growth.

Three types of heat-treatments have explored, and data suggest that using multiple heating steps for a precursor system is beneficial. Only a limited number of heat-treatments have been tested, but many more heat-treatments can be tried and tested. One simple extension of what has already been tried, is to vary the post-processing anneal time. The current data suggests that a step-down film with a post-processing anneal might be able to give the best mobilities and on/off ratios, this also has not been tested.

6.5 References

1. Song, C. et al. Characteristics of pentacene organic thin film transistors with gate insulator processed by organic molecules. *JAPANESE JOURNAL OF APPLIED PHYSICS PART 1-REGULAR PAPERS SHORT NOTES &* **41**, 2730-2734(2002).
2. Mun, S. et al. Determining the optimum pentacene channel thickness on hydrophobic and hydrophilic dielectric surface. *APPLIED PHYSICS LETTERS* **93**, (2008).
3. Shtein, M. et al. Effects of film morphology and gate dielectric surface preparation on the electrical characteristics of organic-vapor-phase-deposited pentacene thin-film transistors. *APPLIED PHYSICS LETTERS* **81**, 268-270(2002).
4. Lee, M. & Song, C. Oxygen plasma effects on performance of pentacene thin film transistor. *JAPANESE JOURNAL OF APPLIED PHYSICS PART 1-REGULAR PAPERS SHORT NOTES &* **42**, 4218-4221(2003).
5. Lim, S. et al. Surface-treatment effects on organic thin-film transistors. *SYNTHETIC METALS* **148**, 75-79(2005).
6. Salih, A. et al. Improved thin films of pentacene via pulsed laser deposition at elevated substrate temperatures. *APPLIED PHYSICS LETTERS* **69**, 2231-2233(1996).
7. Gundlach, D. et al. Pentacene organic thin-film transistors - Molecular ordering and mobility. *IEEE ELECTRON DEVICE LETTERS* **18**, 87-89(1997).
8. Park, J. et al. Characteristics of pentacene-based thin-film transistors. *MATERIALS SCIENCE & ENGINEERING C-BIOMIMETIC AND SUPRAMOLECULAR SYSTEMS* **24**, 27-29(2004).

9. Choi, J. et al. Electrical characteristics of pentacene organic thin film transistors with silicon dioxide gate insulator. *MOLECULAR CRYSTALS AND LIQUID CRYSTALS* **349**, 339-342(2000).
10. Yagi, I., Tsukagoshi, K. & Aoyagi, Y. Growth control of pentacene films on SiO2/Si substrates towards formation of flat conduction layers. *THIN SOLID FILMS* **467**, 168-171(2004).
11. Bouchoms, I. et al. Morphology identification of the thin film phases of vacuum evaporated pentacene on SIO2 substrates. *SYNTHETIC METALS* **104**, 175-178(1999).
12. Lee, J. et al. 10-nm channel length pentacene transistors. *Electron Devices, IEEE Transactions on* **52**, 1874-1879(2005).
13. Fritz, S.E., Kelley, T.W. & Frisbie, C.D. Effect of Dielectric Roughness on Performance of Pentacene TFTs and Restoration of Performance with a Polymeric Smoothing Layer. *The Journal of Physical Chemistry B* **109**, 10574-10577(2005).
14. Gundlach, D. et al. Pentacene organic thin-film transistors-molecular ordering and mobility. *Electron Device Letters, IEEE* **18**, 87-89(1997).
15. Guo, D., Ikeda, S. & Saiki, K. Pentacene films grown on surface treated SiO2 substrates. *Thin Solid Films* **515**, 814-817(2006).
16. Steudel, S. et al. 50MHz rectifier based on an organic diode. *NATURE MATERIALS* **4**, 597-600(2005).
17. Voz, C. et al. Optoelectronic devices based on evaporated pentacene films. *Solar Energy Materials and Solar Cells* **87**, 567-573(2005).

18. Gui-Fang, D. et al. Improvement of Performance of Organic Thin-Film Transistors through Zone Annealing. *Chinese Physics Letters* **22**, 2027-2030(2005).
19. Kang, S.J. et al. Influence of postannealing on polycrystalline pentacene thin film transistor. *J. Appl. Phys.* **95**, 2293-2296(2004).
20. Tunnell, A. et al. Printing-induced improvements of organic thin-film transistors. *Organic Electronics* **9**, 507-514(2008).
21. Sung Kyu Park et al. High-performance polymer tfts printed on a plastic substrate. *Electron Devices, IEEE Transactions on* **49**, 2008-2015(2002).
22. Yong-Hoon Kim, Dae-Gyu Moon & Jeong-In Han Organic TFT array on a paper substrate. *Electron Device Letters, IEEE* **25**, 702-704(2004).
23. Kline, R.J. et al. Significant dependence of morphology and charge carrier mobility on substrate surface chemistry in high performance polythiophene semiconductor films. *Appl. Phys. Lett.* **90**, 062117-3(2007).
24. Coriolis, E.G.D. & Cowan, R.J. Effect of Atmospheres on the Heat Treatment of Metals. *Industrial & Engineering Chemistry* **21**, 1164-1168(1929).
25. Lin, Y. et al. Stacked pentacene layer organic thin-film transistors with improved characteristics. *Electron Device Letters, IEEE* **18**, 606-608(1997).
26. Ji, T., Jung, S. & Varadan, V.K. On the correlation of postannealing induced phase transition in pentacene with carrier transport. *Organic Electronics* **9**, 895-898(2008).

7 Conclusions and Suggestions for Future Work

This work predominantly focused on the formation of pentacene thin films through a precursor system. The reason for using pentacene is because of the potential high mobility promised by this particular semiconductor which rivals the performance of amorphous silicon. Unfortunately the performance of pentacene processed from precursors fall short in performance and is not as high as reported mobility from evaporated pentacene. However, in order to achieve the goals of low-cost electronics, solution processing required and the pentacene precursor still reports one of the higher mobility among solution processable organic semiconductors. In order gain more insight on proper processing of SAP pentacene precursor, a thorough study of the thin film growth mechanisms of SAP to pentacene was performed. The growth mechanism was further tested on various surfaces which are relevant to printed electronics. Finally, electrical performance of pentacene TFTs from SAP was tested using different heat treatment in order to optimize pentacene film to achieve high performance. There is still more work which still can be done in the study of precursor semiconductors for OTFTs.

The study of SAP conversion to pentacene started in chapter 3 with a purely quantitative chemical analysis of the conversion using UV-vis spectroscopy. The degradation rate of SAP was measured at various temperatures and was extracted by looking at the appearance the 667nm peak. In a solid-state reaction the reaction many times is usually in a sigmoidal shape. In the degradation of SAP, the reaction was

properly described by a decaying exponential. This indicates that the conversion of SAP to pentacene is the energetically most expensive step in film formation. It should then be expected that the mechanisms of film formation would be reaction rate dependent. The most important aspect of the degradation rate extraction that now the reaction rate can be used to gauge reaction completion when processing with SAP, which is something which is fundamental, but previously unknown.

Chapter 4, focuses on the understanding of pentacene thin film formation on oxide from SAP. The study found two temperature dependent nuclei. A low temperature nuclei promoted island like growth of films and a high temperature nuclei promoted a layer by layer smooth film growth. The formation of these two types of nuclei was a result of the reaction rate. The island like nuclei forms the bulk-like phase of pentacene. This is the relaxed phase of pentacene and forms due to the slow precursor reaction causing the supply of pentacene molecules for crystal formation to be slow promoting large relaxed crystal. This also decouples crystal interacts with the substrate and resulting films are largely untextured. The high temperature monolayer nucleus forms because of the fast SAP reaction rate at high temperatures. This causes a quick condensation of pentacene, forming the unstable thin-film phase of pentacene. This phase of pentacene caused the resulting film to be highly textured. However, extremely high temperatures, the rapid development of nuclei causes film texturing to be slowly lost and crystals to be small. Based on this study, it can be predicted that when SAP is processed at intermediate temperatures, the presence of texturing and relatively large crystals would give the highest mobility for pentacene TFTs.

Chapter 5 continues to describe pentacene thin film growth on five other substrates, all of which are important for organic electronics, PEDOT on gold, PVP, gold, silver, HMDS on oxide and oxide. Each substrate has a different energetic interaction with pentacene, which would cause pentacene interactions to be more favorable or less favorable. By using the amount of dewetting of pentacene films from the substrate a quick estimate of pentacene stability on the substrate can be measured. As expected, the metallic substrate offered the least stability showing the most dewetting of pentacene form substrate surfaces and organic substrates showed the highest stability with the least pentacene dewetting. The nucleation density of pentacene was found to be constant across all the different substrates. The lateral dimensions of pentacene islands were also constant across the board showing again. This study showed that during the initial stages of film formation, the substrate does not play a significant energetic effect on pentacene film formation, instead the precursor matrix is energetically more important. At the latter part of film formation when the precursor is largely consumed, the substrate starts to play a larger role on the film formation. The substrate interaction then determines the roughness of the pentacene films. The roughest films are the films with unstable interactions with the substrates. The smoothest films are the films grown on substrates which have a stable interaction with pentacene.

Chapter 6 finally describes electrical performance of pentacene TFTs. In this chapter using the knowledge gain from the previous chapters, heat-treatments of the SAP conversion was tested in order to optimize electrical performance on TFT films. TFTs processed at a single temperature followed the predictions from chapter 4. Films processed at intermediate temperatures showed the best mobility because of the presence

of the thin-film phase of pentacene as well as high texturing and low film dewetting. TFTs processed at low temperatures showed low performance due to high disorder of the pentacene crystal orientation. TFTs processed at high temperatures also showed low mobility due to small crystal sizes, high dewetting and loss of film texturing. Furthermore, three different two temperatures SAP processes where tested in TFT fabrication. First, TFTs were made in the standard single temperature heating, but a short high temperature anneal was added after the film was fully processed. This study showed an overall increase in the on/off ratio, since a high temperature anneal is able to fix defects in pentacene crystals. Next, films were made with the step-down processing where, nucleation is initialed at a high temperature and then crystals are grown and films formed at a lower temperature. This process attempts to create films which are well ordered and have large crystal sizes, which should give mobility higher than standard single temperature processing. The step-down process showed the most promise. Mobility was increased simultaneously with the on/off ratio give high performance and low leakage. Finally, the step-up process, which the opposite of the step-down process, was tested and it showed few trends and few conclusion were able to be made. The SEM studies of film growth using these heat treatments showed that the final film morphology is largely determined by film nucleation. Since regardless of the final temperature used to process films, the final film always looks more like films processed exclusively at the nucleation temperature. The use of heat treatments in the processing of semiconducting precursors is promising, because it allows for fine control in order to improve the performance of pentacene TFTs which would hopefully allow for precursor pentacene TFTs to reach the performance of evaporated pentacene TFTs.

The motivating factor of this thesis was the solution processing of organic semiconductors for low-cost electronics. In creating low-cost electronics TFTs are an important component to the realization of this goal. However other devices also need to be made. One particularly elusive device is a solution processed diode. To date no group has been able to report a fully solution processed diode. Many fully evaporated diodes have been reported, even diodes which function well at high frequencies.[1,2] The pentacene precursor used in this study would be a good choice for use in a solution processed diode. However, the requirements for the pentacene to be incorporated into a diode are largely different than when used in a TFT. The processing of the pentacene precursor for such a device may be completely different than what has been reported in this thesis. For the realization of such a device different considerations need to be taken. The processing of the SAP pentacene precursor for a solution processed diode can be a direction for future work.

In conclusion, the formation of pentacene films from SAP has now been explored in great detail and better understood after this study. This knowledge allows for the optimization of the performance of solution processed TFTs using SAP-pentacene. These results may serve as a model semiconducting precursors which may be made in the future.

7.1 References

1. Steudel, S. et al. 50MHz rectifier based on an organic diode. *NATURE MATERIALS* **4**, 597-600(2005).
2. Steudel, S. et al. Comparison of organic diode structures regarding high-frequency rectification behavior in radio-frequency identification tags. *JOURNAL OF APPLIED PHYSICS* **99**, (2006).

9 Appendix (SAP synthesis)

9.1 Introduction

This pentacene precursor, was developed by Afzali, et al.[1] and modified by Steven Volkman.[2] Until recently, SAP was only available by in house synthesis, now it available through Aldrich by special order.

9.2 Chemicals Required

Pentacene $C_{22}H_{14}$

N,O-Bis(trimethylsiyl)-acetamide $CH_3C[=NSi(CH_3)_3]OSi(CH_3)_3$

Thionyl Chloride Cl_2OS

Methyltrioxorhenium(VII) CH_3ReO_3

Chloroform $CHCl_3$

Hexanes C_6H_{14}

Ethyl Acetate $C_4H_8O_2$

Dry Ice CO_2

9.3 Laboratory Equipment

Sublimation Tube (Quartz)

Sublimation Heater System (3 zones with thermocouples and controllers)

Forming Gas Cylinder

Mass Flow Controller and Valve

Vacuum Pump

Bunsen Burner

250 mL Round Bottom Flask

Distillation Apparatus

100 mL Round Bottle

Schlenk Flask

Hot Air gun

50 mL Round Bottom Flask

Glass Reflux Tube for 50 mL Round Bottom Flask

Magnetic Stir Bar and Stirrer

High-Frequency Sound Wave Generator

2000 mL Erlenmeyer Flask

Glass Column

Reservoir

Silica Glass

Silica Gel

Ultra Violet Light Source

9.4 Overview

SAP synthesis is split up into 3 sections. First, pentacene is purified by sublimation using a three zone sublimating tube. Second, the Diels-Alder adduct is made. Lastly, is the Diels-Alder reaction, attaching the adduct to the pentacene molecule.

9.5 Pentacene Sublimation Purification

9.5.1 Preparation

- Thoroughly clean a quartz tube using acetone and IPA
- Dry the quartz tube with a nitrogen gun
- Thoroughly dry the quartz tube and burn off all organic contaminants by baking the tube in sublimation heater for 3 hours under vacuum and nitrogen at 300^0C.
- Cool the furnace and quartz tube to room temperature.

9.5.2 Sublimation

- Warm pentacene up to room temperature. (Pentacene is stored in the freezer. Do not open the bottle until the pentacene is sufficiently warm to prevent condensation on to the pentacene. Pentacene is supplied from TCI)
- Place all of the pentacene ~1g into one end of the quartz tube. ~1 cm from the edge of the quartz tube. Try to keep the pentacene concentrated in a small region.
- Place the quartz tube into the sublimation heater, pentacene end first. Make sure the pentacene is in 1^{st} heating zone of the heater.
- Bring the heater under vacuum and nitrogen condition. The mass flow controller should be set to 3.5 ccm/min flow.
- Set the 1^{st} zone to 260^0C, the 2^{nd} zone to 190^0C, the 3^{rd} zone to 160^0C. Heat for ~48 hours, or until zone one has no more pentacene. There should be some black residual impurities.
- Cool heater and tube to room temperature.
- Using acetone clean off impurities in zone one.

- Scrape out the pentacene from zone 2 and half of zone 3.
- Weigh the pentacene. (Yield should be at least 70%-80%)
- Seal the pentacene in a glass vial and store it in the freeze.

9.6 Diels-Alder Adduct synthesis (NSO)

9.6.1 Preparation

- Clean all necessary glassware. Dry all glassware overnight in an oven. (Make sure the oven is set over 100^0C)
- Right before the reaction
- Seal a magnetic stir bar in a 250mL flask with a rubber septum. Fill the flask with nitrogen (make sure to have a syringe outlet). Flame dry the flask to thoroughly dry the flask, with the nitrogen constantly flowing. This creates a dry oxygen free flask. (Standard flame dry procedures require three heat and cool cycles.)
- Flame dry the schlenk flask, and fill it with nitrogen.

9.6.2 Synthesis

- Add 20 mL of N,O-Bis(trimethylsiyl)-acetamide into the flask through the septum. Use oxygen free techniques to make the acetamide does not get contaminated.
- Add 8 mL of thionyl chloride into the flask. (Add drop by drop, this should take over 20 minutes. Adding the thionyl chloride too quickly makes the solution boil, which is undesireable.)
- Setup the distillation apparatus. Setup the nitrogen to flow nitrogen into the apparatus. Also setup the vacuum. Use a two way value so that the apparatus can be

switched back an forth between vacuum and nitrogen. Flow nitrogen into the apparatus.

- Once the set up is sufficiently cool, attach the NSO filled 250mL flask onto the source side of the apparatus. Attach a 100 mL round bottom flask to the waste side of the apparatus. Flow water through the condensation region.
- Place a crystallization dish with dry ice and acetone under the waste flask.
- Slowly bring the apparatus under vacuum. The NSO may start to bubble, in which case, switch back to nitrogen. Repeat this process until the NSO no longer bubbles under vacuum. Keep the setup under vacuum.
- Slowly apply heat using a hot air gun to the flask and the vertical column. The NSO may start to boil, in which case stop heating. The goal is to heat and evaporate the liquid without boiling. A clear liquid will start to collect in the waste flask, the waste may crystallize. Continue to heat until the waste is no longer clear but yellow. The yellow is desired product and is no longer waste.
- Fill the setup with with nitrogen and remove the waste flask and replace it with the dry schlenk flask. Work quickly to keep the setup oxygen free. The NSO product is oxygen sensitive. Bring the setup back down to vacuum.
- Apply heat to the NSO flask in the same fashion as above. Heat until the flask is completely dry. Black byproducts will be left in the flask. Bring the setup to nitrogen. Seal the schlenk flask and remove it from the setup. Cover the flask with aluminum and store it in a freezer. The NSO compound should be yellow, if it trn reddish brown, the product has reacted with oxygen. There will be enough NSO for several reactions. If oxygen free procedures are followed correctly, the NSO should

be able to be stored for months.

9.7 Diels-Alder Reaction (SAP synthesis)

9.7.1 Preparation

- Clean and oven dry all glassware before hand.
- Before starting the reaction make an dry, oxygen free 50 mL round bottom flask, with a magnetic stir bar sealed inside.

9.7.2 Synthesis

- Bring the NSO and the purified pentacene out of the freezer. Allow to be warmed up to room temperature before use.
- Setup the reflux tube, along with water running through the sleeve. Setup the nitrogen and vacuum to a two way valves and flow nitrogen into the reflux tube.
- Place the round bottom flask on ring stand over stirrer and add 15 mL of anhydrous chloroform, using oxygen free techniques.
- Weigh the pentacene, then weigh out the proper mole ratio of catalyst (Table A.2). Add both pentacene and catalyst into the flask. This requires the flask to be opened, so work quickly. Once the chemicals are added, flow nitrogen through the flask again to exlude oxygen.
- Sonicate this mixture for 1-3 minutes to remove large pentacene flakes.
- Add the proper mole ratio of NSO (Table A.2) using a long needle and syringe.
- Connect the flask to the reflux tube.

- Slowly bring the setup to vacuum. Once again, the chloroform will bubble, in which case, bring the setup back to nitrogen. Go back and forth between vacuum and nitrogen for at least ten times. Finally, bring the setup to nitrogen at the end.
- Heat the round bottom flask with a mineral bath at 71-72^{0}C, make sure that the oil covers the solvent. Heat for 7 hours at 71-72^{0}C. The final product in the flask will look dark. Make sure the solvent does not dry out. This is done by controlling the nitrogen flow through the manifold.

9.8 SAP purification

9.8.1 Preparation

- Clean all necessary glassware before starting
- Prepare the chromatography solutions before hand: 1 4L bottle of 20% ethyl acetate + 80% hexanes (20/80 solution) and 2 4L bottle of 30% ethyl acetate + 70% hexanes (30/70 solution).

9.8.2 Flash Column Purification

- Using a 2L Erlenmeyer flask, mix silica gel with 20/80 solution. Make sure the silica gel is solvated. Pack the column using standard techniques. Make sure the silica gel stays solvated. The packed column should be approximately 2/3 full.
- Allow the excess solution to flow out of the column, but making sure the top of the silica gel does not dry out.
- Load the column with precursor. Make sure to form a smooth, even layer on the top of the silica gel.

- Fill the rest of the column with 20/80 solution being careful not to disrupt the precursor layer.
- Attach the reservoir and continue to fill the setup with 20/80 solution.
- Start running the column, using high pressure for the column to flow faster.
- Fill the reservoir as needed. Use up the 20/80 solution.
- Now switch to the 30/70 solution.
- Once the solvent is switch, start collecting samples, 500mL
- Use TLC to monitor the product.
- Discard all collected samples without the product.
- Using a rotary evaporator, collect the desired product.
- Dissolve the product with chloroform, and transfer it into a vial.
- Using the rotary evaporator, dry off the chloroform.
- Wash the product with hexanes by adding hexanes into the vial and mixing the product around. Centrifuge the vial and remove the hexanes. Do this at least three times.
- Finally dry off the hexane using the rotary evaporator. Store the product in the freezer.
- The final product should colorless, however, a yellow or orange color is also acceptable.

Chemical	Formula	MW (amu)	Mp (°C)	Bp (°C)	d (g/mL)
Pentacene	$C_{22}H_{14}$	278.34	--	--	--
N,O-Bis(trimethylsinyl)-acetamide	$CH_3C[=NSi(CH_3)_3]OSi(CH_3)_3$	203.43	24	71-73	0.832
Thionyl Chloride	Cl_2OS	118.97	-105	78-79	1.635
Methyltrioxorhenium(VII)	CH_3ReO_3	249.23	111	--	--
Chloroform	$CHCl_3$	119.38	-64	62	1.498
Hexanes	C_6H_{14}	86.18	-95	69	0.659
Ethyl Acetate	$C_4H_8O_2$	88.12	-84	77	0.895

Table 9-1 Chemicals Properties of Chemicals

Chemical	Formula	MW (amu)	Density (g/mL)	Molar ratio
Pentacene	$C_{22}H_{14}$	278.34	--	1.0
NSO	$C_2NO_2SH_3$	105.2	1.327g/mL	1.5
Methyltrioxorhenium(VII)	CH_3ReO_3	249.23	--	0.01

Table 9-2: Mole ratios for Diel-Alder reaction

9.9 References

1. Afzali, A., Dimitrakopoulos, C. & Breen, T. High-performance, solution-processed organic thin film transistors from a novel pentacene precursor. *JOURNAL OF THE AMERICAN CHEMICAL SOCIETY* **124**, 8812-8813(2002).
2. Volkman, S. et al. Inkjetted organic transistors using a novel pentacene precursor. *MRS Proceedings* H11.7(2003).